APPLICATION OF GRAVITY DATA IN DETERMINATION OF THE CRUSTAL THICKNESS AND STABILITY OF PARTS OF SOUTHERNNIGERIA

BY

EJEMBI, QueenAjuma
MTech/SPS/2017/7177

DEPARTMENT OF PHYSICS
FEDERAL UNIVERSITY OF TECHNOLOGY
MINNA

JANUARY, 2022

APPLICATION OF GRAVITY DATA IN DETERMINATION OF THE CRUSTAL THICKNESS AND STABILITY OF PARTS OF SOUTHERN NIGERIA

BY

EJEMBI, QueenAjuma
MTech/SPS/2017/7177

A THESIS SUBMITTED TO THE POSTGRADUATE SCHOOL FEDERALUNIVERSITY OF TECHNOLOGY, MINNA, NIGERIA IN PARTIAL FULFILLMENT OF THE REQUIREMENTS FOR THE AWARD OF THE DEGREE OF MASTER OF TECHNOLOGY IN PHYSICS (APPLIED GEOPHYSICS)

JANUARY, 2022

ABSTRACT

This study focuses on the application of gravity data in determination of the distance between the earth surface and moho (crustal thickness) and stability of parts of southern Nigeria. Empirical relations, Spectral analysis and 2-D gravity modelling techniques were utilised on the bouguer gravity data covering the study area. Three empirical relations relating bouguer gravity with crustal thickness were used to calculate the crustal thicknesses within the study area, the depth ranges to the major density interfaces (basement surface, Conrad and crustal thickness) were determined from the spectral analysis of the bouguer anomalies as the bouguer gravity map was divided into thirty (30) sections. The bouguer gravity anomalies were used with the available geological and geophysical information to create two-dimensional (2-D) gravity models of the earth's crut along three profiles trending in NE, SE and SW directions to obtain a correlated crustal thickness for the study area. The obtain results from these 2-D crustal models show's that the upper and lower part of the profiles has a crustal thickness of 28 km to 39 km, bouguer anomaly of the study area varies from 30 mGal to 0 mGal, 40mGal to 0 mGal and 40 mGal to 20 mGal with the three approach has an average crustal thickness ranges from 30 km to 37 km, 30.2 km to 35.6 km, 28 km to 39 km respectively. There is a good correlation in all the average crustal thicknesses obtained using the three different approaches. Based on these results, the study area is made up of high crustal thickness ranging between 28 km to 39 km. The gravity anomaly profiles were model along profile lines (A-A', B-B' and C-C') drawn in different directions and covering a distance between 230 km - 340 km with crustal thicknesses ranges from 30km to 38km in order to ascertain the crustal thickness underlying the study area. The models identified and delineate boundaries between the Upper Crust, Lower Crust and Mantle with densities of 2.7 g/cm^3, 2.8 g/cm^3 and 3.2 g/cm^3. The crustal thicknesses obtained from the study area ranging from 30 km to 37 km, 30.2 km to 35.6 km and 28 km to 39 km and not located in any active plate boundaries (margins) which indicates the tectonic stability of the region. The result from the study area has shown that the crustal thickness and density have influence on the tectonic stability of the study region. Hence, the area is tectonically stable as it is located in a non-major fractured zones.

TABLE OF CONTENTS

Content		Page
Cover Page		
Title Page		i
Declaration		ii
Certification		iii
Dedication		iv
Acknowledgements		v
Abstract		vi
Table of Contents		vii
List of Tables		xi
List of Figures		xii
CHAPTER ONE		
1.0	**INTRODUCTION**	1
1.1	Background of the Study	1
1.2	Crustal Thickness	2
1.3	Mohorovicic Discontinuity	2
1.4	Gravity Method	3
1.5	Location and extent of the Study Area	8
1.6	Climate	9
1.7	Vegetation of the Study Area	9
1.8	Statement of the Research	10
1.9	Aim and Objectives of the Study	10
1.10	Scope of the Study	11
1.11	Significance of the Study	11

CHAPTER TWO

2.0	**LITERATURE REVIEW**	**12**
2.1	Geology of the Study Area	12
2.2	Review of Geophysical Literature	15

CHAPTER THREE

3.0	**MATERIALS AND METHOD**	29
3.1	Materials used for the Study	29
3.1.1	Data acquisition and collection	29
3.1.2	Research methodology	29
3.1.3	Digitisation of the map	30
3.1.4	Gridding	31
3.1.5	Contouring	31
3.2	Theory of the Study	32
3.2.1	Theoretical gravity	33
3.2.2	Observed gravity	34
3.2.3	Gravity field reductions	34
3.2.4	Drift correction	35
3.2.5	Latitude correction	37
3.2.6	Elevation correction (Free Air Correction)	38
3.2.7	Bouguer correction (BC)	39
3.2.8	Tidal correction (TD)	39
3.2.9	Eotvos correction (EC)	40
3.2.10	Gravity anomalies	40
3.2.11	Free air anomaly (FAA)	40

3.2.12 Bouguer anomaly (BA) 41

3.3 Relationship between BG and Crustal Thickness 41

3.4 The Empirical Relations 42

3.5 Spectral Depth Analysis (SDA) 43

3.6 2-D Modelling 45

CHAPTER FOUR

4.0 RESULTS AND DISCUSSION 48

4.1 Bouguer Gravity Anomaly 48

4.2 Empirical Calculations 48

4.2.1 Demenistskaya relation 49

4.2.2 Wollard relation 49

4.2.3 Wollard and strange relation 49

4.2.4 Average empirical relation 50

4.3 Spectral Method of Depth Determination 55

4.3.1 Depth to basement map 59

4.3.2 Conrad discontinuity map 59

4.3.3 Crustal thickness map 60

4.3.4 Average crustal thickness map of empirical and spectral result 63

4.4 2-D Gravity modelling 66

4.4.1 Model line profile AA[1] 67

4.4.2 Model line profile BB' 67

4.4.3 Model line profile CC' 68

4.4.4 The average crustal thickness map of 2D modelling plot 84

4.5 Crustal Thickness and Plate Tectonism 81

CHAPTER FIVE

5.0	**CONCLUSION AND RECOMMENDATION**	**84**
5.1	Conclusion	84
5.2	Recommendation	84
REFERENCES		85
APPENDICES		90

LIST OF TABLES

Table		Page
4.1	Sample Results of Empirical Calculations where H_D, H_W, H_{WS} are the Crustal Thickness using Demenistskaya, Wollard, Wollard and Strange	52
4.2	Basement Depth, Conrad Depth and Crustal Thickness obtained from Spectral Analysis	58
4.3	Basement Depth, Conrad Depth and Crustal Thickness obtained from Spectral Analysis and its location	61
4.4	Result of Average Crustal Thickness obtained from Empirical and Spectral Analysis of the Study area	64
4.5	2D Plot of the Crustal Thickness obtained from 2D Modelling for the Study Area	78
4.6	Parameters deduced from Modelled Gravity Profiles (AA^1, BB^1 and CC^1)	82
4.7	Some Earthquake Countries, their Crustal Thickness, year of recent Earthquake Occurrence and Earthquake Magnitude on Ritchter's scale	83

LIST OF FIGURES

Figures		Page
1.1	Image of the Earth's internal structure showing Crustal thickness	4
1.2	Crustal thickness Map of Africa	6
1.3	Generalized Geological Map of Nigeria showing location of study area	7
2.2	The location Map of the study Area	14
3.1	Base Tie Plot for Two Base Stations A and B	36
3.2	Block diagram of the Methodology of the Research	47
4.1	The Bouguer Anomaly Map of the Study Area	51
4.2	The Contour Map of Crustal Thickness obtained using Demenistskaya empirical relation for the Study Area	53
4.3	The Contour Map of Crustal Thickness obtained using Wollard empirical relation for the study area	53
4.4	The Contour Map of Crustal Thickness obtained using Wollard and Strange Empirical relation for the Study Area	54
4.5	The Contour of average Crustal Thickness obtained using the three empiricalRelations for the Study Area	54
4.6	Showing a graph of log of spectral energy against frequency	57
4.7	The Basement depth Map obtained from Spectral analysis for the Study Area	62
4.8	The Conrad Discontinuity Map from Spectral analysis for the Study Area	62
4.9	The Crustal Thickness Map from Spectral analysis for the Study Area	63
4.10	The Map of Crustal Thickness obtained from the average of empirical and Spectral analysis of the Study Area	65
4.11	The Bouguer gravity map with towns within the study Area	70

4.12 The Bouguer gravity map with towns and locations of 2-D modelling profiles(A-A', B-B' and C-C') 70

4.13 The Geology map of the study area with the model profiles A-A', B-B' and C-C' 71

4.14 The Bouguer Gravity Map of the Study Area Showing Profile AA' 72

4.15 Crustal Modelling for Profile AA' 73

4.16 The Bouguer Gravity Map of the Study Area Showing Area showing Profile BB' 74

4.17 Crustal Modelling for Profile BB' 75

4.18 Bouguer Gravity Map of the Study Area Showing Profile CC' 76

4.19 The Gravity Modelling along Profile C-C' for the Study Area 77

4.20 The 2D plot of the Map of Crustal Thickness obtained from 2D Modelling for the Study Area 80

4.21 The 3D surface plot of the Crustal Thickness obtained from 2D modelling for the Study Area 80

CHAPTER ONE

1.0 INTRODUCTION

1.1 Background of the study

The earth subsurface has been of particular concern to geoscientists, who attempt to research it using different methods, some with the aims of getting data, while others do it for economic resources examination, for instances mineral resources and hydrocarbons. With the advance in technology development and the need for a clearer pictures of the earth subsurface and its substance, the earth scientist have thought of it as essential to utilise the properties associated with the earth interior since the earth shelters life.

Geophysics which entails all portions of the physics of the earth incorporates the utilisation of physical principles and quantitative measurements in order to study the earth interior, its space as well as the atmosphere. Investigation of these measurements can uncover how the earth interior varies vertically and horizontally and the analysis which review important information on the geological structures (Bonde*et al.*,2014). This discovery show scientist that the earth subsurface is divided into three sections the crust, mantle and core. The crust being the upper rigid part of the lithosphere, it is an extremely thin layer of rock that makes up the outermost solid shell of our planet. In relative terms its thickness is like that of apple skin, the base of which is defined by a prominent seismic discontinuity, the mohorovicic discontinuity. The crust is said to be divided into three crustal, the ocean, transition and the continental crust. One of the important of geophysical method is the study of the earth crust in cases of tectonics.

1.2 Crustal Thickness

The distance between the earth surface and moho is crustal thickness. The limit can be controlled by isostatic/gravimetric and seismic strategies. Significant numbers of isostatic speculations, gravimetric and seismic models exist for assessing the crustal thickness (Nafiz*et al.*, 2008). The benefit of utilising an isostatic/gravimetric model to decide the crustal thickness is the uniform scope and generally point by point determination of the presently accessible worldwide geo potential models and satellite information. Crustal thickness is a meticulous parameter for understanding the process of continental rifting and break up. There is need to study crustal thickness in Nigeria since very little portion is known about the structure of the sedimentary basins as it relates to the geosciences development of key tectonic features, such as the west Africa passive margin where some southern part of Nigeria are located (Akpan*et al*.,2015). Some southern part of Nigeria like the Niger delta and Anambra basin is a geographical feature which is the largest wetland and it keeps up the third largest drainage sedimentary basin in Africa. Due to its amazingly oil well and mineral resources. Seismic measurement of crustal thickness is widely used spaced interval and expensive (Huismans & Beaumonth, 2011; Sutra & Manatschal, 2012). The distance between the earth surface and the moho (Nafiz*et al.*, 2008), the interface can be imaged accurately through deep seismic profiling, but for economic considerations make gravity modelling more practical approach for mapping crustal thickness.

1.3 Mohorovicic Discontinuity

This is the boundary between the earth crust and its mantle. The Mohorovicic discontinuity marks the lower limit of earth crust. The Moho separates both the oceanic crust and continental crust from underlying mantle. Mohorovicic was able to use his discovery to study thickness variations of the crust. He discovered that the oceanic crust

has a relatively uniform thickness while continental crust is thickest under mountain ranges and thinner under plains (Matrinic, 1994).

1.4 Gravity Method

Gravity is a potential field; it is a force that acts at a distance which involves the measuring of the acceleration due to the earth gravitational field. The gravity surveying involves the measurement of the earth's gravitational field at particular areas on the earth surface to determine the location of the subsurface density variations which are caused by some rocks having more (or less) density than others, higher residual gravity values are found in rocks that are denser such as igneous and metamorphic rocks, while lower gravity values are found in the sedimentary rocks that are less dense. The density of sedimentary rocks increases with depth which is mainly due to compaction.

The gravity method is typically used for regional geological/geophysical studies, isostatic compensation studies and detection of subsurface cavities (archeo-geophysics), and in geodesy shape of the earth and other planets(Philip *et al*., 2002).

The gravity method is a relatively cheap, non-invasive, non-destructive remote sensing method. It is also passive that is no energy is needed to be put into the ground in order to acquire data; making the gravity method a well suited geophysical method for geophysicist. Data from gravity measurements are relevant in exploring resources and studying the crust. There is need to account for non- geological contributions to the gravity field that obscures actual anomalies and these unwanted effects should be effectively annihilated. In this research work gravity method will be applied to determine the crustal thickness of some southern part of Nigeria, using Bouguer gravity data.

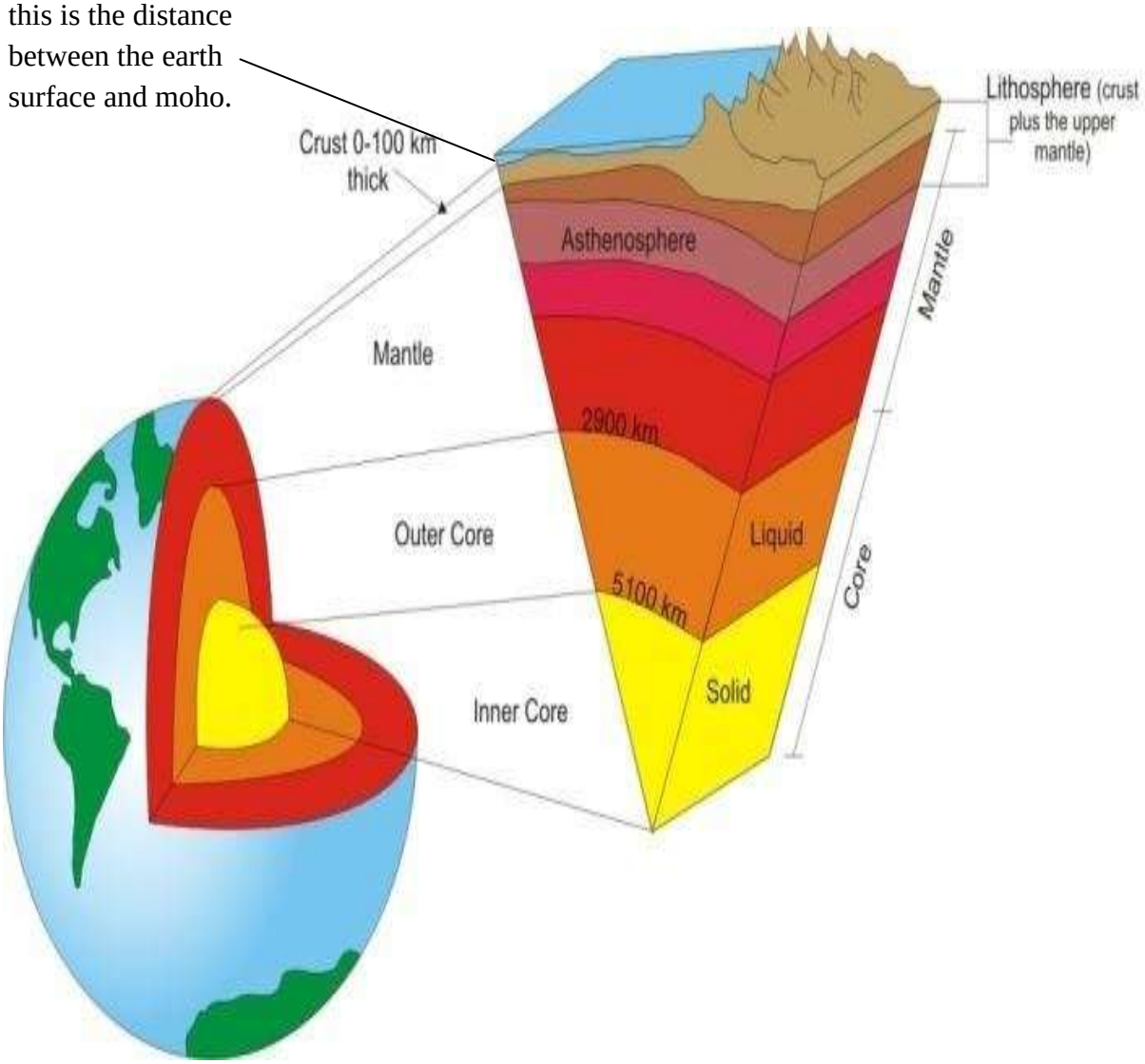

Figure 1.1: Shows the image of the earth's internal structure showing the crustal thickness (Modified after Ozawa, 2011*).*

The distance 0 - 100 km which is the distance between the earth surface and moho is the crustal thickness. Figure 1.2 shows the map of the crustal thickness of Africa, the crust thickness for most of the terrains appear to be similar. The average crust thickness for the entire continent is 0 -100 km and the average depth for most terrains is within the same range, from the map the average crustal thickness of Nigeria is between 40 and 50 km (Modified after Ozawa, 2011*).*

There is need to monitor the tectonic stability of the study region by examining its crustal thickness. The empirical relations, spectral analysis method and 2-D Modelling technique are used on Bouguer Gravity data to estimate the crustal thickness of some parts of the southern Nigeria.

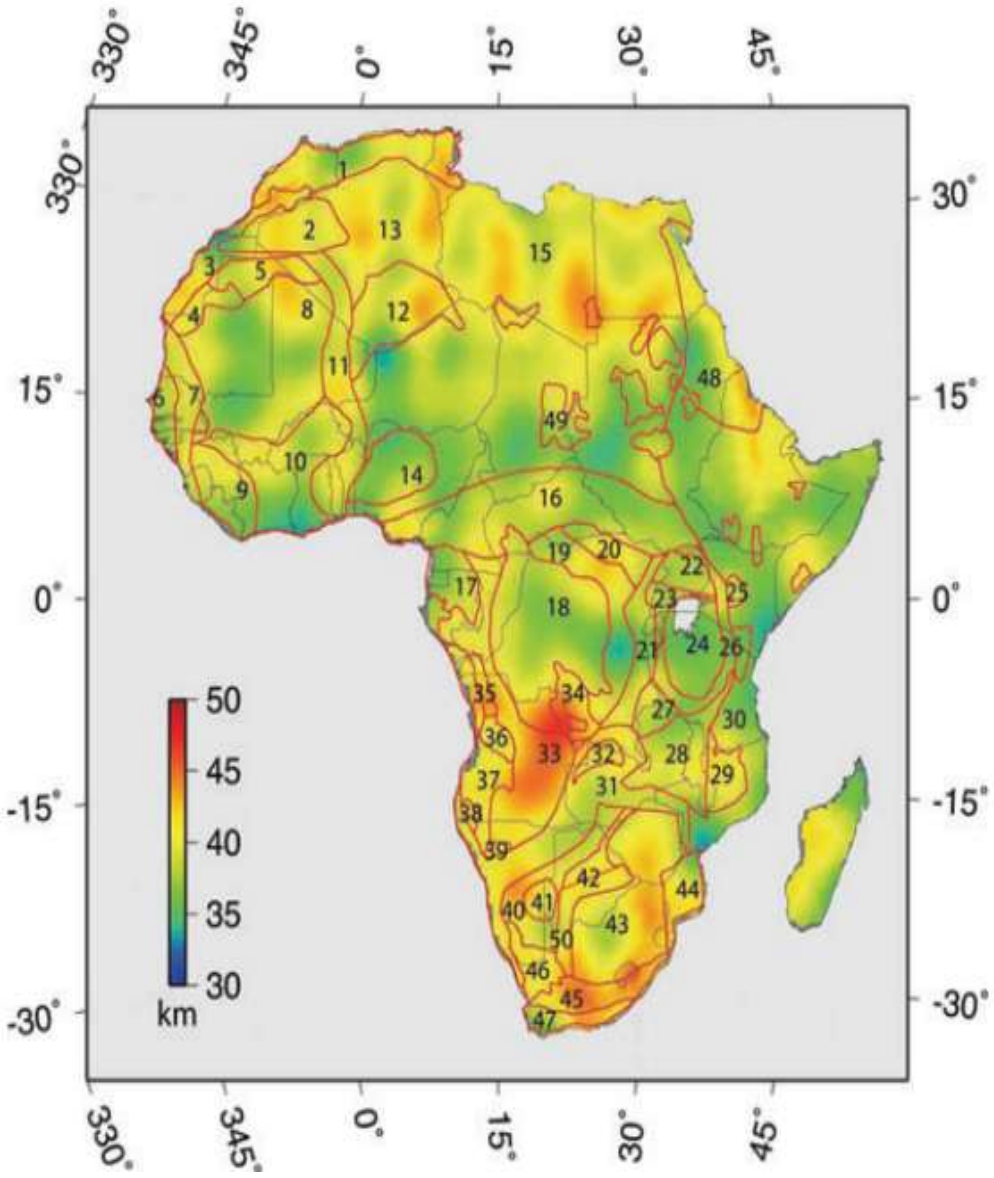

Figure 1.2 Crustal Thickness Map of Africa (Begg*et al.*, 2009).

The Crustal thickness Map of Africa was developed as a new continental scale Crustal model for Africa by modelling the free-air gravity anomaly EIGEN-GL04C, Crustal Thickness is estimated using 3-D Euler deconvolution, a method that does not rely on a priori depth and density constraints. the result is in Good agreement which is 5 km of seismically determined Crustal Depth estimates from across continent, except for narrow tectonic regions, such as rift valleys and areas where seismic velocity models of the crust indicate a gradational Crustal. The results show that Crustal Thickness is fairly

homogeneous, with an average Crustal Thickness for the whole continent of 39 ± 2(SD) km. The average Crustal depth for most terrains is within 5 km of the continental average, and there is little variability between terrains of different age. The average Crustal Thickness most of the location in Africa is from 30 km - 40 km respectively. Crustal Thickness in sedimentary basins across northern and central Africa varies between 33 km and 36 km. Though comparison with global averages for similar - aged terrains, the finding shows that Africa Crustal Thickness does not deviate significantly from the Thickness of crust in other parts of the world (Begg*et al.,* 2009).

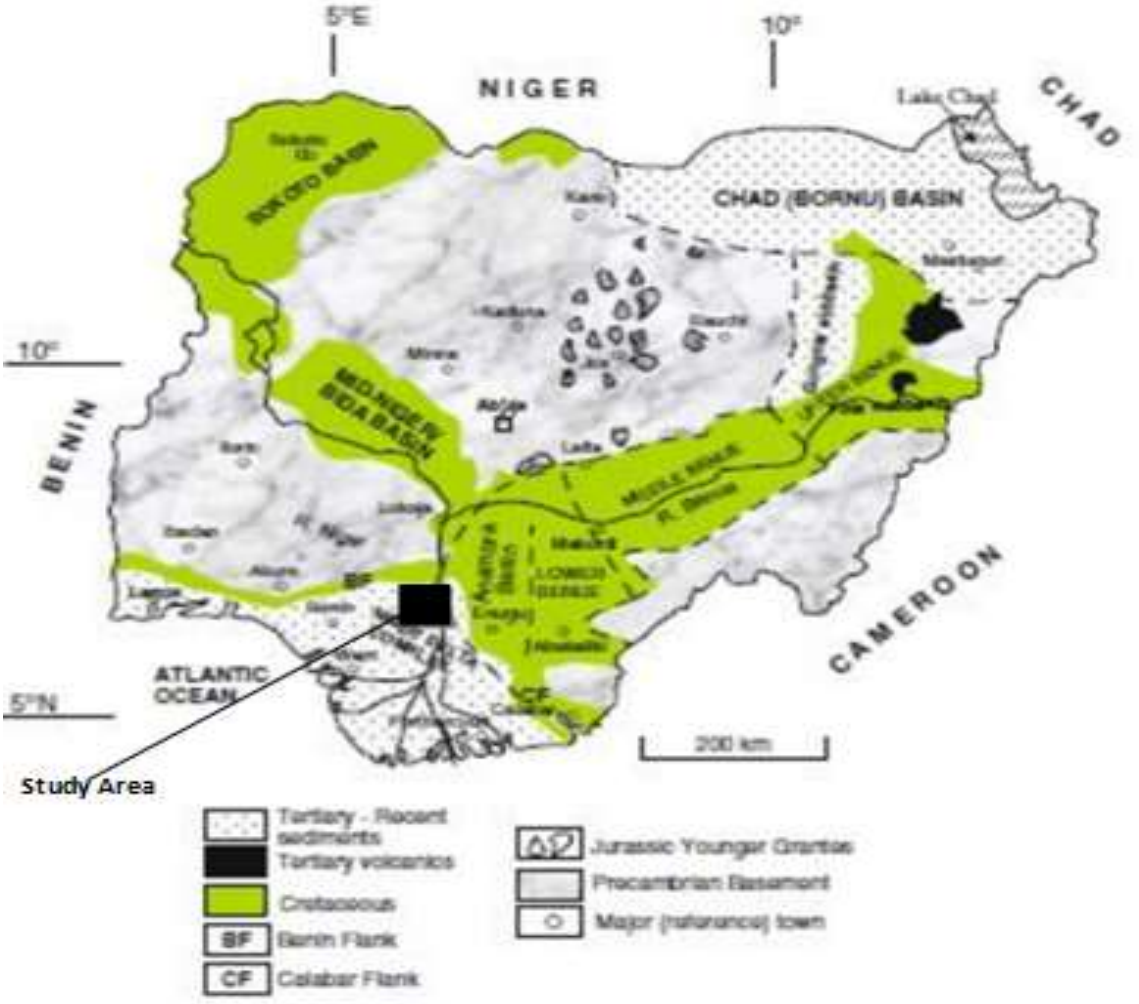

Figure 1.3 The Generalised Geology map of Nigeria showing the location of the study area

The geological map of Nigeria of the study area lies within the crystalline basement complex of Nigeria (Adapted from Obaje, 2009). The land scale consists old hard rocks and domeshaped hills which rise gently across the town. The area covered by Precambrian igneous and metamorphic rocks which extend over state and large quantities of quartzites are found inset too. It is not particularly rich in prominent materials but endowed with a wide distribution sedimentary and metamorphic group of materials, namely: marble, Red clay, Sand, Gravel, Granite, Limestone and Tac. The climate is equatorial, notably with dry and wet seasons with relatively high humidity, the average daily temperature ranges between $25^0C\ and\ 35^0$C across the year.

1.5 Location and Extent of the Study Area

The study area is geographically located in the southern part of Nigeria. It lies between longitude 5.0° E to 8.5° E and latitude 5.0° N to 7.5° N in some southern part of Nigeria. Those areas are situated in the apex of the Gulf of Guinea on the west coast Africa. The structural disposition of those parts of southern Nigeria has been documented by several researchers and workers. Some part of this study area was formed by the build-up of sediments over crustal tract developed by rift faulting during the Precambrian with outlines controlled by deep seated faults associated with rifting. Rifting diminished in the late cretaceous and gravity tectonism became the primary deformational process after the rifting phase in some southern Nigeria.

The study area is one of the important areas in southern Nigeria due to the presence of abundant economic and mineral resources. It is fastest becoming an industrial area with lots of economic activities due to rural-urban discovery in the area of mineral and hydrocarbon resources. Some of the towns within the study area are Benin City, Agbor,

Onitsha, Ekpoma, Auchi, Warri, Kwale, Agbede, Owa, Sapele, Awka, Asaba, Burutu, Port Harcourt, Aba and Abakaliki.

1.6 Climate

The climate is the tropical inland sort with interchanging wet and dry seasons of varying duration. The seasons correspond to the period's dominance of the wet tropical inland air masses. The seasonal distribution of rainfall follows the direction of the inter-tropical divergence (ITD) and varies almost proportionally with distance from the coast. The wet season occur within six months from April to October while the dry season continues from November to March. There is generally a break in rainfall in August precisely, this area has the yearly mean precipitation ranging from 500 to 2780 mm. about 90% of rain falls in seven mouths of April to October. The mean yearly temperature ranges between 24^0C -33^0C, the mean number of hours of sunlight is 5-7 depending on the season. The rate of evaporation is high being the continental interior. The relative humidity is between 60% - 70% per annum depending on the season of the year (dry or rainy). The mean atmospheric pressure is about 1013mb (Ozawa , 2011).

1.7 Vegetation and Land use of the Study Area

The normal vegetation of the study area is the high forest zones, which comprises of numerous assortments of mangrove and rain forest where trees like palms, hardwood timbers are found. The swampy surfaces are the domain of the fresh water swamp forests in the interior and the units of mangrove vegetation near the coast. The sand ridges are characterized by savannah and stunted rain forests. Most areas of the region, the natural vegetation has been very much degraded as a result of human activities. Human interference has led to the presence of plantations for rubber and oil palm as well as forest reserves, extensive exploitation of forest resources; cattle grazing and

persistent bush fires have combined to reduce area of forest vegetation to derived degraded savannah. An important aspect of vegetation of the region is the dominances of tree crops.

1.8 Statement of Research

The crustal thickness of the earth varies from one place to another. It is very important to determine the crustal thickness of the crust, which is the rigid part of the earth. If the crustal thickness of an area is high, it gives an indication of the stability of that area, in terms of tectonic movement. Therefore, the occurrence of natural earthquakes in Nigeria is uncommon because of its location on a passive continental margin with the nearest active plate boundaries lying very far away at the mid-Atlantic ridge; hence the country is referred to as being aseismic (Yakubu *et al.,* 2014). However, recent seismic activities in some parts of the West African sub-region have shown that the West African region may be unstable. Countries like Congo andChad one of Nigeria's not too distant neighbour in 2015 to 2021, Kaduna State, Nigeria in 2016 and Abuja FCT in 2018 have experienced tectonic instability in form of earth's tremor. For this reason, there is need to continuously monitor the crust and the upper mantle to ascertain the tectonic stability of various regions of the country. Therefore this research work is set to apply gravity data method in order to determine the crustal thickness of some part of southern Nigeria which is one of the most important economics areas of the country so as to predict the tectonic stability of the study area.

1.9 Aim and Objective of the Study

The aim of the study is to investigate the distance between the earth surface and moho depth (crustal thickness) and to predict the tectonic stability of some parts of southern Nigeria using bouguer gravity data.

The Objectives of the Study are to:

i. determine the crustal thickness of the area mathematically using empirical relations.
ii. estimate the crustal thickness of the study area using spectral depth analysis method.
iii. using(2-D) dimensional modelling technique to determine the crustal thickness of the study area.
iv. predict the tectonic stability of the study area.

1.10 Scope of the Study

The study is limited to gravity method by choice since the data needed for the study is cheaper and available within the study area.

1.11 Significance of the study

The crustal thickness shows an elevated area which might be prone to earthquake activities and molten magma mobility (mobile zone), so this study is important for tectonic studies and understanding of continental rifting processes. The study of crustal thickness and stability status has been one of the interesting studies of geophysicists in the world as its accurate recognition is important in finding out the tectonic movement of a place. Since the earth is a save place that shelter life, it's necessary to study its stability.

CHAPTER TWO

2.0 LITERATURE REVIEW

2.1 Geology of the Study Area

The study areas are foun1d in Nigeria (Figure 2.1) which is located in the zenith of the Gulf of Guinea on the passive continental margin close to the western coast of Africa at the culmination of the Benue Trough and alongside the basin being one of the most prolific hydrocarbon and minerals provinces in the world (Corredor*et al.,* 2005).The Anambra basin and Abakaliki high to the north, the Cameroun volcanic line to the east, the Dahomey Embayment to the west and the Gulf of Guinea to the south define the boundaries of the southern Nigeria. It is a coastal sedimentary basin which has experienced three depositional cycles. At initial stage, it started with a marine incursion in the middle cretaceous and was concluded by the mild folding phase in Santonian time.The study area is geographically located in the southern part of Nigeria. It lies between longitude 5.0° E to 8.5° E and latitude 5.0° N to 7.5° N in southern part of Nigeria.

The second involved the growth of a proto-Niger delta during the late Cretaceous and terminated in a major Paleocene marine transgression. The third cycle, from Eocene to Recent, marked the nonstop development of the main southern Nigeria. Thickness of the sediments in some southern Nigeria averages 12 km covering a total area of about 140,000 km^2 (Bilotti*et al*., 2005).Triple Lithostratigraphic subdivision is found in some southern Nigeria subsurface, comprising Agbada, Akata and Benin Formation, the upper Benin made up of sand, and prevailing unit alternating sandstone and shale named the Agbada Formation and a lower Akata Formation made of shale. These three units stretch out over some southern parts of Nigeria and ranges in age from early tertiary to recent.

They are related to the present outcrops and environments of deposition, other geologic formations of some southern Nigeria encountered in the basin also includes: Agbor, Onitsha, Ekpoma, Owa, Warri, Kwale, Burutu, Sapele, Agbede, Aba, Auchi, Abakaliki, Port Harcourt,Asaba, Awka, Benin city,Imo,Agbani sand stone/Awgu shale formation Subsurface structures are described as resulting from movement under the influence of gravity and their distribution is related to growth stage of the data. Rollover anticline in front of growth fault from the main objectives of oil exploration, the hydrocarbons being found in sandstone reservoir of the Agbada Formation (Tegbe&Akaegbobi, 2000).

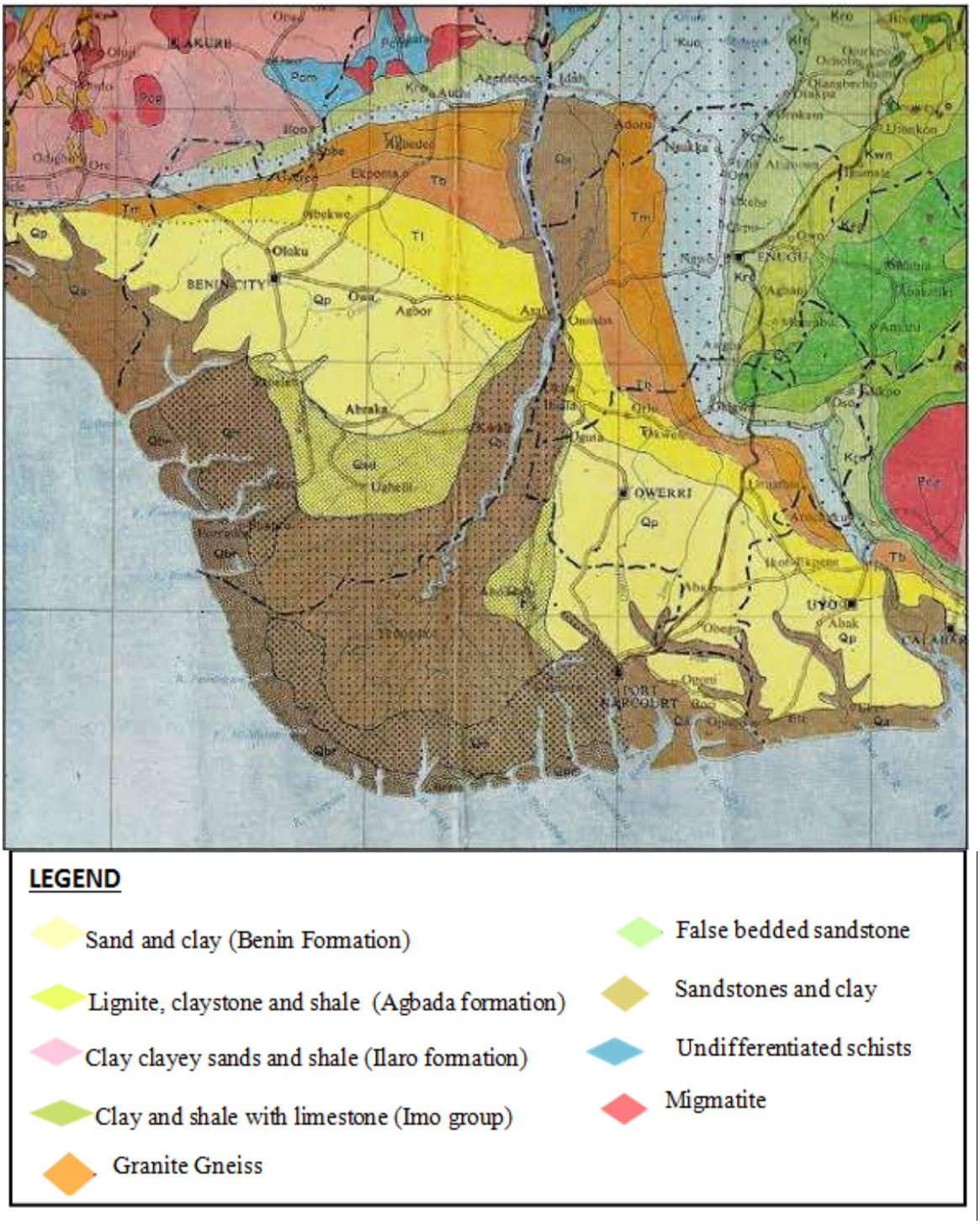

Figure 2.2 The Location map of the study area (Extracted from Geology map of Nigeria obtained from Nigeria Geological Survey Agency NGSA).

The lithostatigraphic subdivision is found in some southern Nigeria subsurface, the southern parts of Nigeria with an area of about 256,000 km^2 and was initially build over an older trangressive paleocene prodelta. The construction proceeded in discrete mini basins ranging in tectonic configuration from extensional, through translational to compressional toe-thrust regions. Outcropping unit of the southern parts like the Imo formation and Anike group consisting of the Anike, Nanka, Nsugbe and Ogwashi-Asaba formations. The subsurface Lithostratigraphic units are the major transgressive marine Akata Shales, the petroliferous paralic Agbada Formation, and the continental Basin Sands. Oil reserves are about 40 billion barrels, with gas reserves of over 40 trillion cubic feet.

2.2 Review of Geophysical Literatures

Gravity method due to its significance is common approach to determine crustal thickness around the world (Nafiz*et al*., 2008). Several studies have been made by cognizant scientists to assess the crustal thickness of different regions of the world using several geophysical method and some are outlined as follows:

Ekwok*et al*. (2021) worked in the Calabar Flank using High-resolution potential field data. The study was aimed at mapping the tectono-sedimentary framework, and determining depth to basement of the area. The smooth magnetic/gravity curves obtained from the 2-D models reflect thick sedimentary series and deeply buried basement rocks with no significant post rift tectonic events. Also, the main basement structures (that is, the horst and graben) and associated normal fault blocks of the Calabar Flank were properly delineated. Thickness of sedimentary series in some locations in the study area was observed to be ~7000 m, and the stacked models showed that the sediment thicknesses dip gently in the south western direction. The models,

particularly the joint gravity and magnetic model, validate the extant conceptual geological model for the area.

Okpoli & Akingboye (2020) in application of Airborne Gravimetry Data for Litho-Structural and Depth Characterization of Precambrian Basement Rock. The study entails the detailed analyses of high-resolution gravimetry dataset using enhancement techniques for characterising and delineating the locations, edges/boundaries, trends, and depths of lithostructural features around Precambrian basement complex of Igabi region, Northwestern Nigeria with a view of evaluating the structural architectures that harbor mineralisation in the study area. The analysed results of the bouguer anomaly and residual maps of study area showed the distribution of the gravity anomalies and magnitudes of the concealed structures based on the observed low to very high gravity anomalies. Bouguer anomalies around Igabi area ranged between -67.77 to -53.34 mGal reflecting the density variations within bedrock. The upward continued bouguer anomaly maps at distance 500 m, 1 km, 2 km, 3 km, and 4 km revealed the variations of the deep-seated basement rocks, the structures and the concealed anomalous bodies with general regional trends in NW-SE, E-W, and NE-SW directions. The bouguer analytic signal and its superimposed maps further revealed that areas with low amplitude signals may be associated with migmatites, schists, less dense felsic rocks (porphyritic granites) and fractures, and areas of high amplitude signals may be associated with denser biotite granitic and gneissic rocks. In addition, the second vertical derivative and tilt derivative maps clearly revealed the density of shallow basement rocks and near circular closures anomalies associated with fractures within the granitic rocks. Spectral analysis suggests depth to gravity sources range between 0.3 km and 0.67 km for shallow, 0.90 km to 0.97 km for intermediate and 1.5 km to 1.86 km for deep sources while Euler sources depths ranged from 2059 m. Based on the calculated bouguer anomalies such as

variation in rocks densities, different structures and varying trends of litho-structures in with subsurface depth may have suggested intense deformation of the Basement rocks with varying tectonic framework in the study area over time.

Nwankwo&Ene (2020) Structural Investigation of Udi LGA of Enugu State, South Eastern Nigeria Using High Resolution Bouguer Gravity and Landsat Data. This was achieved by delineating the regional from the residual, determining the lateral and sedimentary thicknesses of causative structures with their lateral boundaries and corresponding lineaments. Regional-residual separation was employed on the aerogravity dataset while Georeferencing and creation of new coordinate system was undertaken on the Landsat data. Causative sources with short and long wavelength trending in the NE-SW, NNE-SSW, E-W, WNW-ESE, N-S and NW-SE directions were found to exist within the study area as qualitative analysis was applied on the aerogravity and landsat data. The NE-SW and NW-SE trends are possible oil and gas rich belt within the area. Quantitatively, two depth source models D_1 and D_2 were identified. D_1 depicting depth to deeply seated sources varies from 0.00071 to 0.0044 km with true thickness of 0.01 km. The shallow related sources expressed using D_2 lies between 0.0014 to 0.0034 km with true value of 0.0005 km. If other conditions like structural features and depth parameters are met, a true sedimentary thickness of 0.01 km shows that the area will encourage mineral and water exploration rather than hydrocarbon exploration.

Okwesili et al. (2020) in geophysical survey of aero gravity anomalies over Lafia and Akiri regions of middle Benue trough, Nigeria were investigated with the objectives to determine the thickness of the sedimentary basin, establish the basement topography and density contrasts which will give information about variation of geological structures. Two sheets of digital airborne gravity data were used for the study. Power

Spectrum and Source parameter imaging (SPI) techniques were employed in the quantitative interpretation. The Bouguer anomaly of the study area varied from -66.0 mGal to 28.4 mGal while the residual Bouguer anomaly of the study area varies from -30.5 mGal to 27.7 mGal. The result from the Power Spectrum analysis showed that the maximum estimated basement depth obtained is 5.6 km. Oasis Montaj software was employed using the first vertical derivatives and horizontal gradient in computing the SPI depth of the gravity data. The SPI gave depth values ranging from -983.2 to -5572.6 m for shallow and deep lying gravity anomalous bodies. The results obtained from Power Spectrum technique closely agrees with that of the source parameter imaging.

Abraham *et al*. (2020) in integrated geophysical investigation of recent earth tremors in Nigeria using aeromagnetic and gravity data to investigate crustal depths subsurface geologic faults and fractures and the overall subsurface interaction at Mpape region and environs. Estimated depths to the bottom of magnetic crust (basal depths) range between 11.0 and 11.4 km at the Mpape region and decrease further southward towards Guabe town. This signifies the depth range of the active crust within the region. Comparative deeper basal depths (15.0–16.2 km) were obtained at locations farther from Mpape–Guabe towns at Nasarawa, Rubochi, and Fuka regions, showing a more stable region away from Mpape region. Computed Moho depths from gravity data show deeper depths at the Mpape region (~ 34.1 km) suggesting that the active crust exists in the upper crust. Two-dimensional modeling analysis along a profile taken across the Mpape region shows a conspicuous subsurface basement intrusion at the Mpape region with deep faults and fractures reaching depths of 7–14 km. Shallow basal depths at the Mpape region resulting from significant subsurface intrusion and concentrated

subsurface faults at the intruded region may be responsible for the instability of the Mpape region. The most affected area is located within the Mpape–Guabe towns.

Nyakundi *et al*. (2020) carried out Gravity survey at the Eburru area to estimate the source depth locations and delineate the fault boundaries using 3D Euler deconvolution. Gravity data was collected using CG-5 gravimeter. Gravity data reductions were done by applying drift correction, latitude correction, free air correction, Bouguer correction and terrain correction to the observed raw data to obtain complete bouguer anomaly (CBA). The CBA data was transferred to Oasis montaj software for Euler deconvolution processing. The 3D Euler deconvolution was carried out to determine and estimate the depth of the density bodies. Euler deconvolution locates the gravity anomaly source and estimates its depth from the gravity observation level. Euler deconvolution was preferred to other filtering methods in this study as solutions are only determined over identified analytic signal peaks, the window size varies according to anomaly size and the final solution involves only a few more precise depth estimates. The Euler deconvolution was performed using structural indices of 0.5, 1.0 and 2.0. Results from this analysis indicated that the CBA values in this study area range from gravity values of -272 mGal to -286 mGal and residual Bouguer anomaly amplitude range between -3 mGal and 3.4 mGal. The 0.5, 1.0 and 2.0 structural indices generated five solutions at depth range of 433 m - 2269 m, 801 m - 1433 m and 1170 m - 2246 m respectively occurring almost at the same locations on gravity highs. The deep structures were observed to occur in the northern part of the study area, and interpreted to be dense intruding masses likely to be trapped by the overlying cap rock at these depths. These could be geothermal heat sources that can be exploited to generate geothermal energy

Abraham*et al*. (2019) worked on Geothermal Energy Reconnaissance of Southeastern Nigeria from Analysis of Aeromagnetic and Gravity Data. The aim of locating and

mapping regions of shallow Curie point depths (CPDs), crustal thickness, and geologic structures supportive of a geothermal system. Result reveals deeper CPDs within central and southern regions of Okposi, Afikpo and Biase towns in an approximate range of 18.4 to 19.3 km. Shallow CPDs (9.8–17.4 km) have also been obtained within Obubra and Abakaliki regions. Estimated crustal thickness (Moho) ranges between 26.5 and 35.8 km. Part of the region with shallow CPD correlates with regions of shallow Moho depths, particularly in Abakaliki, and deeper Moho depths coincide with deeper CPD estimates at the Afikpo location. The estimated geothermal gradient and heat flow values range between 29.0 and 45.0 ºC and 52.2–101.5 mW/m2, respectively, and fall within values evaluated from deep wells drilled for oil exploration within the adjoining Anambra Basin region. This study recommends the regions with shallow depths for possible geothermal power plant location. Gravity data evaluations also reveal significant subsurface intrusions within Ugbodo, Obubra and Abakaliki locations of south eastern Nigeria.

Abdullahi *et al*. (2019) in Mapping magnetic lineaments and subsurface basement beneath parts of Lower Benue Trough (LBT), Nigeria: Insights from integrating gravity, magnetic and geologic data. Lineament analysis of the aeromagnetic data demonstrated four tectonic trends of the basement terrain. The lineaments are in the northeast to southwest (NE–SW), east, northeast to west, southwest (ENE–WSW), north to south (N–S), and east, southeast to west, northwest (ESE–WNW) directions. The NE–SW and ENE–WSW are the most dominant whereas the N–S and ESE–WNW are the minor trends. The estimated magnetic basement using spectral analysis varies between 3.5 and 5 km and the shallow magnetic sources (depth to top of intrusions) vary between 0.24 and 1.2 km. The sedimentary basin (5 km) is estimated using GPSO algorithm and Oasis Montaj (Geosoft).

Akiishi *et al*. (2019) in determination of hydrocarbon potentials in Masu area northeast Nigeria using forward and inverse modeling of aeromagnetic and aerogravity data covering Masu area, which lies within latitudes 12°00′ and 13°00′ North and longitudes 12°30′ and 14°00′ East in Nigerian sector of Chad Basin have been interpreted qualitatively and quantitatively. Regional-residual separation was carried out by applying polynomial fitting (first order), which was fitted by least square method. First order was used because it is the best regional fit for data as it reflected the available geological information of the area. The residual values of both magnetic and Bouguer anomalies obtained were used to produce the residual magnetic intensity and residual gravity maps respectively. These maps show intrusive basement rocks in the eastern part of Masu. The forward and inverse of aeromagnetic data modeling estimated basement depths for profiles P1 and P2 were 4300 and 1195 m, with respective magnetic susceptibility values of 0.0003 and 0.0250, which indicate minerals like limestone and marble. Similarly, the estimated basement depths from the forward and inverse of aerogravity data modeling are 6524 and 4312 m for P1 and P2 with density contrasts of 0.72 and 0.255 g/cm^3. The results from this work indicate that the area has some geologic features suitable for hydrocarbon and mineral deposits.

Okpoli & Akingboye (2019) work on application of high-resolution gravity data for litho-structural and depth characterisation around Igabi area, Northwestern Nigeria. Theaero gravity dataset was interpreted to delineate litho-structural architectures that could favour the exploitation of potential economic minerals. The distribution of the gravity anomalies over the area ranged from –67.77 to –53.34 mGal. The upward continued bouguer anomaly maps at distance 500 m, 1 km, 2 km, 3 km, and 4 km revealed the variations of anomalous bodies with general regional trends in NW-SE, E-W, and NE-SW directions. The superimposed analytic signal indicated low amplitude

signals for migmatites, schists, less dense felsic rocks (porphyritic granites) and fractures, while areas of high amplitude signals correlated with biotite granitic and gneissic rocks because of the denser mafic minerals in them. The second vertical derivative and tilt derivative maps revealed the anomaly patterns of shallow basement rocks and near circular closures anomalies that are associated with fractures within the granitic rocks. Spectral analysis suggested depth to gravity sources ranging between 0.3 km and 0.67 km for shallow, 0.90 km and 0.97 km for intermediate and 1.5 km to 1.86 km for deep sources, while Euler solution depths ranged from <1392.3 m to >2059 m. The results, therefore, suggested intense deformation of the basement rocks with tectonic framework suitable for mineralisation.

Balogun (2019) carried out preliminary interpretation of isostatic residual gravity anomalies within the central portion of the Equatorial Atlantic African region. Airy'sisostatic residual gravity anomaly map and profiles were interpreted for the central portion of the Equatorial Atlantic African region with a view to understanding the lithospheric dynamics, hence imminent vertical crustal movements and thus predict the future outlook of evolving landscape within the study area. In order to compute the isostatic residual gravity anomaly, the AIRYROOT algorithm of the United States Geological Survey was used and isostatic all overcompensated, undercompensated and completely compensated portions were identified on the isostatic residual gravity anomaly map and profiles. The Airy'sisostatic residual gravity anomaly map showed three distinct parts which were the oceanic south-western part characterized by negative isostatic residual gravity anomaly values (− 11 to − 200 mGal), the volcanic eastern and extreme north central parts characterized by positive isostatic residual gravity anomaly values (+ 10 to + 90 mGal) and the central part having a network of sedimentary basins, characterized by isostatic residual gravity anomaly values that approach zero (− 10 to

+ 9 mGal). It was discovered that the oceanic south-western part was isostatically overcompensated, the uplifted eastern part and the Younger Granite Province of the extreme northcentral part were undercompensated and the central part consisting of the Niger Delta, Benue Trough and the Mid-Niger (Nupe) Trough was completely compensated. It was consequently predicted that vertical uplift is imminent in the isostatically overcompensated oceanic region while subsidence is expected over the region of the eastern upland and the Younger Granite Province which were associated with isostatic under compensation. The sedimentary basins within the study area are expected to remain stable.

Ekpa *et al*. (2018) in investigation of gravity anomalies in parts of Niger Delta Region in Nigeria using aerogravity data with the objectives to determine the thickness of the sedimentary basin, establish the basement topography, density contrasts and the geological models which will give information about variation of geological structures. Four sheets of digital airborne gravity data were used for the study. Source parameter imaging (SPI), Standard Euler deconvolution and forward and inverse modelling techniques were employed in quantitative interpretation. The Bouguer anomaly of the study area varied from -20.0 to 37.7 mGal, while the residual Bouguer anomaly varied from -19.6 to 25.7 mGal. The SPI gave depth values ranging from -539.7 to -4276.0 m for shallow and deep lying gravity anomalous bodies. The windowed Euler-3D for Bouguer gravity result revealed the depth range of 1355.5 to -1518.1 m for structural index of one; 2384.5 to -3283.2 m for structural index of two and 2426.0 to -5011 m for structural index of three. The forward and inverse modelling gave the density values for the modelled profiles 1, 2, 3, 4 and 5 as 1.820, 2.410, 0.720, 2.310 and 2.100 gcm-3, respectively, with their respective depths of 3872, 4228, 4880, 3560 and 2527 m.

Mbah *et al*. (2017) in possible cause of gravity anomalies in parts of the Niger Delta Basin, Nigeria was investigated using three methods of gravity data interpretation; Euler-3D deconvolution, source parameter imaging (SPI) and forward and inverse modelling. The estimated depths from the interpretation techniques used show much similarity. Quantitatively, the results obtained from the SPI method showed a minimum to maximum depth of 1264.11 to 9354.57 m to the anomalous body. The results obtained from Euler-3D deconvolution method showed a depth range of 2136.40 to 9167.57 m to the anomalous body using a structural index of 3. The results from the forward and inverse modelling revealed a depth range of 793 to 7586 m to the anomalous body. Qualitatively, the gravity signatures in profiles 1, 2 and 3 possibly depict antiformal geologic features whereas the gravity signatures in profiles 4 and 5 possibly depict synformal features/basin geometries.

Alaneme & Okotete (2018) in critical evaluation of seismic activities in Africa and curtailment policies, evidences available show that most of the devastations are accentuated by tremor induced collapse of buildings and civil structures.

Ali & Suardi (2018) also revealed a depth to basement range between 0 to 10.7 km in the lower Niger Delta Basin which is similar to the depth range obtained in this research (1.3 to 9.4 km for SPC A, 3.1 to 9.4 km for Euler 3D deconvolution and 0.8 to 7.6 km for forward and inverse modelling).

Sunday &Samuel (2013) discriminated the regional from residual structures within the study area through aeromagnetic study. This was done in order to define thicker sedimentary section by subjecting the data into various geophysical techniques like tilt depth, Euler Deconvolution, Analytic signal, derivatives and 2D derivatives. Tectonic trends with strike direction of NE-SW, NW-SE and E-W directions were observed.

In order to examine the relationship between deep basement shape and size and the hydrocarbon target. (Okiwelu *et al.*, 2012) used airborne magnetic data covering Niger Delta area to investigate the relationship between deep basement architecture and hydrocarbon target. Varying basement structures which would have significant control on oil and gas within the Tertiary strata of the Niger Delta were established.

Aeromagnetic data covering parts of Imo River was used by Chikwendu & Diugo (2011) in identifying basement features associated within the basin and then deduced the influence of the basement features in hydrocarbon exploration by subjecting the data to various filtering actions. This art revealed tectonic features trending in the NE-SW direction.

Hospers (1965) studied the gravity field and structure of the Niger delta, Nigeria using gravity data. The interpreted data revealed the NE-SW and NW-SE trends as the mega tectonic framework of the Niger Delta. A combination of the NE-SW, E-W and N-S structures from the residual and enhanced maps resulting from the shear/wrench-fault tectonics involving the basement created faulting, fracturing, down warp and epeirogenic warping along zones of basement weakness. He concluded from his result that both horizontal and vertical movements are involved in wrench-fault system but the horizontal movement predominated.

Jorgense *et al.* (2004) observed from their results that small offsets in the basement structure can generate hydrocarbon traps by creating structural or stratigraphic traps in the overlying sediment. Using magnetic and gravity data He mapped the basement geology and compared it to know the oil and gas pool locations. The information from his study revealed clearly the association between magnetic patterns and known oil and gas pools. It is interesting to note that gravity and aeromagnetic methods applied

separately could not give robust results but integrating these methods will give detailed information about the subsurface and better delineation of subsurface structures.

It is pertinent to apply the combination of both so that the result may throw more light to the understanding of such investigation. (Ikumbur*et al.,* 2013) subjected the geophysical anomalies to both map and profile analysis using Discrete Fourier Transform method. The result of their study revealed two depth source models in the area; deeper sources with range of 2.81 to 3,24km and the shallower sources of range 0.45 to 1.49km. The deeper magnetic sources identified with crystalline basement, while the shallower magnetic sources could be associated to near surface magnetic sources. They also observed linear depression with sedimentary accumulation trending E-W and the average sedimentary thickness determined as 2.90km.

Ako *et al.* (2014) Work on gravity data, that the most promising area of hydrocarbon accumulation are the zones of structural lows, which are deeper than 3900ft (1300m) and signify the sub-basin in the southern parts and neighbouring basins such as Anambra basin and the Benue trough.

Gomez-Ortiz *et al.* (2005) applied spectral analysis method to gravity data of central Spain to investigate the crustal density structure. Power spectral analysis of the data set reveals the existence of two distinct layer segments. The slope of the shallowest depth segment (11.6km) correspond to the mean depth of the upper crust base and the depth given by the steepest slope (31.1km) correspond to the mean Moho depth.

Lefort & Agarwel (2002) analysed a complete gravity data set from France and part of the neighboring countries to compute the topography of the Moho undulation and obtain 33.5km which correspond to a mean Moho depth using spectral analysis techniques.

Udensi & Osazuwa (2002) performed a quantitative interpretation of the residual magnetic field over the Bida Basin using 2-D modelling. The technique reveals that the thickness of the basin varies from 0.2km to 4.63km. The width of the basin is not uniform, but the largest width of the basin is 160km while the shortest width of the basin is 87km. those width agree considerably with the geology. The area with the largest thickness of sediments (4.63km) is located in the North of Pategi and southeast of the basin had sedimentary thickness of 4.50km.

Bansal & Dimri (2001) presented a technique to estimate the depth to anomalous sources for scaling power spectra for long non-stationary gravity profiles. They tested power spectrum technique along a synthetic gravity profile and applied this technique to Jaipur- Raipuer Geo-transect in western and central India. The Geo-transect has been divided into four stationary parts. They interpreted four depth of deeper interfaces (37km, 32km, 29km and 31.5km) that could be the Moho depth using power spectral technique.

Nnange *et al*. (2000) carried out depths to density discontinuities beneath the Adamawa Plateau region, Central Africa, from spectral analyses of new and existing gravity data.New gravity data from the Adamawa Uplift region of Cameroon have been integrated with existing gravity data from central and western Africa to examine variations in crustal structure throughout the region. The new data reveal steep northeast-trending gradients in the Bouguer gravity anomalies that coincide with the Sanaga Fault Zone and the Foumban Shear Zone, both part of the Central African Shear Zone lying between the Adamawa Plateau and the Congo Craton. Four major density discontinuities in the lithosphere have been determined within the lithosphere beneath the Adamawa Uplift in central Cameroon using spectral analysis of gravity data: (1) 7–13 km; (2) 19–25 km; (3) 30–37 km; and (4) 75–149 km. The deepest density

discontinuities determined at 75–149 km depth range agree with the presence of an anomalous low velocity upper mantle structure at these depths deduced from earlier teleseismic delay time studies and gravity forward modelling. The 30–37 km depths agree with the Moho depth of 33 km obtained from a seismic refraction experiment in the region. The intermediate depth of 20 km obtained within region D may correspond to shallower Moho depth beneath parts of the Benue and Yola Rifts where seismic refraction data indicate a crustal thickness of ~ 23 km. The 19–20 km depths and 8–12 km depths estimated in boxes encompassing the Adamawa Plateau and Cameroon Volcanic Line may correspond to mid-crustal density contrasts associated with volcanic intrusions, as these depths are less than depths of 25 and 13 km, respectively, in the stable Congo Craton to the south.

Udensi (2000) carried out estimate of the Moho depth of the Minna Area using Bouguer Gravity Anomaly data obtained a Moho depth of maximum thickness of 46km at the deepest part of Minna Batholith using Empirical relation.

Poudjom Djomani*et al.* (1992) applied spectral analysis to Bouguer gravity data to estimate the depth to the major density contrast within the lithosphere of the Adamawa Plateau. A depth between 18km and 38km which corresponds to the crust-mantle interface was obtained. For the purpose of this research, structural evaluation will be carried out by integrating qualitative and quantitative analyses and interpretation of the residual bouguer gravity data

CHAPTER THREE

3.0 MATERIALS AND METHOD

3.1 Materials used for the study

The materials used for this study include the following:

(1) Gravity data covering areas such as some southern parts of Nigeria

(2) Hp Envy corei7 16inchs Laptop (3G RAM, 64 bits, 1.67 GHz)

(3) Computer software's

(i) Oasis Montaj version 6.4.2

(ii) Sulfer 13

(iii) Microsoft Excel software

(iv) Mat lab

3.1.1 Data acquisition

The study area – parts of Southern Nigeria is covered by sixteen Bouguer Anomaly maps in half – degree sheets. The maps obtained for the research work are onshore gravity data which covers an area of longitude 5.0^0E to 8.5^0E and latitude 5.0^0N to 7.5^0N.These maps were obtained from the department of physics, Federal University of Technology Minna. The Microsoft Excel, surfer 13, oasisMontaj and Matlab Geophysics software were used for the data analysis, processing and interpretation.

3.1.2 Research methodology

Bouguer gravity anomalies are necessary for determining crustal thickness, deducing the geological history of an area, and even for predicting future geological movements. It is also of great interest in tectonic studies (Udensi, 2000). The following procedures were carried out on Bouguer gravity data to obtain an estimate of the crustal thickness

for the study area as well as to ascertain the tectonic stability of the study area from the average crustal thickness determined.

3.1.3 Digitisation

The bouguer gravity (BG) map of the study area was digitised using picture of unknown estimated value that fall between known valuemethod to obtain data on grid layout to be used for qualitative interpolation. Digitisation is a process of converting information into a digital (discrete) format so that computers and many devices with computer capacity can process.

Digitization is not a trivial process since a host of potential pitfalls are lurking within this simple step. Nothing is more important since improperly recorded digital data can be totally worthless or completely misleading. And once the data have been improperly recorded digitally, correct data cannot be recovered. The latitude and longitude position must be added to the data showing its position when imputing it into the system. For example a data to be imputed into a computer system must be represented as (4, 2, 7. 0). This means longitude 4, latitude 2, Data 7.0.

The entire available bouguer gravity anomaly map will be grided at an interval of 10 km as gridding at smaller intervals may introduce aliasing (Noise) since the area is a sedimentary terrain and also, crustal thickness is a regional feature and as such does not vary rapidly as most surface features. The data from each digitised map is recorded in a coding sheet which contains the longitude, latitude and the bouguer gravity anomaly data (BG).

3.1.4 Gridding

Gridding is the first step in the data processing which interpolates the bouguers anomaly values of the data base to a square grid. The term grid refers to the files that contain location (x,y) and data (z) gravity observation values, which was interpolated to create a regular and smoothly sampled representation of the locations and data. The interpolation methods of (x,y and z) data within Geosoft oasis Montaj software are Bi-directional, Minimum curvature and gridding.

For this research work, the Bi-Directional Gridding was used as it interpolates the (x,y,z) data by fitting a two dimensional surface to the (x,y,z) data, in the case the curvature of surface is minimised.

3.1.5 Contouring

Contours are one of several common methods use to denote elevation or altitude and depths on maps. From the contours, a sense of the general terrain can be determined. Contour maps are topographical maps on which the shape of the land surface is shown by contour lines which joins point of equal elevation about a given level. These maps are used to show the below ground surface of geologic strata, fault surfaces (especially low angle thrust faults) and unconformities. These contour maps are the bases of the gravity interpolation before the development of the computer programs. Software such as sulfer 13 produces this contour.

Nowadays, the gravity data is displayed as colour maps, where the colour represent different gravity anomaly from high to low within the gravity map using advance Geosoft software like the oasis Montaj. The oasis Montaj is a program written to pick data points row by row, calculate the longitude and latitude using base values already supplied and produces the coloured map of the bouguer gravity data of the study area

with a contour interval of 5milligals. Therefore, at this stage, the gravity grid produced using the Bi-directional gridding is displayed in coloured shaded grid.

3.2 Theory of the study

The underlying support of the gravity survey methods is Newton's law of gravitation which states that the force of attraction F between two masses m_1 and m_2, whose dimensions are small with respect to the distance r between them, is given by Newton. Newton proposed a theory known as the Newton's gravitational law on which this study is based. The Law states that "Every particle in the universe attracts every other particle with a force directly proportional to the product of their masses and inversely proportional to the square of the distance between them". If m_1 and m_2 are the masses of two particles separated by distance r, then the gravitational force of attraction between them is given as:

$$F = \frac{Gm_1m_2}{r^2} \tag{3.1}$$

where G =universal gravitational constant (6.67 x 10^{11} Nm^2Kg^2) (Philip *et al.*, 2002)

Considering the gravitational attraction of a spherical, non-rotating homogenous earth of mass M and radius R on a small mass m on its surface. It is relatively simple to show that the mass of a sphere acts as though it were concentrated at the centre of the sphere and by substitution in equation

$$F = \frac{GM}{R^2}m = mg \tag{3.2}$$

Force is related to mass by acceleration and the term $g = GM/R^2$ is known as the gravitational acceleration or simply gravity.

The gravitational field is most usefully defined in terms of the gravitational potential U

$$U = \frac{GM}{r} \tag{3.3}$$

Whereas the gravitational acceleration g is a vector quantity having both magnitude and direction (vertically downwards), the gravitational potential U is a scalar having magnitude only. The first derivative of U in any direction gives the component of gravity in that direction. Consequently, a potential field approach provides computational flexibility. Equipotential surfaces can be defined on which U is constant. The sea level surface is the most easily recognised equipotential surface, which is everywhere potential, that is at right angles to the direction of gravity (Philip *et al*., 2002).

3.2.1 Theoretical gravity

Theoretical gravity is a value of the true effective or clearly visible gravity on Earth's surface by means of mathematical model representing (a physical method) Earth. The formula for computing the theoretical gravity is referred to as the International Gravity Formula. The first formula was proposed in 1930 by the international association of Geodesy.

$g(\phi)=g_e[1 + A\sin^2(\phi) – B\sin^2(2\phi)]$(3.4)

where

$g(\phi)$ = gravity as a function of the geographic latitude

ϕ = geographic latitude of the position whose gravity is to be determined

g_e = The gravity at the equator

A and B = parameters that must be selected to produce a good global fit to true gravity

3.2.2 Observed gravity

The observed gravity reading is obtained from the gravity survey which reflects the gravitational field due to all masses in the earth and the effect of the earth's rotation. It is also the gravity readings observed at each gravity station after corrections have been applied for instrument drift and Earth tides

3.2.3 Gravity reductions

The interpretation of potential field anomalies for example gravity is naturally unclear. The unclear arises because any given anomaly could be brought on by a vast number of possible sources. The measurement of an absolute value of gravity is difficult and requires complex apparatus and a lengthy period of observation and rigorous reductions or corrections. The measurement of relative values of gravity, that is the differences of gravity between locations is simpler and is the standard procedure in gravity surveying. Absolute gravity at survey stations are obtained by reference to base stations at which the absolute values of gravity have been determined by reference to sites of absolute gravity measurements. (Philip *et al*., 2002)

It is necessary to make many corrections to the raw meter readings to obtain the gravity anomalies that are the target of a survey. This is because geologically uninteresting effects are significant and must be removed. Before the results of a gravity survey can be interpreted, it is necessary to correct for all variations in the earth's gravitational field which do not result from the differences of density in the underlying rocks. This is known as gravity reduction or reduction to the geoid, as sea-level is usually the most convenient datum level.

The geoid is an equipotential surface corresponding to mean sea level. On land it corresponds to the level that water would reach in canals connecting the seas. The geoid

is a conceptual surface, which is warped due to absence or presence of attracting material. It is warped up on land and down at sea.

3.2.4 Drift correction

Gravimeters are instrument used for taking gravity readings as it detects gravity changes within a region. As with all man-made instruments, gravimeters are not without shortcomings. The shortcoming of gravimeters is the phenomenon of drift. (Philip *et al*., 2002)

Drift refers to gradual change in reading with time observable when the instrument is left at a fixed location. Instrument drift in gravimeter is monitored by repeated meter readings at a fixed location for example the laboratory within a time frame to determine if the gravimeter is fit to be used in the field by ascertaining the linearity of the gravimeter when the meter readings taken is plotted against time. If linear for most hours of the day, the gravimeter is said to be fit to be used in field.

On field, Gravity readings taken are usually started on points of known gravity relative to the geoid and to end a series of measurements within hours on the same or another point with known gravity. These standard points are known as Base Stations or Control Stations.

These measurements taken with gravimeter on the base stations (say A and B) are taken in the form A ⟶ B ⟶ AB ⟶

In plotting the base tie plot as shown in Figure 3.1 below.

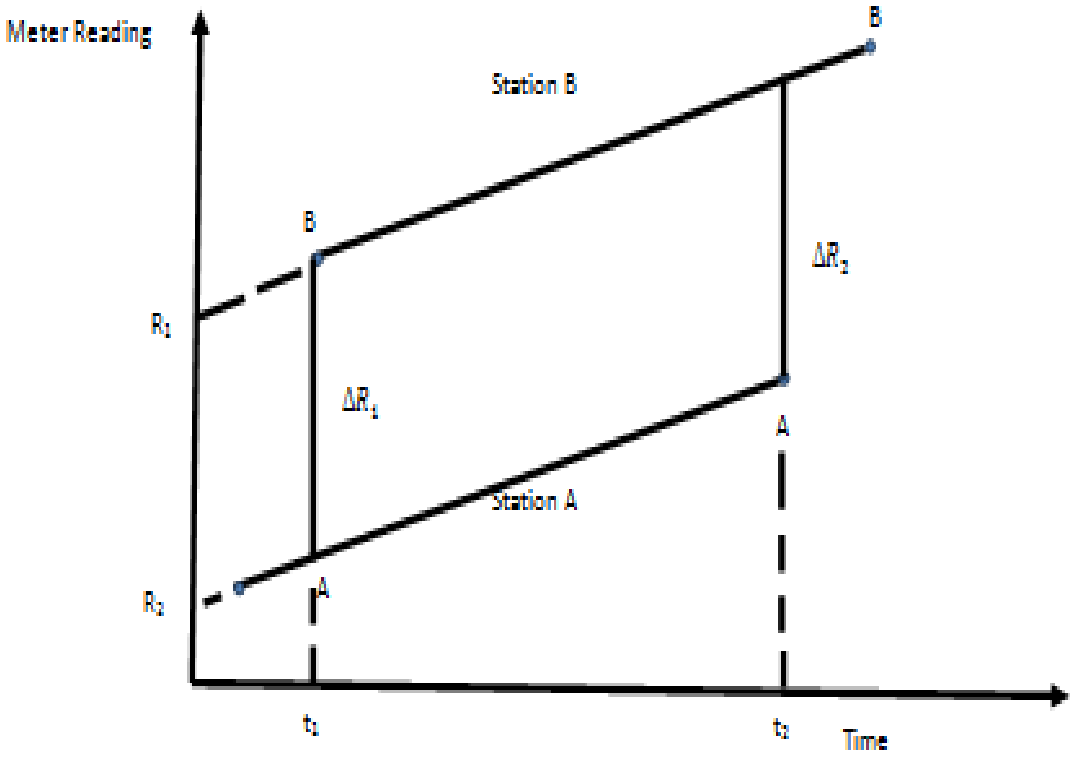

Figure 3.1: Base Tie Plot for Two Base Stations A and B

Meter reading from the base stations is plotted as a function of time and the difference determined. By so doing, instrumental drift, uncompensated temperature effects and tidal effect on gravity data would have been corrected for after the application of equation 3.4, 3.5, 3.6. Using the base tie plot ABAB in Figure 3.1, Drift ∇ can be calculated as follows:

$$\Delta R = \frac{\Delta R_1 + \Delta R_2}{2} \tag{3.4}$$

$$\nabla = \frac{(R_1 - R_2) - \Delta R}{t_2 - t_1} \tag{3.5}$$

Applying the drift∇ to carry out the drift correction, we have that

$$g_{obs} = g_1 + k\,(R_1 - R_s) + \nabla(t_s - t_1) \tag{3.6}$$

where:

g_{obs}=observed gravity of each detail station

g_1=absolute gravity for reference base station

k = instrument constant

R_1 = meter reading for reference base station

R_s= meter reading for each detail station

∇= drift

t_s= measurement time at each detail station

t_1 = measurement time at reference base station (Telford *et al*., 2001)

3.2.5 Latitude correction

Gravity varies with latitude because of the non-spherical shape of the Earth and because the angular velocity of a point on the earth's surface decreases from a maximum at the equator to zero at the poles. The centripetal acceleration generated by this rotation has a negative radial component that consequently causes gravity to decrease from pole to equator. The true shape of the Earth is an oblate spheroid or polar flattened ellipsoid whose difference in equatorial and polar radii is some 21 km. Consequently, points near the equator are farther from the centre of mass of the Earth than those near the poles, causing gravity to increase from the equator to the poles.

The amplitude of this effect is reduced by the differing subsurface mass distributions resulting from the equatorial bulge, the mass underlying equatorial regions being greater than that underlying Polar Regions. The net effect of these various factors is that gravity at the poles exceeds gravity at the equator by some 51 860 mGal, with the north–south

gravity gradient at latitude $\emptyset$ being 8.12 sin $2\emptyset$ mGalkm^{-1}.Clairaut's formula relates gravity to latitude on the reference spheroid according to an equation of the form:

$$g_{\emptyset} = g_0(1 + k_1 \sin^2\emptyset - k_2 \sin^2 2\emptyset) \quad (3.7)$$

where;

$g_{\emptyset}$= the predicted value of gravity at latitude$\emptyset$,

g_0= 9780327mGal is the value of gravity at the equator

k_1= 0.0053024

$k_2 = 0.0000058$

And bothk_1 and $k_2$are constants dependent on the shape and speed of rotation of the Earth. Hence equation becomes

$$g_{\emptyset} = 9780327\,(1 + 0.0053024\ \sin^2\emptyset - 0.0000058\ \sin^2 2\emptyset) \quad (3.8)$$

The value $g_{\emptyset}$ gives the predicted value of gravity at sea-level at any point on the Earth's surface and is subtracted from the observed gravity to correct for latitude variation.(Philip *et al.*, 2002) This is the international Gravity formula (IGF) for 1967.

3.2.6 Elevation correction

Elevation corrections sometimes called the Free air correction (FAC) corrects for the decrease in gravity with height in free air resulting from increased distance from the centre of the earth or the increase in gravity with height as a result of decreased distance from the centre of the earth according to Newton's Law. For this reason, all measurements are taken to the geoid and hence for an observation taken at height h (in meters),

$$\mathrm{FAC} = 3.086\mathrm{h} \quad (\text{h in meters}) \tag{3.9}$$

The FAC is positive for an observation point above geoid to correct for the decrease in gravity with elevation and negative for an observation point below geoid to correct for the decrease in gravity with elevation. The FAC accounts solely for variation in the distance of the observation point from the center of the Earth but do not consider the gravitational effect of the rock present between the observation point and datum (Philip *et al.*, 2002).

3.2.7 Bouguer correction (BC)

The BC sometimes known as mass correction considers the gravitational effect of the rock present between the observation point and datum by approximating the rock layer beneath the observation point to an infinite horizontal slab with a thickness equal to the elevation of the observation above geoid. The BC makes the assumption that the topography around the gravity is flat. This is rarely the case.

$$\mathrm{BC} = 0.4191\rho\mathrm{hgu} \tag{3.10}$$

where ρ is the density of the rock

On land the Bouguer correction must be subtracted, as the gravitational attraction of the rock between observation point and datum must be removed from the observed gravity value. The Bouguer correction of sea surface observations is positive to account for the lack of rock between surface and sea bed. The Free-air and Bouguer corrections are often applied together as the "Combined elevation correction".

3.2.8 Tidal correction (TD)

This is usually neglected for gravity readings taken offshore since solid earth tides are considerably smaller than oceanic tides and lag further behind the lunar motion. They

cause the elevation of an observation point to be altered by a few centimetres and thus vary its distance from the centre of mass of the earth. Earth tide period and the tidal variations are usually automatically removed during the drift correction. If a meter with a low drift rate is employed, base ties are normally made only at the start and end of the day so that the tidal variation has undergone a full cycle. In such a case, a separate tidal correction may need to be made (Philip *et al.,* 2002).

3.2.9 Eotvos correction (EC)

When gravity measurements are taken from a moving vehicle such as an aircraft or a ship, Eotvos Correction (EC) needs to be applied. Depending on the direction of travel, vehicular motion will generate a centripetal acceleration which either reinforces or opposes gravity. The correction required is

$$\mathrm{EC} = 75.03\mathrm{V}\sin\alpha\cos\emptyset + 0.04154\mathrm{V}^2 \qquad (3.11)$$

where:

V =Speed of the vehicle in knots,

α= The heading and

$\emptyset$= The latitude of the observation.

3.2.10 Gravity anomalies

3.2.11 Free air anomaly (FAA)

The FAA may be thought of as squashing up all the mass above sea level into an infinitesimally thin layer at sea level, and measuring gravity there. The FAA is mostly used for marine surveys and for investigating deep mass distribution such as testing theories of isostasy.

$$\mathrm{FAA} = \mathrm{g_{obs}} - \mathrm{g_{\emptyset}} + \mathrm{FAC}\ (\pm\mathrm{EC}) \tag{3.12}$$

3.2.12 Bouguer anomaly (BA)

The main end-product of gravity data reduction is the Bouguer anomaly, which should correlate only with lateral variations in density of the upper crust or near-surface environment and which is of most interest to applied geophysicists and geologists. The Bouguer anomaly is the difference between the observed gravity value (g_{obs}), adjusted by the algebraic sum of all the necessary corrections, and that at some base station ($g_{\emptyset}$). The variation of the Bouguer anomaly should reflect the lateral variation in density such that a high-density feature in a lower-density medium should give rise to a positive Bouguer anomaly. Conversely, a low-density feature in a higher density medium should result in a negative Bouguer anomaly.

After all reductions or corrections have been carried out, the Bouguer Anomaly (BA) forms the basis for the interpretation of gravity data on land. The Bouguer anomaly (BA) is the difference between the observed value (g_{obs}) duly corrected, and a value at a given base station ($g_{\emptyset}$) such that:

$$\mathrm{BA\ g_{obs}} - \mathrm{g_{\emptyset}} + \ \mathrm{Correction} \tag{3.13}$$

$$\mathrm{BA} = \ \mathrm{g_{obs}} - \mathrm{g_{\emptyset}} \mp \mathrm{FAC} \pm \mathrm{BC} + \mathrm{TC}(\pm\mathrm{EC}) \tag{3.14}$$

3.3 Relationship between BA and Crustal Thickness

The empirical relations, spectral analysis method and 2-D Modelling technique are used on Bouguer Gravity data to estimate the crustal thickness of some parts of the southern Nigeria (Tealeb *et al*., 1986).

3.4 The Empirical Relations

The empirical relations were developed by Demenitskaya (1958), Wollard (1959), Wollard & Strange (1962). The respective empirical relations are:

$$H_D=35*(1-TANH(0.0037)*BG) \tag{3.15}$$

$$H_W = 32.0 - 0.08 * BG \tag{3.16}$$

$$H_{WS} = 40.50 - 32.50 * TANH\left(\frac{BG+75}{275}\right) \tag{3.17}$$

But from Hyperbolic function,

$$TANH\ (X) = \frac{SINH(X)}{COSH(X)} = \frac{1-e^{-2X}}{1+e^{-2X}} \tag{3.18}$$

Where X = $\frac{BG+75}{275}$ from equation 3.17, Therefore equation 3.17 can then be rewritten as

$$H_{WS} = 40.50 - 32.50 * \left[\frac{1-e^{-2\left(\frac{BG+75}{275}\right)}}{1+e^{-2\left(\frac{BG+75}{275}\right)}}\right] \tag{3.19}$$

where;

H_D = Crustal thickness by Demenistkaya in kilometre

H_W= Crustal thickness by Woollard in kilometre

H_{WS}=Crustal thickness by Woollard and Strange in kilometre

BG =Bouguer gravity anomaly in milligal (mGal).

To estimate the Moho depths from equations 3.15, 3.16 and 3.17, the average result obtained from these three relations at any given location is taken as the estimated Moho depth at that particular location.

3.5 Power Spectral Depth Analysis (SDA)

Determination of the depth to Mohorovicic discontinuity is one of the principal applications of gravity data. This statistical approach has been found to yield good estimates of mean depth to basement underlying a sedimentary basin (Udensi *et al.,* 2001).

Spectral analysis of gravity data uses the 2- D Fast Fourier Transform and first transforms gravity data from the space domain to the wave number domain and then analysing their frequency characteristics. Thus, if b(x) represents the discrete N data array of gravity data obtained by sampling a continuous profile at evenly spaced intervals Δx, the finite mean depth z= h; Δρ is the density contrast between two layers; F(k) is the Fourier transform off(x), the derivation of the interface from the mean depth z; G is the gravitational constant. Parker (1973) suggested equation 3.16

Thus, the power spectrum of B (k) is simply:

$$E = (2\pi\Delta\rho G)^2 . l\, F(k)\, 1^2 \exp(-4\pi kh) \qquad (3.16)$$

The expected values of the power spectrum are expressed as the product of a depth factor and a size. This power spectrum exhibits intervals of wave numbers in which the logarithm of increasing wave number within discrete segments of the spectrum and the slopes of these linear segments are proportional to the depths of the possible layers in this case the Moho and Conrad discontinuity.

The total gravity anomaly values are used to obtain the two dimensional Fourier Transform from which the spectrum is to be extracted consisting M rows and N columns in X-Y. For the purpose of easier handling of the large data involved, the four residual blocks of the study area was divided and sectioned into nine (9) spectral cells

labelled section 1-9. Each section was subjected to spectra analysis using Oasis Montaj software.

The depth to causative mass distributions was obtained by analysing a plot of the logarithm of the power spectrum as a function of the wave number or frequency. Taking the logarithm of both sides of equation (3.17), one has:

$$\text{LogE} = \text{Loga(k)}_{z=0} - 4\pi kh \tag{3.17}$$

where:

K = the wave number

h = the depth to boundary surfaces;

A (k) = the amplitude spectrum.

One can plot the wave number k against LogE to obtain the average depth to the Moho interface and the Conrad discontinuity. The interpretation of LogE against the wave number k requires the best-fit line through the lowest wave number of spectrums. The most commonly encountered situation is the one in which there are two ensembles of sources; deep and shallow. These ensembles are recognizable by a change in the rate of decay of the power spectrum with wave number. The mean ensemble depth dominates the spectrum so that a significant change in depth of the ensemble results in a significant change in the rate of decay. Then the average depth can be estimated by plotting equation (3.18) as:

$$\text{H} = -\frac{\Delta LogE}{4\pi\Delta k} \tag{3.18}$$

where

h= the average depth to boundary surfaces;

$\Delta LogE = VariatiosofEnergylog$

$\Delta k = Variationsofwavenumber$

The graph of each energy spectra was obtained with the aid of a MATLAB software specifically designed to accept the longitude and latitude values alongside with its respective gravity values for each of the spectra sections where the log of spectra energy against frequency was plotted. To evaluate the corresponding depths from the slopes of the plotted graph, Equation 3.19 is used as it gives a relationship between the obtained slopes and the various depths to be calculated.

$$h = -\frac{m}{2\pi} \tag{3.19}$$

where:

m = m1, m2 or m3 slope of the best fitting straight

h = h1, h2 or h3 which is sedimentary thickness, Conrad depth and Moho depth in kilometres

3.6 2-D Modelling

The 2-D modelling is useful in geophysics both as a tool to interpret data in a research setting and as a tool to develop physical understanding in an educational setting. Modelling is usually the final step in interpretation for it helps compare the output of the finite element calculations with analytical solutions and demonstrate that these are in excellent agreement. It is used in analysis of data to generate reasonable models and

predictions about the properties and structures of the subsurface which is a primary concern of geophysicists in this case the Moho depth.

Moho depth may be estimated using 2-D modelling with the aid of the computer installed Geosoft packages for example the GM-SYS package. The software allows the digitizing of a profile from maps in Geosoft. In general, the extent (x-coordinate) and depth (z-coordinate) of the profile to be modelled are defined. In the environment, the user interactively adjusts the model parameters in order to improve the fit between the calculated and the observed Moho depth. In modelling operation, profiles are spaced out and drawn through relatively less disturbed area (Udensi & Osazuwa, 2002) perpendicular to the striking length across the Bouguer gravity anomaly map in order to estimate the Moho depth. Less disturbed areas are chosen so that the effects of topography rather than lithology will account more for modelling. Hence modelling is used to correlate the calculated Moho depth of gravity anomaly with the observed results to then estimate the average Moho depth of the study area. The computer program gives a composite model of the Moho depth, the surface topography of the basement below the basin and depth of any intrusions in the basement. Figure 3.2 gives the summary of the research methodology in a flowchart. The computer program gives a composite model of the crustal thickness, the surface topography of the basement below the basin and the structure and depth of any intrusions in the basement. Figure 3.2 gives the summary of the methodology in a block diagram.

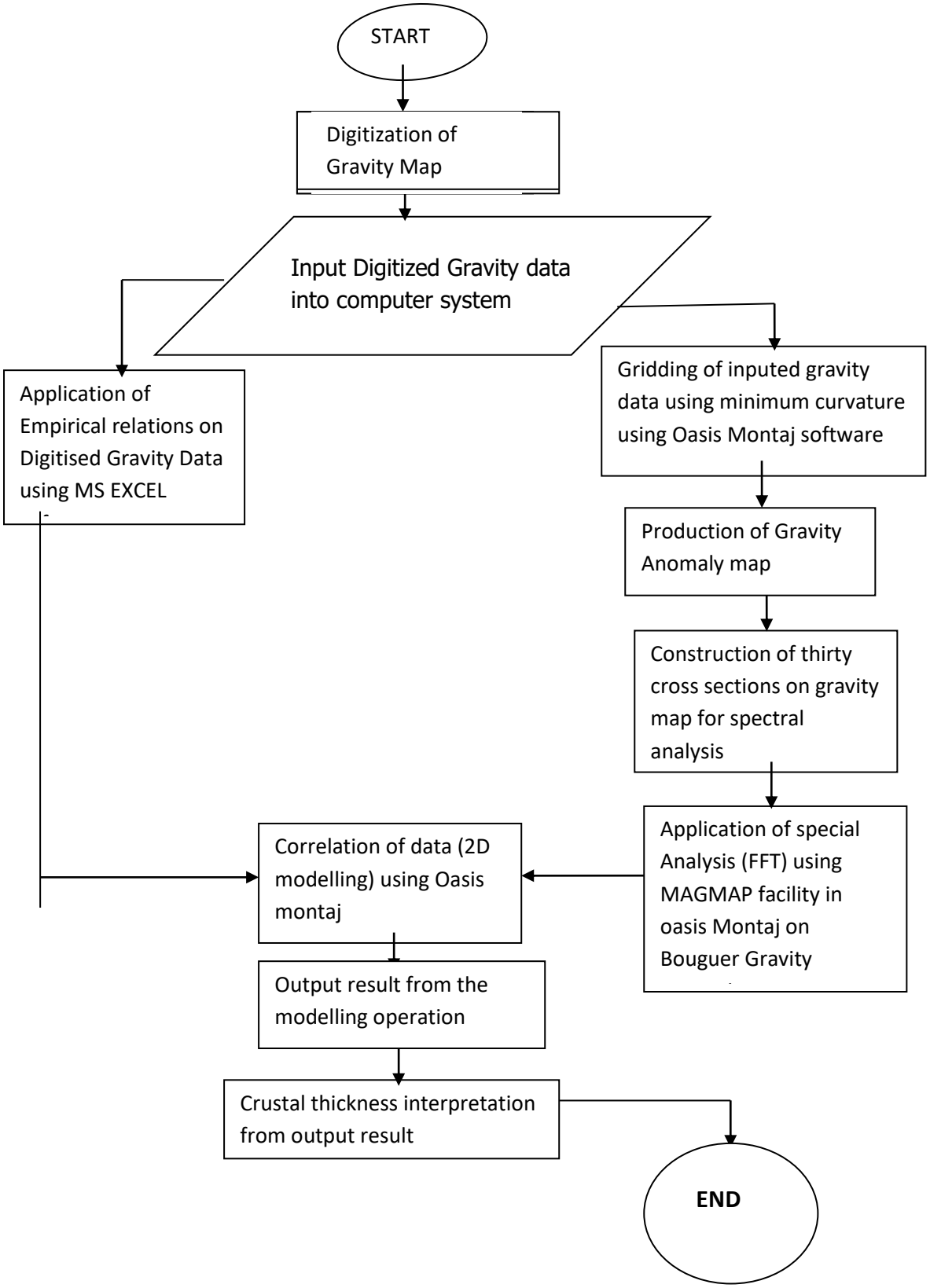

Figure 3.2: Block diagram of the Methodology of the Research

CHAPTER FOUR

4.0 RESULTS AND DISCUSSION

4.1 Bouguer Anomaly

The Bouguer gravity anomaly map of the study area (Figure 4.1). It is contoured at interval of 5mGal; which was produced using the "Surfer" package. The Bouguer gravity map of the study area (Figure 4.1) reveals that the gravity field trends in South-west (SW) and North-East (NE)direction.

The Bouguer anomaly value follows a regular trend across the map. The values are seen to take a regular reduction pattern as one move from north toward south wards direction. A wide range in gravity values ranging from -40mGal at the south-eastern parts of the study area which increases northward and reaches 30mGal at the north-western part is observed in the study area. The Bouguer anomaly value ranges from -40mGal to 30mGal that covers almost all part of the study area may be as a result of density bodies of the crust within the location with density contrasts within the basement. The NW-SE trend of the gravity field has a minimum value of -40mGal which are found around north west and maximum value of 30 mGal found at south east part of the study area is in line with the trend of geologic features within the study area.

4.2 Empirical Calculations

The digitised gravity data were inputted into the Microsoft Excel program to calculate the Crustal thickness depth using equations 3.15, 3.16 and 3.17 and the average Crustal thickness depth for each point calculated and also the average Moho depth for each point calculated. Table 4.1 shows the sample results of the empirical relation while the complete result is shown in Appendix A. The empirical relation used was developed by

Demenitskaya (1958), Wollard (1959), Wollard & Strange (1962). The Crustal Thickness of the study area obtained from the three empirical relations was averaged as shown in Appendix A and contoured using ‘’SURFER’’ graphic package as shown in figure 4.5. The average values obtained from the three relations at any given location is the crustal thickness at that location.

4.2.1 Demenistskaya Relation

The result obtained from the empirical relation was contoured as shown in Figure 4.2. The Contour maps of crustal thickness obtained using Demenistakaya. Figure 4.2 follows a SW - NE trend as in the case of the Bouguer anomaly map. Obtained crustal thickness using this relation ranges from 31 km around the north western region of the study area to 40 km at the south-eastern with an increase of 0.5mGal contour interval in the region of the study area.

4.2.2 Wollard Relation

Figure 4.3 is the map of the Wollard empirical relation with values ranging from 29.6 km to 35.2 km with a contour interval of 0.5 mGal, the highest value is found around the North Eastern and some parts of South west region while, the lowest value is found around the north west region of the study area

4.2.3 Wollard and Strange Relation

Figure 4.4 The map of Wollard and Strange relation, the crustal thickness of the study area has a value ranges from 28.5 km to 36.5 km. with a contour interval of 0.5 mGal the maximum value is found around some parts of South Eastern, Nouth Eastern region while the lowest value is found around the North west region of the study area.

4.2.4 Average Empirical Relation

Figure 4.5 the average empirical relation of Demenistskaya, Wollard, Wollard and Strange. The average empirical map showed that the crustal thickness of the study area ranges from 30 km and 37.5km with an increase in interval of 0.5. The highest crustal thickness varies from maximum value of 37.5km to a minimum value of 30 km. The maximum Crustal Thickness is located around the South West region while its minimum Crustal Thickness is located around the North West region of the study area.

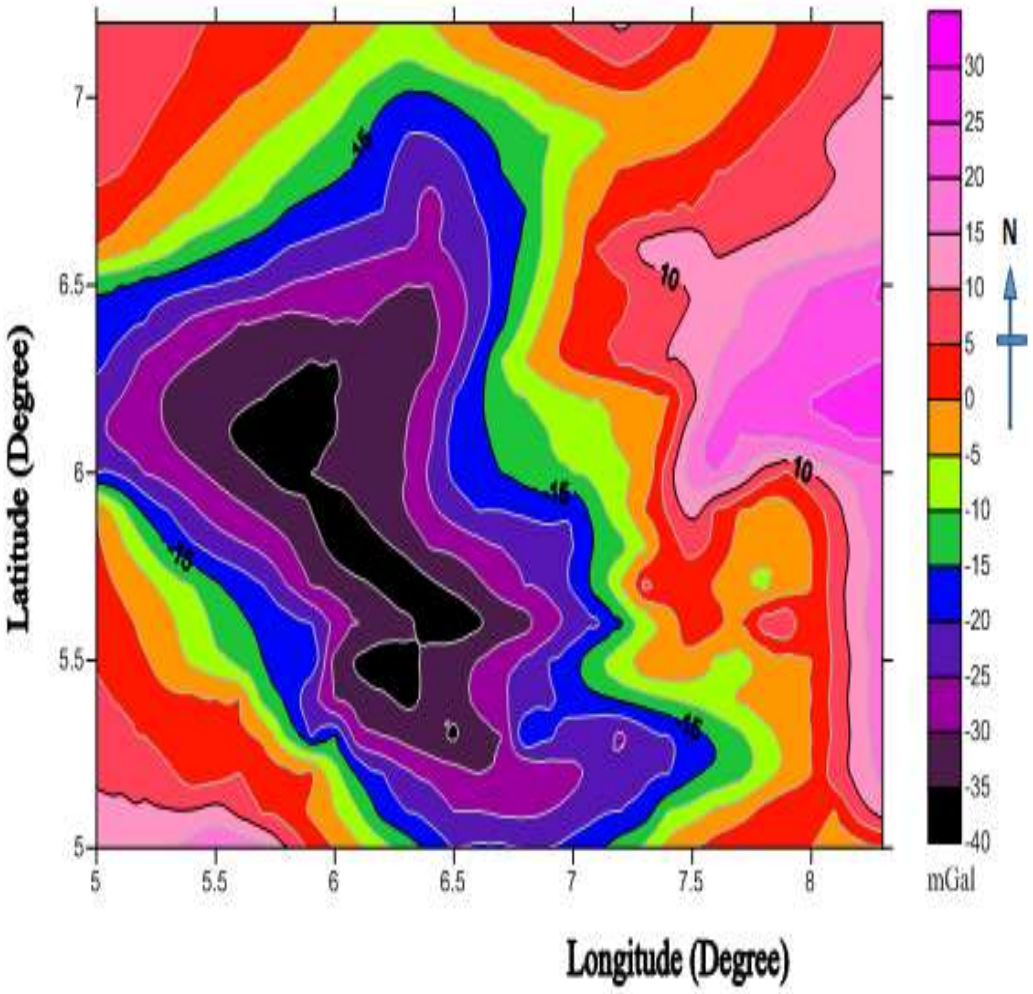

Figure 4.1: The bouguer Anomaly Map of the study area

Table 4.1: Sample result of Empirical calculations

Longitude (Degree)	Latitude (Degree)	BG (mGal)	H_D (km)	H_W (km)	H_{WS} (km)	Average= ((H_W+H_{WS}+ H_D)/3) (km)
5.00	5.00	32.00	31.84	32.94	35.00	
5.10	5.00		35.00	32.00	31.84	32.94
5.20	5.00		35.00	32.00	31.84	32.94
5.30	5.00		35.00	32.00	31.84	32.94
5.40	5.00		35.00	32.00	31.84	32.94
5.50	5.00	20.00	32.41	30.40	29.69	30.83
5.60	5.00	19.00	32.53	30.48	29.80	30.94
5.70	5.00	17.00	32.79	30.64	30.01	31.15
5.80	5.00	10.00	33.70	31.20	30.76	31.88
5.90	5.00	4.00	34.48	31.68	31.41	32.52
6.00	5.00	0.00	35.00	32.00	31.84	32.94
6.10	5.00	-4.00	35.51	32.32	32.29	33.37
6.20	5.00	-8.00	36.03	32.64	32.73	33.80
6.30	5.00	-12.00	36.55	32.96	33.18	34.23
6.40	5.00	-16.00	37.07	33.28	33.63	34.66
6.50	5.00	-20.00	37.58	33.60	34.08	35.09
6.60	5.00	-19.00	37.46	33.52	33.97	34.98
6.70	5.00	-19.00	37.46	33.52	33.97	34.98
6.80	5.00	-20.00	37.58	33.60	34.08	35.09
6.90	5.00	-20.00	37.58	33.60	34.08	35.09
7.00	5.00	-18.00	37.33	33.44	33.85	34.87
7.10	5.00	-16.00	37.07	33.28	33.63	34.66
7.20	5.00	-12.00	36.55	32.96	33.18	34.23
7.30	5.00	-9.00	36.16	32.72	32.84	33.91
7.40	5.00	-3.00	35.38	32.24	32.18	33.26
7.50	5.00	0.00	35.00	32.00	31.84	32.94

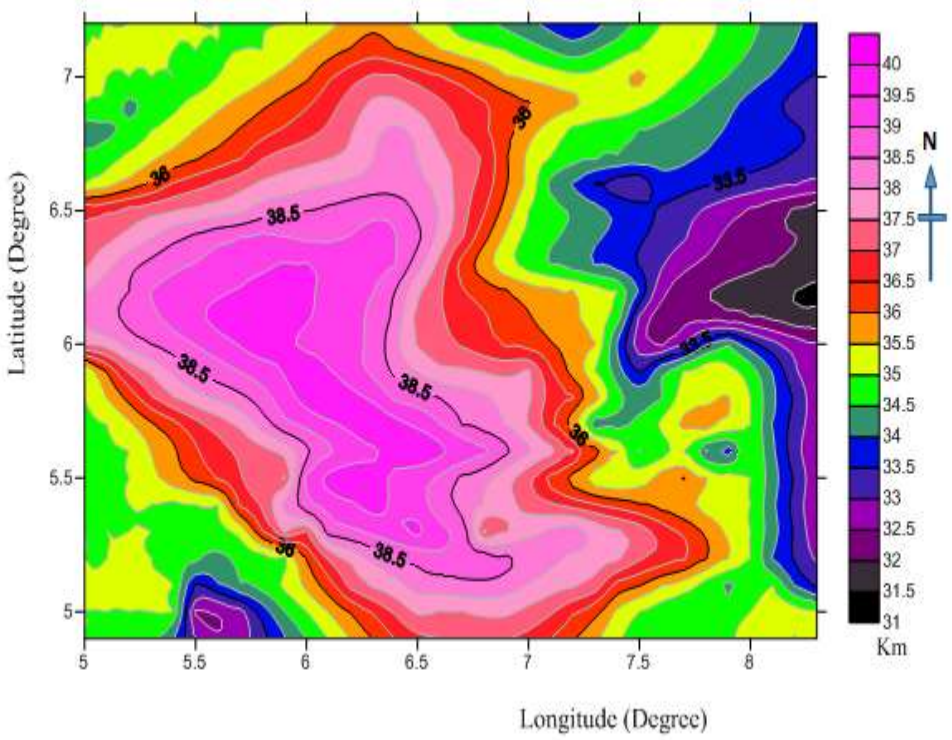

Figure 4.2: The Contour map of crustal thickness depth obtained using Demeniskaya empirical relation for the study area

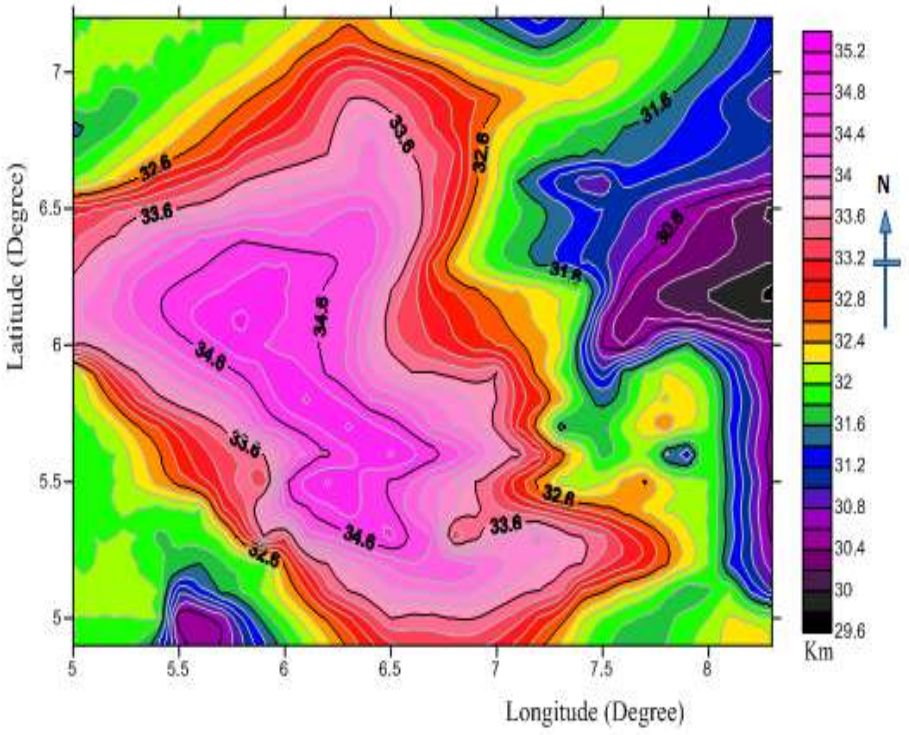

Figure 4.3: The Contour map of crustal thickness depth obtained using Woolard empirical relation for the study area

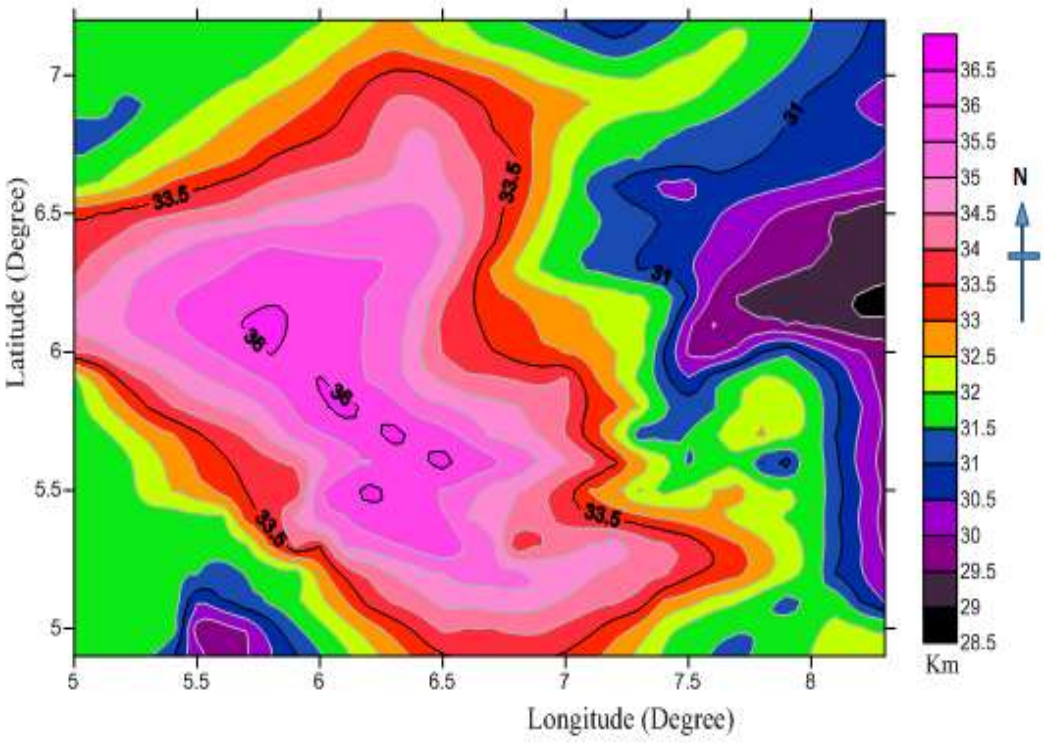

Figure 4.4: The Contour map of crustal thickness depth obtained using Woolard and Strange empirical relation for the study area

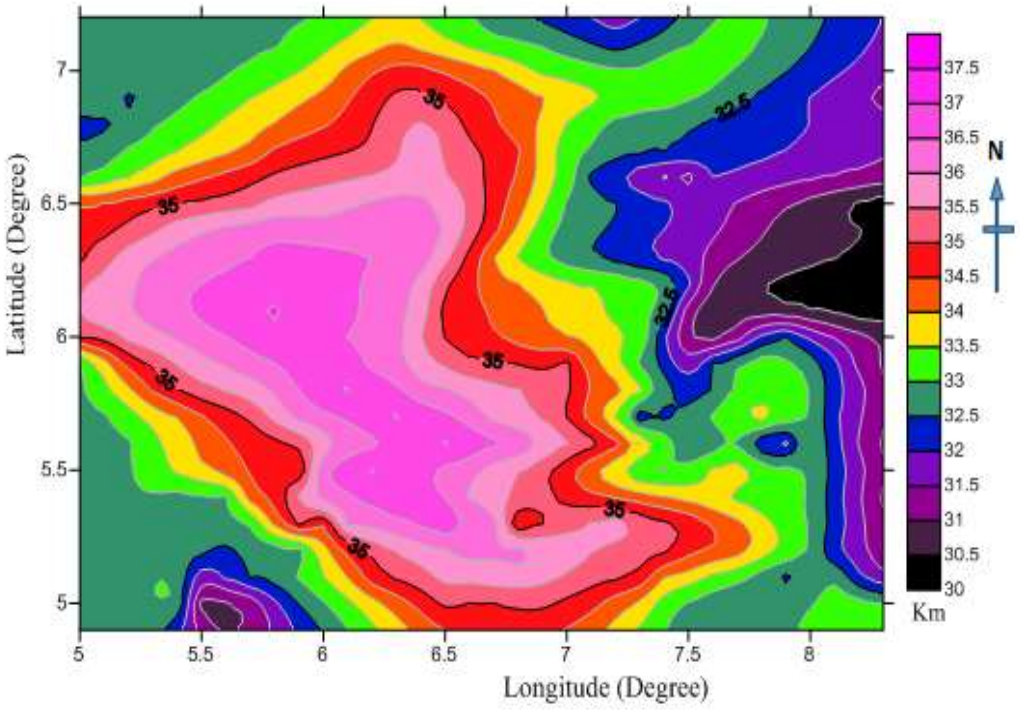

Figure 4.5: The Contour map of average crustal thickness depth obtained using the (3) empirical relations for the study area

4.3 Spectral Method of Depth Determination

The depths to the gravity sources can be calculated from power spectrum profiles computed from the Potential Field data. The spectral method allows the estimation of depths to the top of assemblages of source bodies from the wavelengths of gravity fields. Frequency analysis using the Fast Fourier Transform (FFT) which is widely utilised technique for processing and interpretation of the potential field data, particularly for depth estimation method has been applied to the digitised Bouguer gravity data for the estimation of average depths to different density discontinuities within the study area. At this stage, the MAGMAP facility in Geosoft Oasis is used to process the original grid map- total gravity anomaly map in order to enhance it. Thirty cross sections are constructed from the gravity anomaly map and Fast Fourier Transform (FFT) applied using the MAGMAP facility in Oasis Montaj software in order to analytically estimate the crustal thickness of the study area.

Gridding and Sectioning of the Bouguer anomaly map into thirty spectral sections (SPCA-SPCAD which is equivalent to SPC1-SPC 30) was carried out using Oasis Montaj Geosoft and the radial spectral energies were plotted within it. The *SPC files for the thirty spectral sections obtained from the radial spectral energy were exported into the Microsoft excel worksheet one after the other on a comma separated values (*csv*) file format. The Microsoft excel worksheets file data obtained was then used as an input file into a spectral program plot developed with Matlab software. Graphical Results of logarithm of spectra energy with respect to the frequency in cycles per kilometre which gives the spectra energy section generated from the Matlab program are shown in Appendix B of which Figure 4.6shows the sample result. The results of the depth estimate for the 30 spectral sections (SPCA-SPCAD) are given in Table 4.2.

The inspection of the results in Figure 4.6 reveals that three main slopes m_1, m_2 and m_3 representing slopes for shallow depth which is the basement, Conrad discontinuity and the crustal thickness was obtained.

From the earth's surface downwards, the slope (m_1) may be attributed to average depth of shallow sources from the crystalline rocks (basement and /or intrusions). Meanwhile, the slope m_2 is associated with the average depth to Conrad discontinuity which reflects a change in the rock type within the crust from dense silicon-aluminium rock type at the upper crust to denser silicon-magnesium rock type at the lower crust. However, slope m_3 may be connected with the average depth of the crustal thickness which comes about as a result of density contrast between the overlying crust and the underlying mantle.

To evaluate the corresponding depths from the slopes, Equation 3.23 is used as it gives a relationship between the obtained slopes and the various depths to be calculated. Table 4.2gives summary of spectral result and obtained depths for Basement depth (shallow depth) h_1, the Conrad discontinuityh_2, and the Crustal thickness(depth) h_3.

There is need to contour the obtained depths from spectral technique in order to obtain a view of the crustal thickness across the study area in 2-Dimension and as such the average longitude and latitude values for each spectra section was included into the spectral result table as shown in Table 4.3.

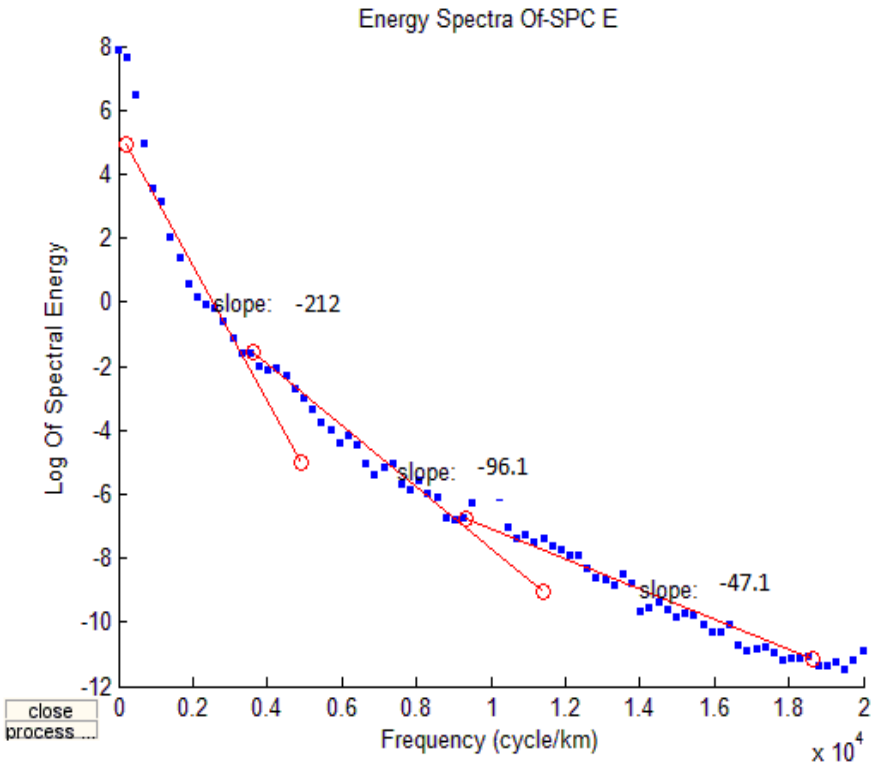

Figure 4.6: A graph of Log of Spectral energy against Frequency Spectral Section E (SPC E)

Table 4.2: Basement depth, Conrad depth and crustal thickness obtained from Spectral analysis

SPECTRAL SECTIONS	m_1	m_2	m_3	BASEMENT DEPTH h_1(km)	CONRADDEPTH h_2 (km)	CRUSTAL THICKNESSh_3(km)
SPC A	31.2	68.4	191	4.96	10.89	30.39
SPC B	46.4	74.1	201	7.38	11.79	31.99
SPCC	48.2	74.3	207	7.67	11.83	32.95
SPCD	55.9	92.6	223	8.89	14.74	35.49
SPCE	47.1	96.1	212	7.49	15.29	33.74
SPCF	48.5	79.6	206	7.72	12.67	32.79
SPCG	51.9	94.5	208	8.26	15.04	33.10
SPC H	49.5	92.4	204	7.88	14.71	32.47
SPC I	32.5	85.5	197	5.17	13.61	31.35
SPC J	33.2	74.7	205	5.28	11.89	32.63
SPC K	31.6	83.5	211	5.03	13.28	33.58
SPC L	36.8	86.6	202	5.86	13.78	32.15
SPC M	32.5	97.7	206	5.17	15.55	32.79
SPC N	32.3	95.8	204	5.14	15.25	32.47
SPC O	56.7	87.7	214	9.02	13.96	34.06
SPC P	48.3	82.2	209	7.69	13.08	33.26
SPC Q	50.2	80.4	208	7.99	12.79	33.10
SPC R	46.5	82.3	219	7.40	13.09	34.85
SPC S	49.9	80.6	206	7.94	12.83	32.79
SPC T	58.5	82.3	209	9.31	13.09	33.26
SPC U	51.3	81.9	202	8.16	13.03	32.15
SPC V	54.2	90.5	212	8.63	14.40	33.74
SPC W	48.9	89.2	212	7.78	14.19	33.74
SPC X	47.7	91.3	208	7.59	14.53	33.10
SPC Y	48.4	92.3	204	7.70	14.69	32.47
SPC Z	55.5	92.7	206	8.83	14.75	32.79
SPC AA	52.5	89.7	215	8.36	14.28	34.22
SPC AB	53.3	91.4	212	8.48	14.55	33.74
SPC AC	47.5	73.4	206	7.56	11.68	32.79
SPC AD	47.4	76.5	208	7.54	12.18	33.10

4.3.1 Depth to basement map

The basement depth map produced from Tables 4.3 in Figure 4.7 Is the depth to the basement surface (sedimentary thickness) within the area which trend toward NW and SE region, ranges approximately from 4.8 km at it minimum level to 9.4 km at it maximum level with an interval of 0.2 km. This thickness is below the stated maximum Crustal thickness of the Niger delta of 14.2 km and Anambra (Emujakporue & Ofoha, 2015). The map exhibits common thickening of sedimentary cover towards the central region of the study area.

4.3.2 Conrad discontinuity map

The Conrad Depth map Figure 4.8 Is the depth of the Conrad discontinuity. This is the depth beneath the continent where the continental crust becomes close in physical properties to the oceanic crust. This is due to the change in velocity of seismic wave at this sub horizontal boundary. This depth ranges from 10.8 km at the minimum to 15.6 km at the maximum level with interval of 0.2 km within the study area. The low Conrad depth of 10.8 km shows that in the Niger delta and Anambra basin, the basement rock underlying the sediments is interpreted to be oceanic crust unlike other Sedimentary basins in Nigeria that are underlain by continental crust. This explains why the Conrad depth looks like the Depth to Basement as the range of the Conrad depth is interwoven with the range of the sedimentary thickness. The Conrad depth with highest thickness is seen at Longitude 8.5^0W and Latitude 15.5^0N and maximum value with the highest depth trending toward NW and shallow depth toward SE region within the study area.

4.3.3 Crustal thickness map

The crustal thickness map Figure 4.9 Reveals that the basement depth to the Moho achieves its maximum value of about 35.6 km along longitude 9.0^0E. This depth decreases gradually southward and westward reaching its minimum value of 30.2 km and maximum value of 35.6 km with an interval of 0.2 km which trend toward the SE at the deepest depth and SW at the shallowest region of the study area. Depth to crust from this map can be said to approach its maximum thickness at the southward and eastward and approach its minimum thickness at southward and westward region of the study area.

Table 4.3: Basement Depth, Conrad depth and Crustal thickness obtained from Spectral Analysis and its location

SPECTRAL SECTIONS	LONGITUDE (˚E)	LATITUDE (˚N)	AVERAGE LONGITUDE X (Degree)	AVERAGE LATITUDE Y(Degree)	BASEMENT DEPTH h1 (km)	CONRAD DISCONTINUITY h2 (km)	CRUSTAL THICKNESS h3 (km)
SPC A	5.00 – 6.00	5.00 – 5.50	5.50	5.25	4.96	10.89	30.39
SPCB	5.50 – 6.50	5.00 – 5.50	6.00	5.25	7.38	11.79	31.99
SPCC	6.00 – 7.00	5.00 – 5.50	6.50	5.25	7.67	11.83	32.95
SPCD	6.50 – 7.50	5.00 – 5.50	7.00	5.25	8.89	14.74	35.49
SPCE	7.00 – 8.00	5.00 – 5.50	7.50	5.25	7.49	15.29	33.74
SPC F	7.50 – 8.50	5.00 – 5.50	8.00	5.25	7.72	12.67	32.79
SPCG	5.00 – 6.00	5.50 – 6.00	5.50	5.75	8.26	15.04	33.10
SPCH	5.50 – 6.50	5.50 – 6.00	6.00	5.75	7.88	14.71	32.47
SPC I	6.00 – 7.00	5.50 – 6.00	6.50	5.75	5.17	13.61	31.35
SPC J	6.50 – 7.50	5.50 – 6.00	7.00	5.75	5.28	11.89	32.63
SPC K	7.00 – 8.00	5.50 – 6.00	7.50	5.75	5.03	13.28	33.58
SPC L	7.50 – 8.50	5.50 – 6.00	8.00	5.75	5.86	13.78	32.15
SPC M	5.00 – 6.00	6.00 – 6.50	5.50	6.25	5.17	15.55	32.79
SPC N	5.50 – 6.50	6.00 – 6.50	6.00	6.25	5.14	15.25	32.47
SPC O	6.00 – 7.00	6.00 – 6.50	6.50	6.25	9.02	13.96	34.06
SPCP	6.50 – 7.50	6.00 – 6.50	7.00	6.25	7.69	13.08	33.26
SPCQ	7.00 – 8.00	6.00 – 6.50	7.50	6.25	7.99	12.79	33.10
SPCR	7.50 – 8.50	6.00 – 6.50	8.00	6.25	7.40	13.09	34.85
SPCS	5.00 – 6.00	6.50 – 7.00	5.50	6.75	7.94	12.83	32.79
SPC T	5.50 – 6.50	6.50 – 7.00	6.00	6.75	9.31	13.09	33.26
SPCU	6.00 – 7.00	6.50 – 7.00	6.50	6.75	8.16	13.03	32.15
SPC V	6.50 – 7.50	6.50 – 7.00	7.00	6.75	8.63	14.40	33.74
SPC W	7.00 – 8.00	6.50 – 7.00	7.50	6.75	7.78	14.19	33.74
SPC X	7.50 – 8.50	6.50 – 7.00	8.00	6.75	7.59	14.53	33.10
SPC Y	5.00 – 6.00	7.00 – 7.50	5.50	7.25	7.70	14.69	32.47
SPC Z	5.50 – 6.50	7.00 – 7.50	6.00	7.25	8.83	14.75	32.79
SPC AA	6.00 – 7.00	7.00 – 7.50	6.50	7.25	8.36	14.28	34.22
SPC AB	6.50 – 7.50	7.00 – 7.50	7.00	7.25	8.48	14.55	33.74
SPC AC	7.00 – 8.00	7.00 – 7.50	7.50	7.25	7.56	11.68	32.79
SPC AD	7.50 – 8.50	7.00 – 7.50	8.00	7.25	7.54	12.18	33.10

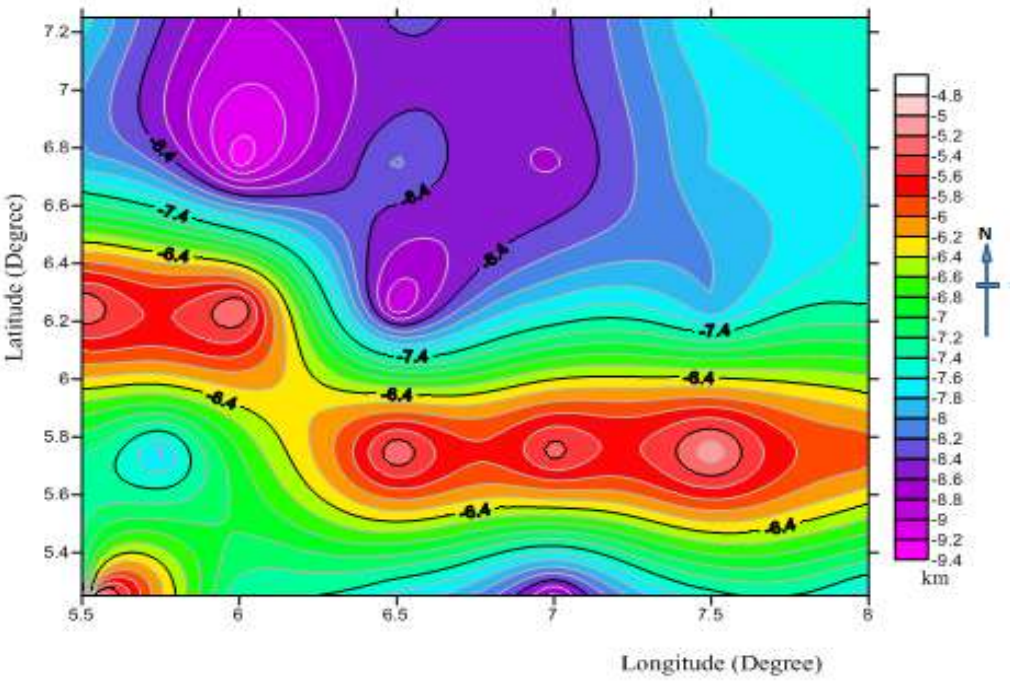

Figure 4.7: The contour map of basement depth obtained from spectral analysis for the study area

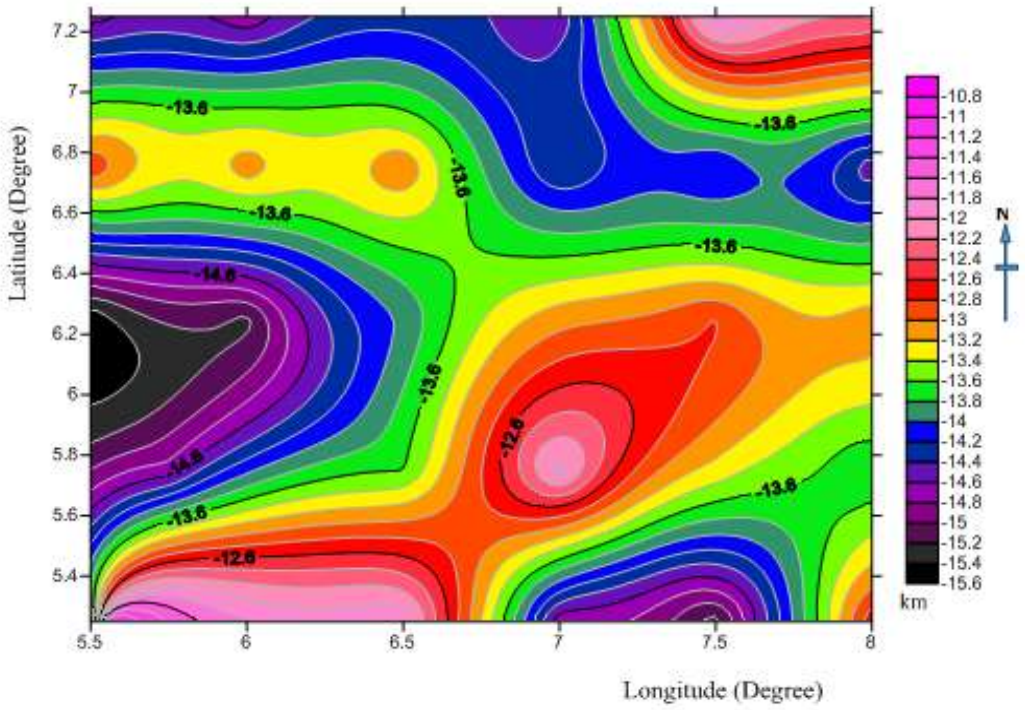

Figure 4.8: The contour map of Conrad discontinuity obtained from spectral analysis for the study area

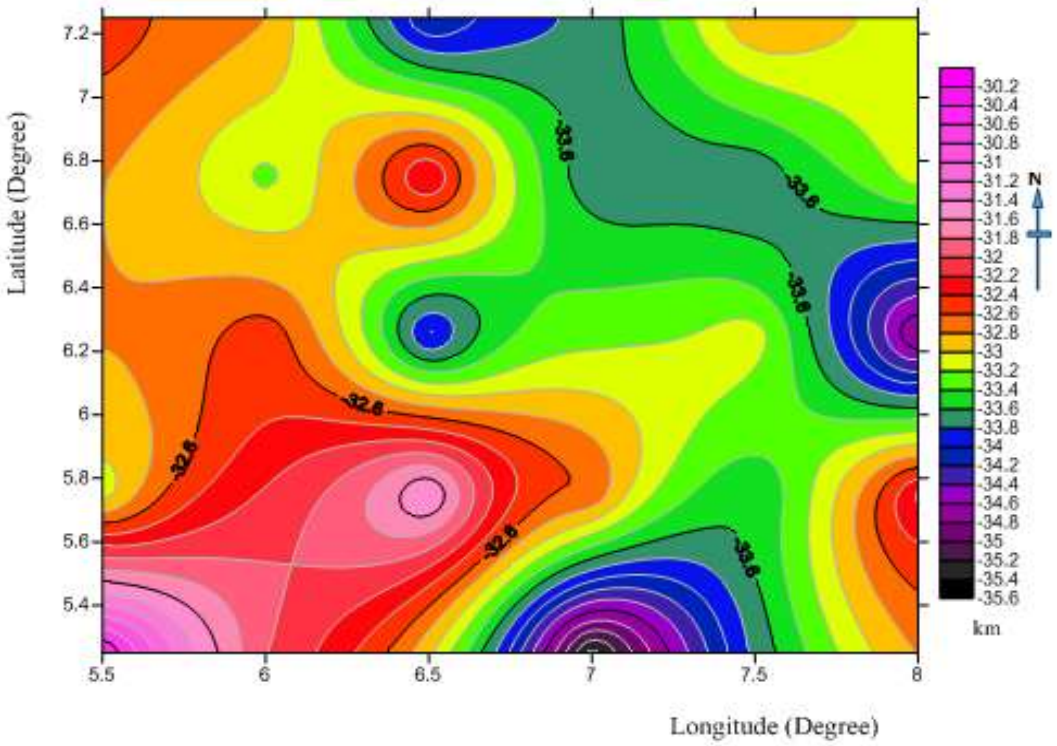

Figure 4.9: The contour map of the Crustal thickness obtained from spectral analysis for the study area

4.3.4 Average crustal thickness map of empirical and spectral result

The average crustal thickness map of empirical and spectral result (Figure 4.10) shows that the basement to the depth achieves its maximum value of about35.6 km. This depth decreases gradually reaching its minimum value of 31.4 km with a contour interval of 0.2 km and an average maximum value of 35.6 km which trend toward the NE and minimum average value of 31.4 km trending SE region of the study area. Depth to crust from this average empirical and spectral map can be said to approach its maximum thickness at the southward and eastward and approach its minimum thickness at southward and westward region of the study area.

Table 4.4 Average crustal thickness obtained from Empirical and Spectral Analysis Results.

S/N	LONGITUDE (Degree)	LATITUDE (Degree)	BG (mGal)	EMPIRICAL RESULT (km)	SPECTRAL RESULT (km)	AVERAGE CRUSTAL RESULT (km)
A	5.50	5.25	2.42	32.67	30.39	31.53
B	6.00	5.25	-12.36	34.35	31.99	33.17
C	6.50	5.25	-32.26	36.4	32.95	34.675
D	7.00	5.25	-24.17	35.55	35.49	35.52
E	7.50	5.25	-17.67	34.83	33.74	34.285
F	8.00	5.25	1.33	32.74	32.79	32.765
G	5.50	5.75	-18.61	34.85	33.10	33.975
H	6.00	5.75	-34.82	36.63	32.47	34.55
I	6.50	5.75	-31.08	36.35	31.35	33.85
J	7.00	5.75	-19.19	34.4	32.63	33.515
K	7.50	5.75	4.34	32.52	33.58	33.05
L	8.00	5.75	1.23	32.82	32.15	32.485
M	5.50	6.25	-32.16	36.38	32.79	34.585
N	6.00	6.25	-35.06	36.73	32.47	34.6
O	6.50	6.25	-22.33	35.42	34.06	34.74
P	7.00	6.25	-1.65	33.06	33.26	33.16
Q	7.50	6.25	10.4	31.8	33.10	32.45
R	8.00	6.25	23.67	30.47	34.85	32.66
S	5.50	6.75	-5.27	33.50	32.79	33.145
T	6.00	6.75	-15.68	34.62	33.26	33.94
U	6.50	6.75	-22.28	35.37	32.15	33.76
V	7.00	6.75	-3.14	33.36	33.74	33.55
W	7.50	6.75	4.37	32.48	33.74	33.11
X	8.00	6.75	9.48	31.95	33.10	32.525
Y	5.50	7.25	4.45	32.95	32.47	32.71
Z	6.00	7.25	-1.11	33.10	32.79	32.945
AA	6.50	7.25	-2.92	33.25	34.22	33.735
AB	7.00	7.25	6.89	33.20	33.74	33.47
AC	7.50	7.25	2.76	32.66	32.79	32.725
AD	8.00	7.25	3.40	33.61	33.10	33.355

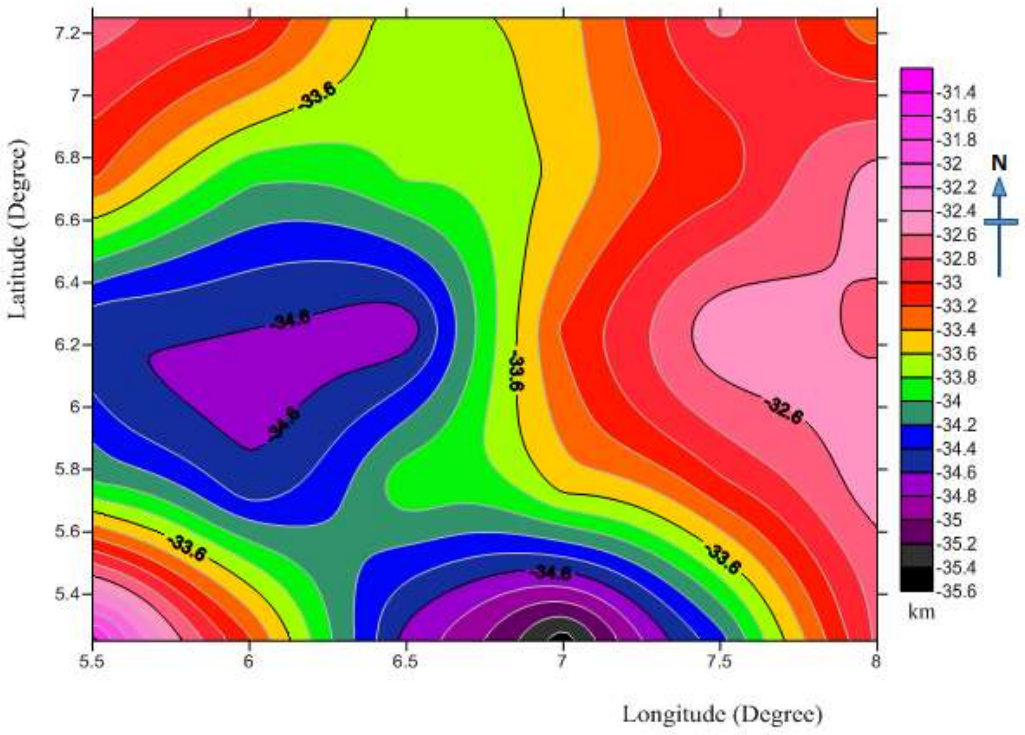

Figure 4.10: Average crustal thickness map obtained from empirical and spectral result for the study area

4.4 2-D Gravity Modelling

Gravity modelling is considered an important implement to study the crustal structures. Gravity data indicate that there is a regular relationship between crustal structure, crustal density and the surface elevation. For regional scale, Bougueranomalies are enough to give clear evidence of changes in mass distributions in the lower and upper crust as well as distributions in the upper mantle. Recent studies indicate that Bouguer anomalies and surface relief are closely connected with crustal thickness.

In modelling, profiles are usually run across the map. For this research work, three profiles A-A', B-B' and C-C', were selected to be investigated with the 2-D modelling approach. The A-A' profile as shown in Figure 4.13 whichcut across the NSand profile B-B' shown in Figure 4.14cut across a basement complex at the WE and also profile C-C' shown in Figure 4.15 cut across SW. The positions of this profiles are also shown on the geological map of the study area and the Bouguer gravity map with towns and locations of the study area (Figure 4.11 and 4.12). The profiles are taken along the NS,WE and SW direction to include the negative and positive Bouguer anomalies values.

In this modelling work, three crustal model profiles, based on gravity data have been generated, using 2-D modelling techniques program, with aslightly change of the model parameters and to obtain high quality model results and good fitness between the observed and calculated curves as illustrated in the modelling below.

The upper half of the model figures represents the observed which is the dotted lines, and the calculated which is the solid lines gravity profiles. While the lower half of these profilesshows the model crustal layers. The vertical axis y shows two different parts, the

upper half represents the gravity anomaly scale in mGal. And the lower half shows the latitude depth scale in kilometres (km). The horizontal x-axis represents the horizontal longitude distance in kilometres(km) along the profile respectively.

4.4.1 Model line profile A-A'

The profile A-A' in Figure4.10 Model profile A-A' line runs across SW and NE through cities like Auchi, Agbede, Ekpoma and Kwale direction. Auchi is at longitude 6.2°E and at latitude 7.0°N, Agbede is at longitude 3.5°E and at latitude 6.6°N, Ekpoma is that longitude 6.0°E and at latitude 6.7°N and Kwale is that longitude 3.9°E and at latitude 4.1°N. The horizontal longitude line of profile A-A' covered the minimum distance of about 0 km and a maximum longitude line covered the distance of 238 km and with a vertical latitude line of profile A-A' which has the minimum latitude depth ranges from 0 km and a maximum latitude depth to be 50 km and the crustal thickness has a minimum value of 28 km along the upper crust which has a density of D = 2.7 and a maximum value of 36 km along the lower crust with a density of D = 2.9 while the mantle has a density of D = 3.2, with a Gravity Bouguer anomaly values ranging from -40 - 0 mGal. And the crustal model for profile A-A' described two major layers above the Moho discontinuity line which are differ in thickness and density underlying the study area with the average models identified and delineated boundaries between the Upper Crust, Lower Crust and Mantle with densities of 2.7g/cm^3, 2.9g/cm^3 and 3.2g/cm^3 respectively. Table 4.5 and 4.6 gives the parameters deduced from the modelled gravity profiles.

4.4.2 Model line profile B-B'

Figure 4.13 gives the modelresult line profile B-B', the model profile B-B' line cut across WE and EW and pass in-between cities like Agbor, Asaba, Owa, Awka and

Abakaliki direction. Agbor is at longitude 6.2°E and at latitude 6.2°N, Asaba is at longitude 6.6°E and at latitude 6.1°N, Owa is at longitude 6.2°E and at latitude 6.1° N, Awka is at longitude 7.0°E and at latitude 6.2°N and Abakaliki is at longitude 8.1°E and at latitude 6.3°N. The horizontal longitude line of profile B-B' covered the minimum distance of about 0 km and a maximum longitude line covered the distance of 340 km and with a vertical latitude line of profile B-B' which has the minimum latitude depth ranges from 0 km and a maximum latitude depth to be 50 km. And the crustal thickness has a minimum value of 29 km along the upper crust which has a density of D = 2.7 and a maximum value of 38 km along the lower crust with a density of D = 2.9, while the mantle has a density of D = 3.2, with a Gravity Bouguer anomaly values ranging from -40 to -20 mGal. And the crustal model for profile B-B' described two major layers above the Moho discontinuity line which are differ in thickness and density underlying the study area with the average models identified and delineated boundaries between the Upper Crust, Lower Crust and Mantle with densities of 2.7g/cm^3, 2.9g/cm^3 and 3.2g/cm^3 respectively. Table 4.5 and 4.6 gives the parameters deduced from the modelled gravity profiles.

4.4.3 Model line profile C-C'

Model profile C-C' line slant through and pass cities like, Benin city, Sapele and warri respectively. Benin city is at longitude 5.6°E and at latitude 6.3°N, Sapele is at longitude 5.6°E and at latitude 5.8°N, Warri is at longitude 5.7°E and at latitude 5.5°N. The horizontal longitude line of profile C-C' covered the minimum distance of about 0 km and a maximum longitude line covered the distance of 238 km and with a vertical latitude line of profile C-C' which has the minimum latitude depth ranges from 0 km and a maximum latitude depth to be 50 km. And the crustal thickness has a minimum

value of 28 km along the upper crust which has a density of D = 2.7 and a maximum value of 38.5 km along the lower crust with a density of D = 2.9, while the mantle has a density of D = 3.2, with a Gravity Bouguer anomaly values ranging from -30 - 0 mGal . And the crustal model for profile C-C' described two major layers above the Moho discontinuity line which are differ in thickness and density underlying the study area with the average models identified and delineateboundaries between the Upper Crust, Lower Crust and Mantle with densities of 2.7g/cm^3, 2.9g/cm^3 and 3.2g/cm^3 respectively. Table 4.5 and 4.6 gives the parameters deduced from the modelled gravity profiles.

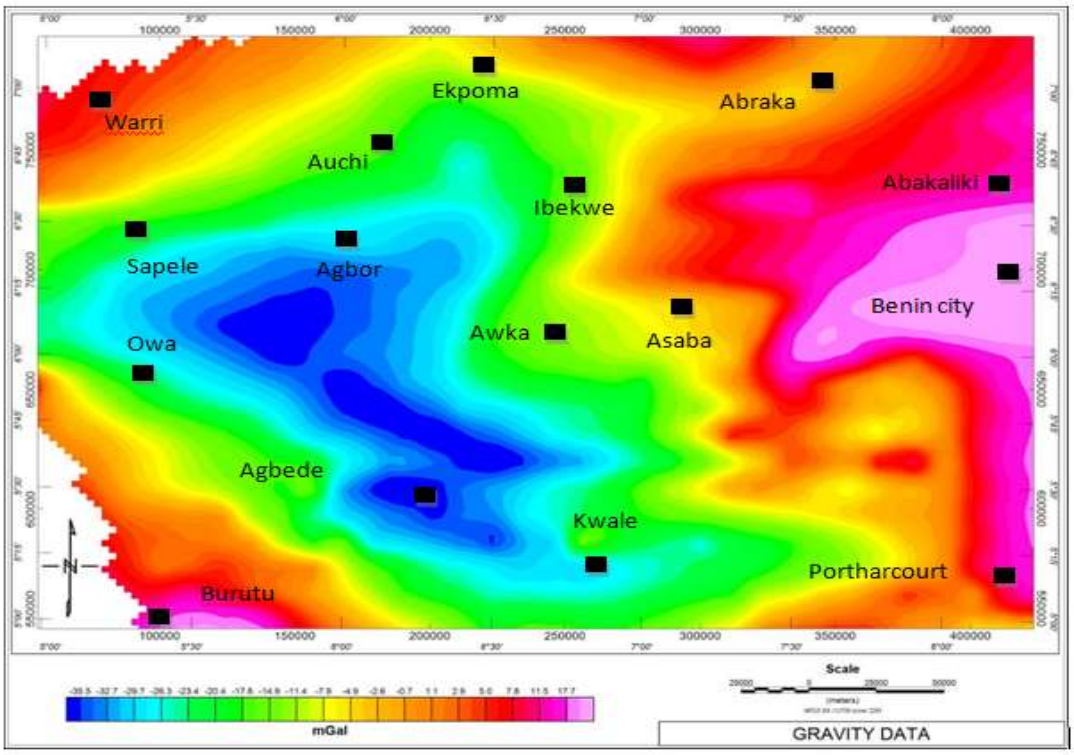

Figure 4.11: Bouguer gravity map with towns within the study area

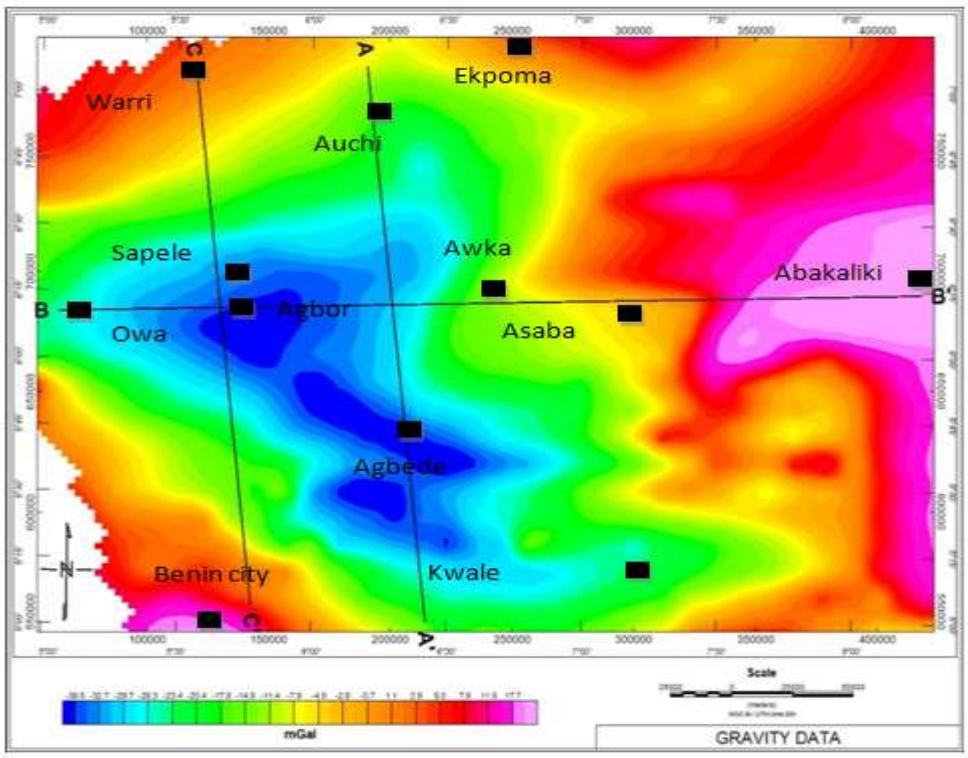

Figure 4.12 Bouguer gravity map with towns and locations of 2-D modelling profiles (A-A$^{|}$, B-B$^{|}$and C-C$^{|}$)

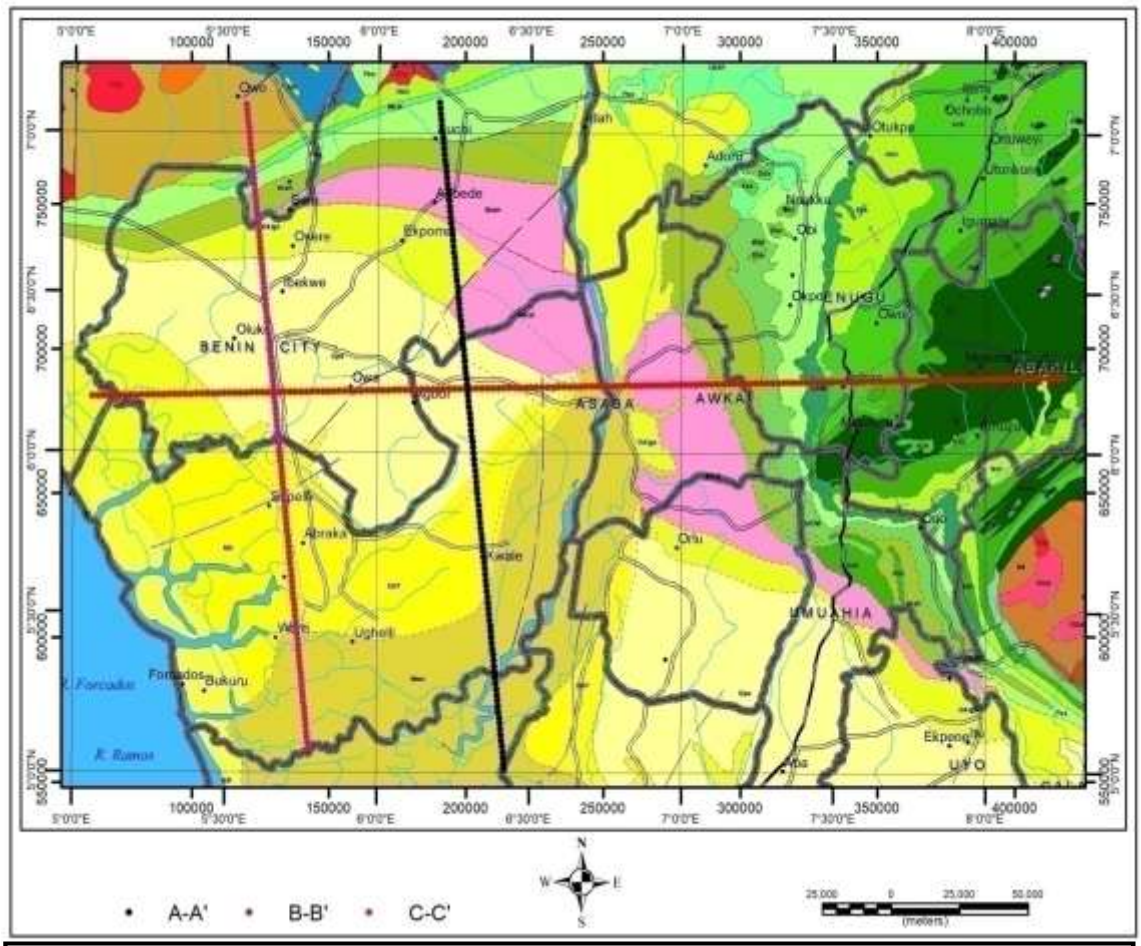

LEGEND

Sand and clay (Benin Formation)

Lignite, claystone and shale (Agbada formation)

Clay clayey sands and shale (Ilaro formation)

Clay and shale with limestone (Imo group)

Migmatite

Granite Gneiss

False bedded sandstone

Sandstones and clay

Undifferentiated schists

Figure 4.13: The Geology map of the study area with the model profiles A-A$^{|}$, B-B$^{|}$ and C-C$^{|}$.

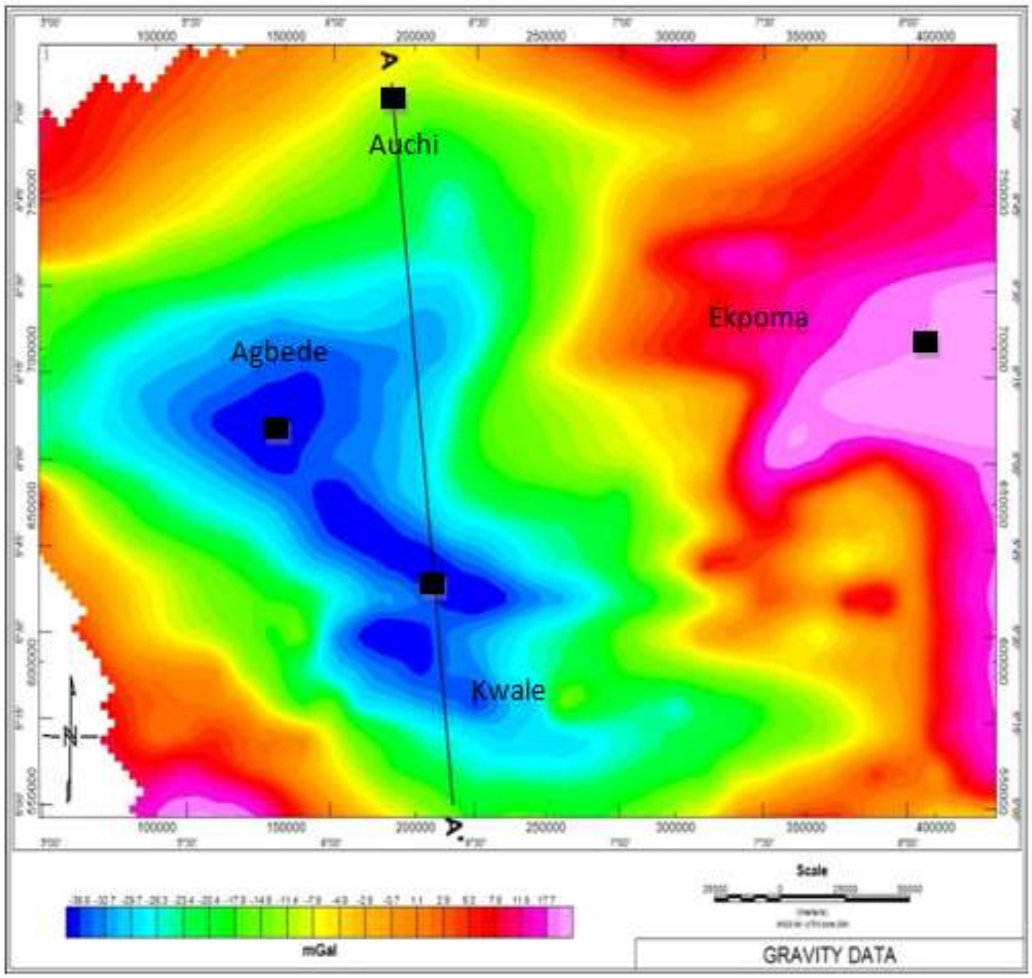

Figure 4.14: Bouguer gravity map of 2-D modelling profile A-A'.

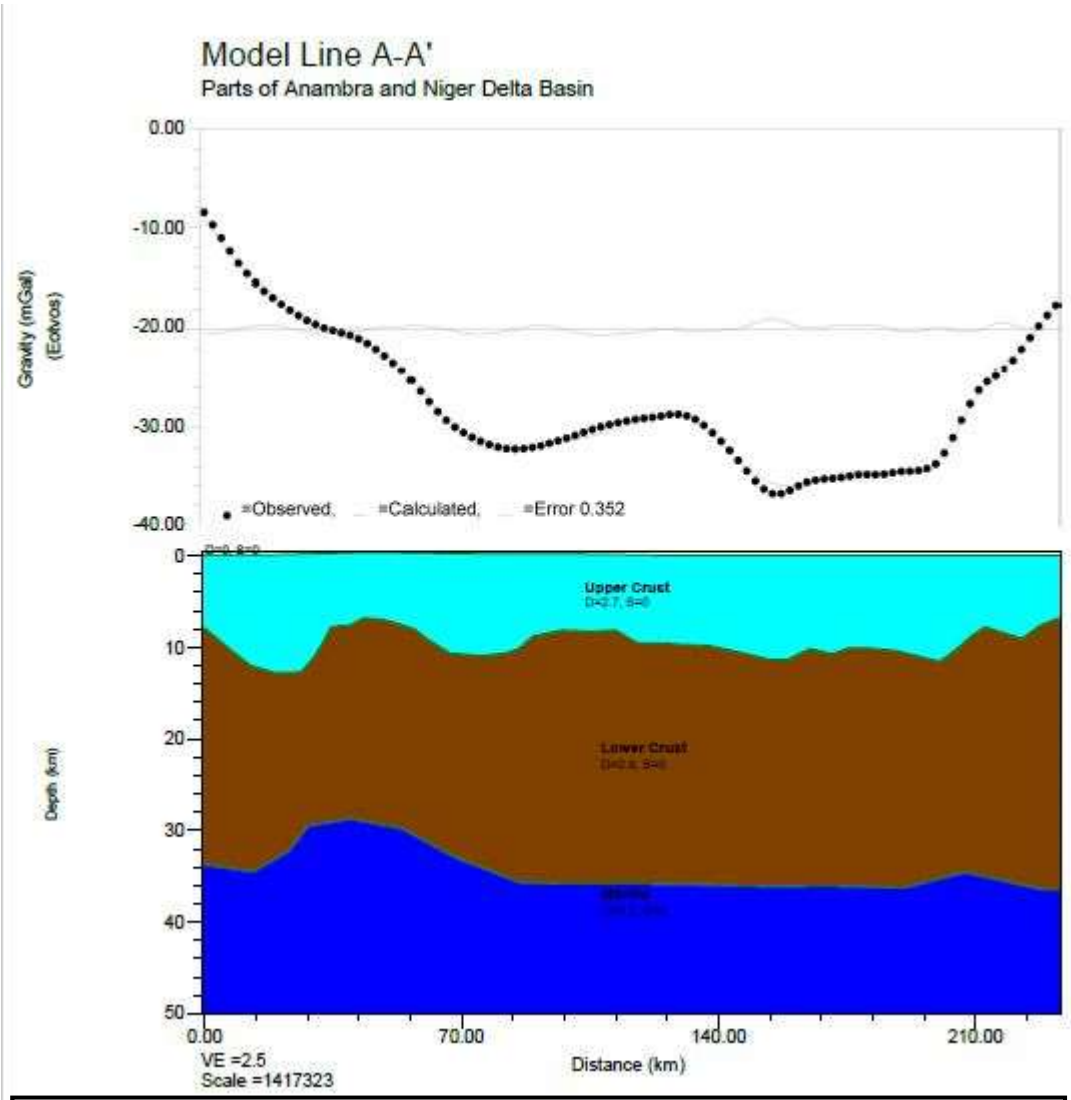

Figure 4.15: Crustal Modelling along Profile A-A'.

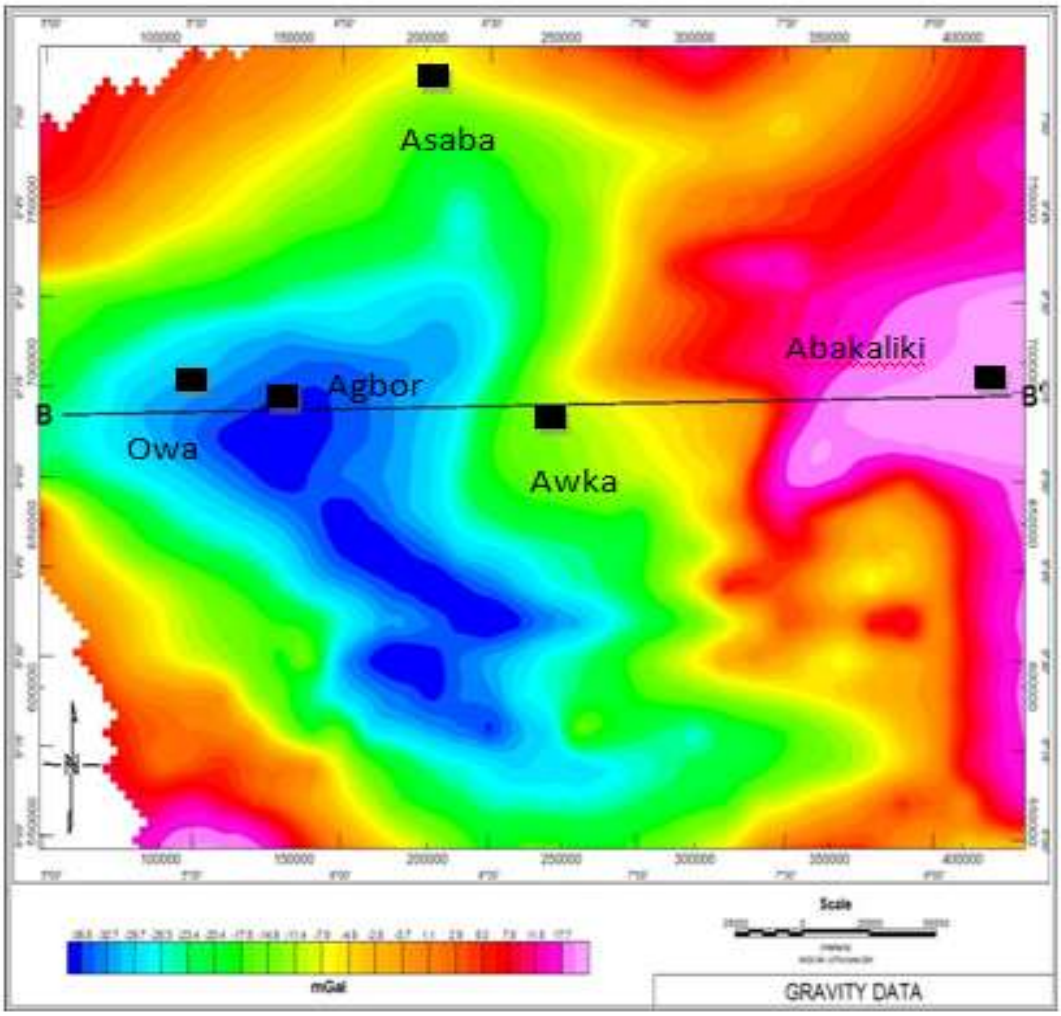

Figure 4.16: Bouguer gravity map of 2-D modelling profile B-B'.

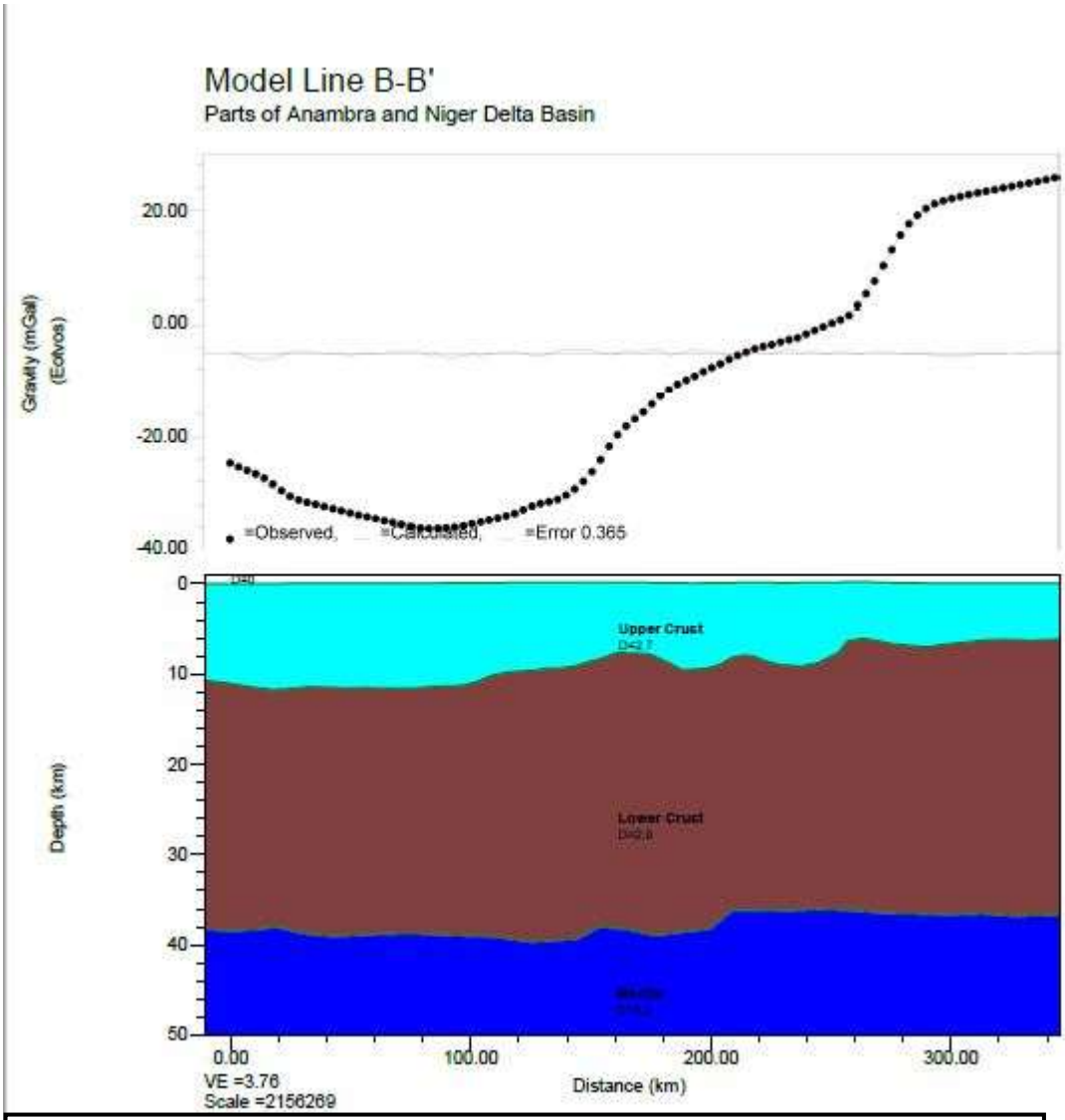

Figure 4.17: Crustal Modelling along Profile B-B'.

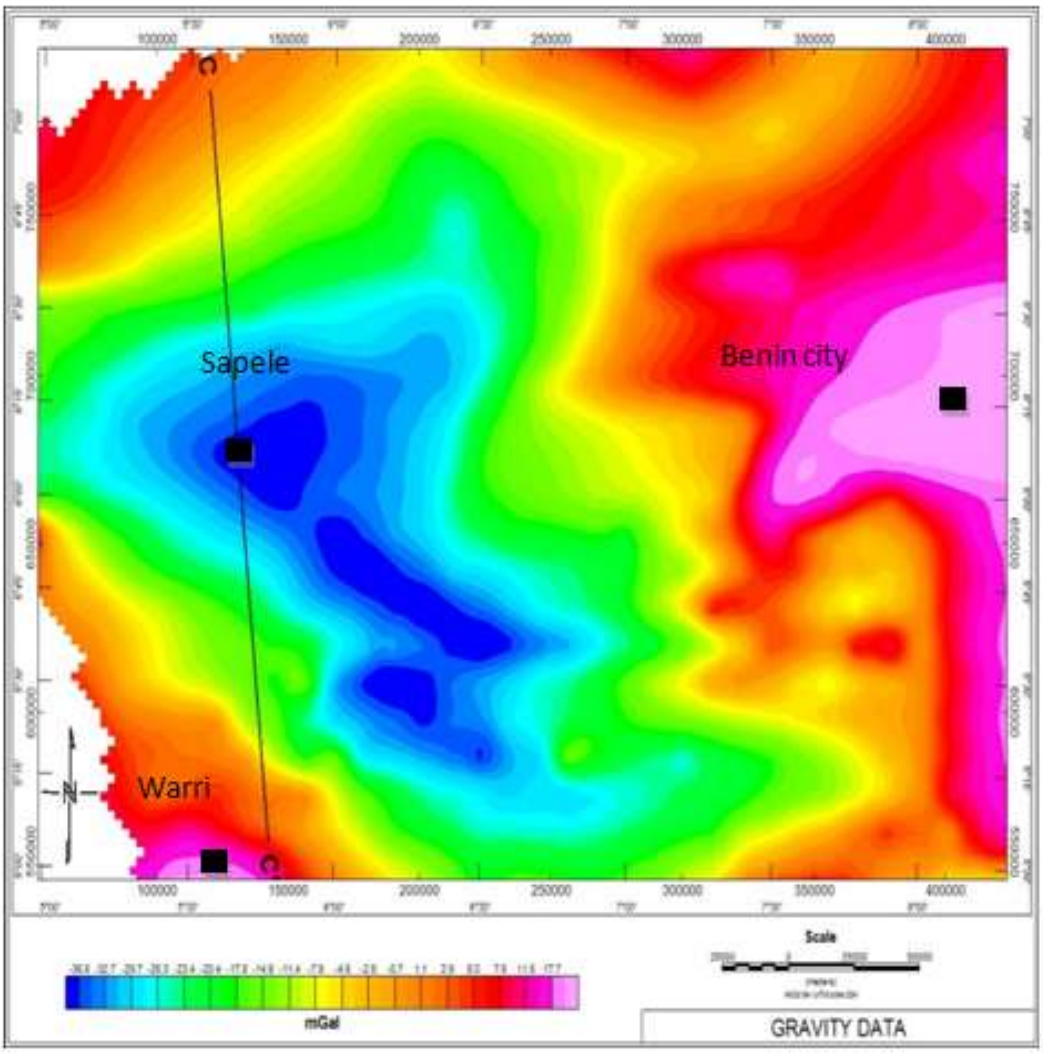

Figure 4.18: Bouguer gravity map of 2-D modelling profiles C-C[l.

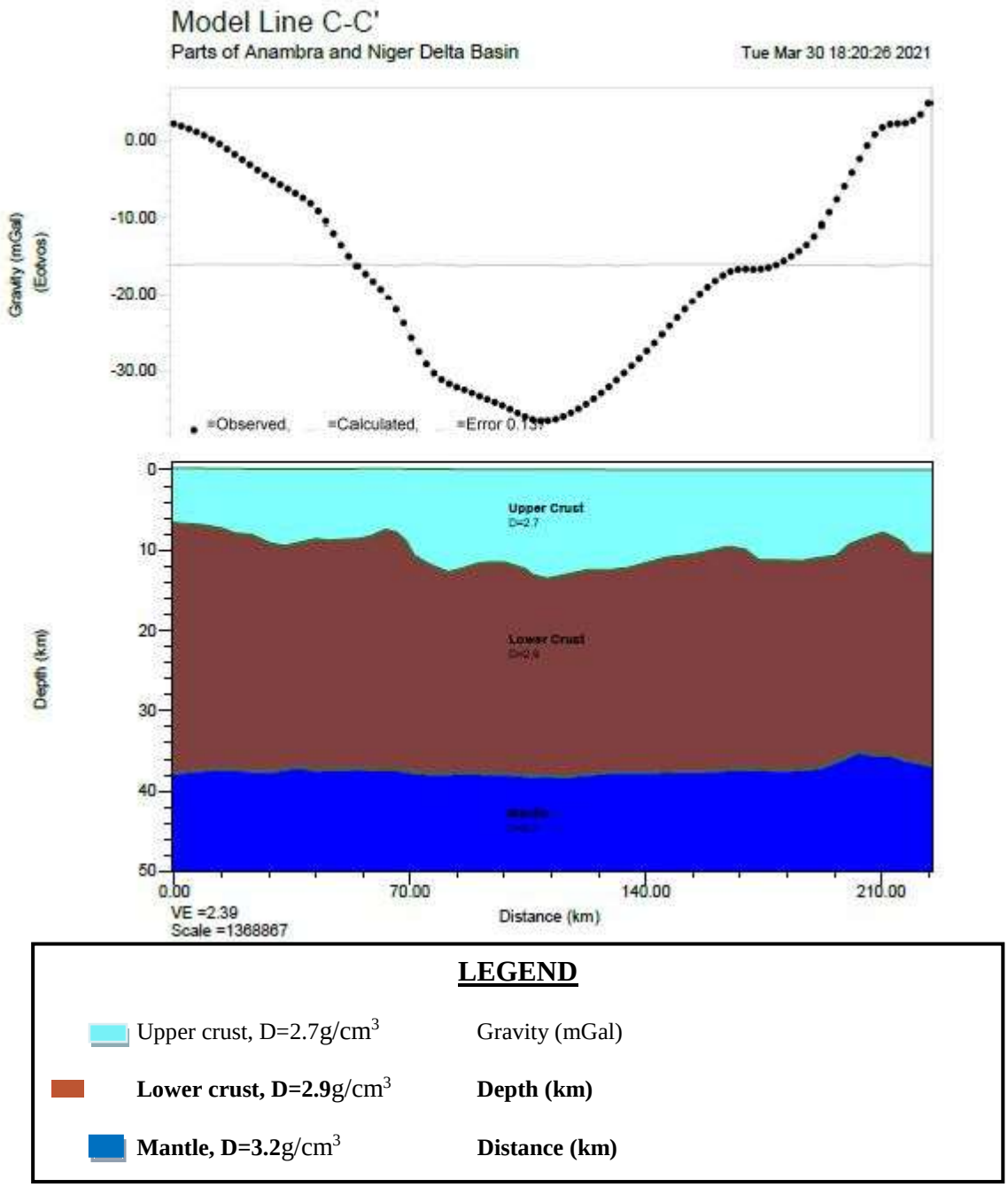

Figure 4.19: Crustal Modelling along Profile C-C'.

Table 4.5 Sample Results of Average crustal thickness obtained from 2-D modelling of 2D plot and 3D surface plot.(Complete result is shown in Appendix C)

LONGITUDE (Degree)	LATITUDE (Degree)	CRUSTAL THICKNESS(km)
6.22	7.08	-34
6.26	6.95	-35
6.63	6.62	-28
6.31	6.65	-29
6.37	6.95	-32
6.33	5.95	-34
6.32	5.94	-35
6.31	6.13	-35
6.23	5.88	-36
6.27	5.89	-35
6.33	5.97	-34
6.37	6.95	-33
6.22	5.89	-35
6.16	5.87	-36
6.22	5.89	-32
6.37	6.95	-34
6.63	6.62	-36
6.54	6.06	-38
5.12	6.26	-38
5.32	6.31	-37
5.42	6.31	-39
5.52	6.26	-38
5.55	6.28	-39
5.32	6.31	-37
5.19	6.28	-38
5.11	6.25	-39
5.27	5.84	-38
5.29	5.71	-39
5.29	5.61	-37
5.29	5.42	-36
5.22	5.73	-35
5.31	5.86	-36
5.35	5.85	-35
5.39	5.86	-38
5.11	6.25	-37
5.19	6.28	-39
5.66	7.14	-38

4.4.4 The average crustal thickness map of 2-D modelling Plot

The average crustal thickness map of 2-D modelling profile result using 2D plot in Figures 4.20 & 21 The basement depth to the deepest depth of 2D plot achieves its value of about 28 km to 39 km at the depth, this depth decreases gradually reaching its minimum value of 28 km at the shallow part it increases with an average maximum value of 39 km which trend toward the NW and minimum average value of -28km trending NE region of the study area. Depth to crust from this average 2D profile plot map can be said to approach its maximum thickness (deep) at the northward and westward and approach its minimum thickness (shallow) at northward and eastward region and also the basement to the depth of 2D plot achieves its maximum value of about 39 km. This depth decreases gradually reaching its minimum value of 28 km with a maximum average Crustal Thickness value of 39 km which trend toward the NW and minimum average value of 28 km trending NE region of the study area. Depth to crust from this average 2D profile plot map can be said to approach its maximum thickness at the northward and westward and approach its minimum thickness at northward and eastward region of the study area.

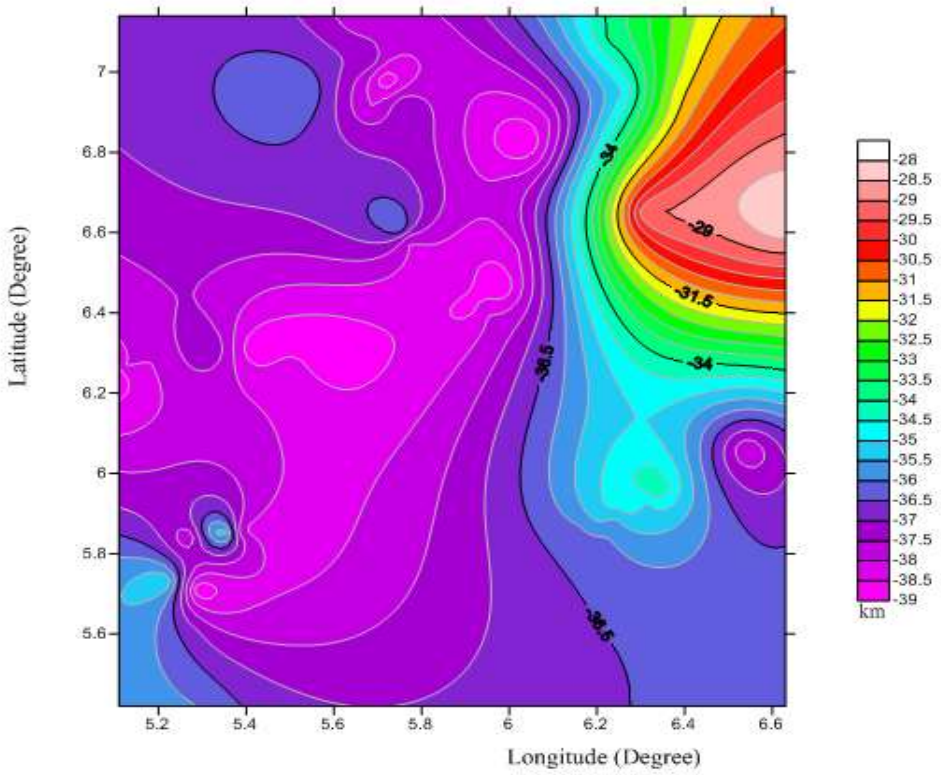

Figure 4.20: 2D profile plot of the crustal thickness obtained from 2D modeling of the study area

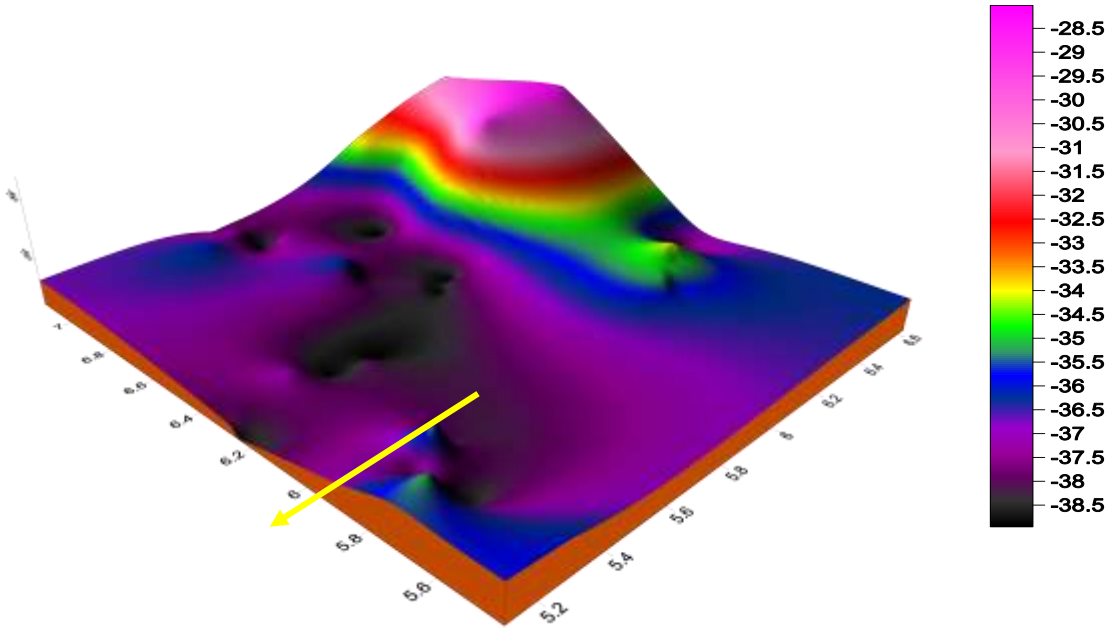

Figure 4.21: 3D Surface plot of the crustal thickness obtained from 2D modelling for the study area

4.5 Crustal Thickness and Plate Tectonism

The average crustal thickness parameters within the study area obtained from 2-D modelling profile plot below is ranging from minimum of 28.3 km to maximum of 38.3 km. Table 4.6 and 4.7 shows an average crustal thickness value of other study region and countries that have recently experience earthquake with their respective crustal thickness range. Comparison of the crustal thickness of the study area with the crustal thickness of some earthquake countries as shown in Table 4.8, it was observed that counties like India, China, Mexico, Japan and Congo have maximum crustal thickness above the obtained maximum crustal thickness for the study area and countries like Chad, Philippines, Indonesia and Libya are seen to have a minimum crustal thickness within the obtained value range for the study area. This can therefore mean that tectonic stability of an area is not characterized base on a crustal thickness of the area. Nigeria as a study area (Africa) lies far from the plate boundaries unlike Countries like Japan that lies in plate boundaries where tectonic activity occurs.

Nigeria's location also on the eastern part of the Atlantic Ocean which is not described by subduction tectonics and occurrence of devastating earthquakes gives an added advantage of being tectonically stable. Though earthquakes are determined by location on tectonic boundaries and not crustal thickness, yet, high crustal thickness within a tectonically stable zone may further enhance the tectonic stability of an area. For this study, the Study area can hence be said to be tectonically stable as it is located in a stable zone and the considerable crustal thickness the area has, gives the area an added advantage.

Table 4.6: Parameters deduced from Modelled gravity profiles (AA[1], BB[1] and CC[1])

Profile Number	Crustal Thickness (Km) Min.	Maximum	Density (g/cm^3) Upper crust	Lower crust	Density (g/cm^3) Mantle
AA[1]	29	37	2.7	2.9	3.2
BB[1]	28	39	2.7	2.9	3.2
CC[1]	28	39	2.7	2.9	3.2
Average	28.3	38.3	2.7	2.9	3.2

Table 4.7: Some earthquake countries, their Moho depth range, year of recent earthquake occurrence and earthquake magnitude on Richter's scale

Countries	Range of Crustal thickness (km)	Year of Recent earthquake occurrence	Magnitude on Richter's scale
Japan (Fukushima)	29 - 63	2021	2.9
Congo(Kinshasa)	46 - 92	2021	4.6
Libya(East Darnah)	35 - 37	2021	3.5
Mexico (Colima)	43 - 83	2021	4.0
Phillipines (Mamburao)	30 - 54	2021	2.1
Chad(Massakory)	35 - 54	2021	4.8
Indonesia(Sumatra)	32 - 52	2021	3.6
China (Xinjiang)	64 - 94	2021	4.6
Indian (Dehli)	177 - 289	2021	4.2

CHAPTER FIVE

5.0 CONCLUSION AND RECOMMENDATIONS

5.1 Conclusion

The results obtained from the interpretation of gravity data covering the study area based on empirical analysis, revealed that the study area have an average Crustal thickness ranges from 30 km to 37 km, while the spectral analysis revealed three major depths with an average crustal thickness ranges from 30.2 km to 35.6 km. The 2-D modelling, it showed the shape and variations in the Crustal thickness with a fit between the observed and calculated curves, and it depicts the upper and lower part of the profiles with an average crustal thickness of 28 km to 39 km. The study area has a good correlation in all the average crustal thicknesses obtained using the three different approaches. Based on these results, the Crustal thickness of the study area is made up of high crustal thickness (deepest depth) ranging from 30 km to 37 km, 30.2 to 35.6 km and 28 km to 39 km respectively and not located in any active plate boundaries (margins) which indicates that the region is tectonically stable in terms of volcanic eruption and earthquake activities.

5.2 Recommendations

It is recommended that seismic survey should be carried out so as to compare the result of both methods in the determination of crustal thickness of the study area.

REFERENCES

Abdullahi, M., Singh, U.K. &Roshan, R. (2019) Mapping magnetic lineaments and subsurface basement beneath parts of Lower Benue Trough (LBT), Nigeria: Insights from integrating gravity, magnetic andgeologic data. *J Earth SystSci*. 128,17.https://do.org/10.1007/s12040-018-1038-9

Abraham, E., Itumoh, O., Chukwu, C. & Onwe, R (2019) Geothermal Energy Reconnaissance of Southeastern Nigeria from Analysis of Aeromagnetic and Gravity Data. *PureAppl.Geophys.* 176, 1615–1638. https://doi.org/10.1007/s0 n0024-018-2028-1

Abraham, E.M., Nkitnam, E.E. &Itumoh, O.E. (2020) Integrated geophysical investigation of recent earth tremors in Nigeria using aeromagnetic and gravity data. *Environ Monit Assess*,192, 352. https://doi.org/10.1007/s10661-020-08339-6

Akiishi, M., Udochukwu, B.C. &Tyovenda, A.A. (2019) Determination of hydrocarbon potentials in Masu area northeastern Nigeria using forward and inverse modelingof aeromagnetic and aerogravitydata. *SN Appl.Sci*. 1, 911. https://doi.org/10.1007/s42452-019-0898-1

Ako, B. D., Ojo, S. B. , Okereke, C. S. , Fieberg, F. O. , Ajayi, T. R. , Adepelum, A. A. , &Afolayan, J. F. (2014) Observation from gravity / magnetic data interpretation of the Niger Delta. Nigeria *Association of Petroleum Exploration's bulletin*,13(1),50 – 69.

Akpan, O., Nyblade, A., Okereke, C., Oden, M., Emry, E., &Jordi, J., (2015).Crustal structure of Nigeria and Southern Ghana, West Africa from P-wave receiver functions. *Tectonophysics journal*, 2, 1-10.

Alaneme, K.K & Okotete, E.A. (2018).Critical evaluation of seismic activities in Africa and curtailment policies – a review. *Geoenviron Disasters*,5, 24. https://doi.org/10.1186/s40677-018-0116-2

Ali, Y. H., &Suardi, I. (2018).Moho Depth and Crustal Architecture beneath the Levant Basin from Global Gravity Field Model Geosciences, 8(6), 200; https://doi.org/10.3390/geosciences80602000

Balogun, O.B. (2019) Preliminary interpretation of isostatic residual gravity anomalies within the central portion of the Equatorial Atlantic African region. *SN Appl. Sci*. 1, 495. https://doi.org/10.1007/s42452-019-0440-5

Bansal, A. R., &Dimri, V. P. (2001).Depth Estimation from the scaling Power Spectral Density of n-stationary Gravity Profile.*Pure and applied Geophysics*, 158, 799-812

Begg, G.C., Griffin, W.L., Natapov, L.M., O'Reilly, S.Y., Grand, S.P., O'Neill, C.J., Hronsky, J.M. A., Djomani, Y.P., Swain, C.J., Deen, T., & Bowden, P (2009). The lithospheric architecture of Africa: seismic tomography, mantle petrology and tectonic evolution. Geosphere 5, 23–50.

Bilotti, F., Shaw, J. H., Cupich, R. M. & Lakings, R. M. (2005) Detachment fold, Niger Delta, in J. H. Shaw, C. Connors, and J. Suppe, eds., Seismic interpretation of contractionalfaultrelated folds*: AAPG Studies in Geology*,53,103–104.

Bilotti, Frank & Shaw, John. (2005). Deep-water Niger Delta fold and thrust belt modeled as a critical-taper wedge: The influence of elevated basal fluid pressure on structural styles. Aapg Bulletin - AAPG BULL. 89. 1475-1491. 10.1306/06130505002.

Bonde D.S., Udensi, E. E., Rai, J. k., Joshua, B. W., & Abbas, M. (2014). Basement Depth Estimates of Sokoto Sedimentary Basin, Northwestern Nigeria, using Spectral Depth Analysis. *Standard Global Journal of Geology and Explorational Research*, 1(4), 078-085.

Chikwendu, N.O.,&Diugo, O.I.(2011) Structural analysis of aeromagnetic data of part of Imo River basin, Southeastern Nigeria. *Natural and Applied Science Journal*;12(1):48-59.

Corredor, F., Shaw, J. H &Bilotti, F. (2005) Structural styles in the deepwater fold-and-thrust belts of the Niger Delta: *AAPG Bulletin*, 89, 6, 753–780.

Demenitskaya, R. M. (1958). Planetary structure and their reflection in Bougueranomalies.*Geology Bulletin*, 8, 52-62

Ekpa, M. M. M., Okeke, F. N., Ibuot, J. C., Obiora, D. N., &Abangwu, U. J. (2018). Investigation of gravity anomalies in parts of Niger Delta Region in Nigeria using aerogravitydata.*International Journal of Physical Sciences*, 13(4), 54-65.

Ekwok, S.E., Akpan, A.E. &Ebong, E.D. (2021) Assessment of crustal structures by gravity and magnetic methods in the Calabar Flank and adjoining areas of Southeastern Nigeria—a case study. *Arab J Geosci*,14, 308. https://doi.org/10.1007/s12517-021-06696-1

Emujakporue G., & Ofoha C. (2015) Spectral depth estimate of subsurface structures over parts of offshore Niger Delta, Niger. *The International Journal of Engineering and Science*.4(10),42-53.

Gomez-Ortiz, D., Tejero-Lopez, R., Babin-Vich, R., & Rivas-ponce, A. (2005). Crustal Density Structure in the Spanish central system derived from gravity data analysis (Central Spain). *Tectonophysics*, 327, 37-59

Hosper, J. (1965). Gravity field and structure of the Niger Delta, Nigeria, West Africa. Geol. Soc. Am. Bull. 76:407-4222.

Huismans, R., & Beaumont, C. (2011). Depth – dependent Extension, Two – Stage break up and CratonicUnderplating at Rifted Margins. *Nature*, 473, 74 – 78. Doi. 10./038/Nature 09988

Ikumbur, E. B., Onwuemesi, A. G., Anakwuba, E. K., Chinwuko, A. I., Usman, A.O. & Okonkwo, C. C. (2013) Spectral Analysis of Aeromagnetic Data over Part of the Southern Bidabasin,West-Central Nigeria. *International Journal of Fundamental Physical Sciences*. 3(2), 27-31.

Jørgensen, Bo Barker, Böttcher, Michael, E., Lüschen, Holger.,Neretin, Lev N, Volkov, & Igor, I (2004). Chemical composition and stable sulfur isotopes in sediment core KOT97-5GC. *PANGAEA*, https://doi.org/10.1594/PANGAEA.267348.

Lefort, J. P., &Agarwal, B. N. P. (2002). Topography of the Moho Undulations in France from Gravity data: their age and origin. *Tectonophysics*, 350, 193-213.

Matrinic, Z. (1994). The Minimum Depth of Compensation of Topographic masses.*Geophysical Journal International*, 117, 545 – 554

Mbah, David &Obiora, Daniel &Oha, Andrew &Terhemba, Bem&Ossai, Cornelius &Igwe, Emmanuel. (2017). Investigation of possible cause of gravity anomalies in parts of the Niger Delta Basin, Nigeria.*International Journal of physical sciences*. 12. 103-117.

Nafiz, M., Kenan, G., Yener, E., & Osman, B. (2008).Two& Three Dimensional Moho depth of the Eastern Pontides (NE TurkeyMarita, N. O. (2007)).*Turkish Journal of Earth Sciences*, 18(2009), 225-238

Nnange, J. M., Ngako, V., Fairhead, J. D. &Ebinger, C. J. (2000). Depths to density discontinuities beneath the Adamawa Plateau region, Central Africa, from spectral analysis of new and existing gravity data.*Journal of African Earth Sciences*, 30, 887-901.

Nwankwo, C. N., & C. Ene, E. (2020). Structural Investigation of Udi LGA of Enugu State, South Eastern Nigeria Using High Resolution Bouguer Gravity and Landsat Data. *Asian Journal of Research and Reviews in Physics*, *3*(1), 17-32. https://doi.org/10.9734/ajr2p/2020/v3i130112

Nyakundi, E., Githiri, J. & K'Orowe, M. (2020) Depth Estimation of Geothermal Heat Structures by Euler Deconvolution of Gravity Data at EburruArea, Kenya. *Journal of Geoscience and Environment Protection*, **8**, 148-158. doi: 10.4236/gep.2020.83011.

Obaje, N. G. (2009). Geology and Mineral Resources of Nigeria (Volume 120).Berlon (Germany),*Springer*. Retrieved from: http://dx.doi.org/10.1007/978-3-540-92685-6

Okiwelu, A.A., & Ude, I.A. (2012). 3D Modelling and Basement Tectonics of the Niger Delta Basin from Aeromagnetic Data, Tectonics - Recent Advances, *EvgeniiSharkov*, *IntechOpen*, DOI: 10.5772/48158. Available from: https://www.intechopen.com/books/tectonics-recent-advances/3d-modelling-and-basement-tectonics-of-the-niger-delta-basin-from-aeromagnetic-data

Okpoli, C. C. & Akingboye, A. S. (2020) Application of Airborne Gravimetry Data for Litho- Structural and Depth Characterisation of Precambrian Basement Rock (Northwestern Nigeria). *Geophysica*, 55(1–2), 3–21

Okpoli, C. C., & Akingboye, A. S. (2019) Application of high-resolution gravity data for litho- structural and depth characterisation around Igabi area, Northwestern Nigeria, *NRIAG Journal of Astronomy and Geophysics*,8,1, 231 241, DOI: 10.1080/20909977.2019.1689629

Okwesili., Agatha Ngozi, Okeke, Francisca Nneka & Orji, Prince Orji (2020) Geophysical survey of aerogravity anomalies over Lafia and Akiri regions of middle Benue trough, Nigeria, employing Power Spectrum and Source Parameter Imaging technique. *IOSR Journal of Applied Physics (IOSR-JAP)*, 12, 5,58-68

Ozawa, H. (2011). Phase Transition of FeO and Stratification in Earth's outer Core. *Science*, 334, 792-794

Parker. (1973). Fourier Transforms used to calculate the Magnetic or Gravitational anomaly caused by an unseen non- uniform layer of material. *Geophysical Journal International* 31 (4), 447-455

Philip, K., Michael, B., & Ian, H. (2002).An Introduction to Geophysical Exploration. First Edition (125-145). United Kingdom, Blackwell Science Press

Poudjom Djomani, Y. H., Diament M., & Albouy Y. (1992). Mechanical Behavior of the Lithosphere beneath the Adamawa Uplift (Cameroun, West Africa) based on Gravity data. *Journal of African Earth Sciences*, 15, 81-90

Sunday, O., & Samuel B. (2013) Basement architecture in part of the Niger Delta from aeromagnetic data and its implication for hydrocarbon prospectively.*The pacific Journal of Science and Technology*. 14(2):512-521.

Sutra, E., & Manatschal, G. (2012). How does the Continental crust thin in a hyper extended rifted margin? Insights from the Iberia margin. *Geology*, 40, 139-142

Tealeb, A., & Riad, S. (1986). Investigation of gravity anomalies of western Sudia Arabia and their geological significance. Proceed of the5^{th} Anniversary Meeting of E. G. S. Cairo, 50-89

Tegbe, O. O., & Akaegbobi, I. M. (2000) Reservoir heterogeneities as a controlling factor to abnormal production performance of the oilfield. Y. N E, Niger Delta. *Bulletin of Nigerian Association Petroleum Explorationists*, 15 (1), 81- 91.

Telford, W. M., Geldert, L. P., Sheriff, R. E., &Kets, D. A. (1980). Applied Geophysics Cambridge University, Press London: page 860

Udensi, E. E. (2000). Estimation of the Moho depth of the Minna Area using Bouguer Gravity Anomaly data. *Journal of Science, Technology and Mathematics Education (JOSMED)*, 3(1), 10-18

Udensi, E. E. (2001). Basement Depth Estimates of Sokoto Sedimentary basin, North western Nigeria, using Spectral Depth Analysis. *International Journal of Engineering and Science*, 3(6), 10-14

Udensi, E. E., & Osazuwa, I. B. (2002). Two and Half dimensional Modelling of the Major structures underlying the Nupe Basin, Nigeria using Aeromagnetic data. *Nigeria Journal of Physics*, 14(1), 55-61.

Woolard, G. P. (1959). Regional variation in gravity, in the Earth's crust and upper Mantle.*Journal of Geophysics,* 13, 320

Woolard, G. P., & Strange, W. E. (1962). Gravity anomalies and Crust of the Earth in the Pacific Basin: The crust of the Pacific basin Geophysical monograph, *Journal of Geophysics*, 67, 6-12

Yakubu, Tahir A. Ofonime U Akpan, Monday A.Isogun, Abraham A Adepelumi, Chiedu S Okeke, Adetola S (2014). An evaluation of earthquake and its implication for understanding the seismotectonic of south western Nigeria. *Open Journal of Geology* 4 (10), 542, 2014

APPENDIX A

Results showing the empirical calculations carried out on the study area.

LONG.	LAT	Z	HD	HW	HWS	A=(HD+HW+HWS)/3
5	5		35	32	31.84978	32.94992533
5.1	5		35	32	31.84978	32.94992533
5.2	5		35	32	31.84978	32.94992533
5.3	5		35	32	31.84978	32.94992533
5.4	5		35	32	31.84978	32.94992533
5.5	5	20	32.41001	30.4	29.69901	30.8363395
5.6	5	19	32.53951	30.48	29.80426	30.94125781
5.7	5	17	32.79851	30.64	30.01553	31.15134603
5.8	5	10	33.70501	31.2	30.76268	31.88922873
5.9	5	4	34.482	31.68	31.41226	32.52475483
6	5	0	35	32	31.84978	32.94992533
6.1	5	-4	35.518	32.32	32.29069	33.37622935
6.2	5	-8	36.036	32.64	32.73486	33.80361725
6.3	5	-12	36.55399	32.96	33.18212	34.23203774
6.4	5	-16	37.07199	33.28	33.63232	34.66143794
6.5	5	-20	37.58999	33.6	34.0853	35.09176342
6.6	5	-19	37.46049	33.52	33.97181	34.98409834
6.7	5	-19	37.46049	33.52	33.97181	34.98409834
6.8	5	-20	37.58999	33.6	34.0853	35.09176342
6.9	5	-20	37.58999	33.6	34.0853	35.09176342
7	5	-18	37.33099	33.44	33.85848	34.87648848
7.1	5	-16	37.07199	33.28	33.63232	34.66143794
7.2	5	-12	36.55399	32.96	33.18212	34.23203774
7.3	5	-9	36.16549	32.72	32.84639	33.91062761
7.4	5	-3	35.3885	32.24	32.18015	33.26954977
7.5	5	0	35	32	31.84978	32.94992533
7.6	5	2	34.741	31.84	31.63058	32.73719535
7.7	5	3	34.6115	31.76	31.52131	32.63093854
7.8	5	3	34.6115	31.76	31.52131	32.63093854
7.9	5	1	34.8705	31.92	31.74007	32.84352454
8	5	0	35	32	31.84978	32.94992533
8.1	5	-3	35.3885	32.24	32.18015	33.26954977
8.2	5	-2	35.259	32.16	32.06982	33.16293872
8.3	5	-1	35.1295	32.08	31.95969	33.05639698
5	5.1		35	32	31.84978	32.94992533

5.1	5.1		35	32	31.84978	32.94992533
5.2	5.1		35	32	31.84978	32.94992533
5.3	5.1		35	32	31.84978	32.94992533
5.4	5.1		35	32	31.84978	32.94992533
5.5	5.1	12	33.44601	31.04	30.54801	31.67800424
5.6	5.1	8	33.964	31.36	30.97829	32.10076574
5.7	5.1	4	34.482	31.68	31.41226	32.52475483
5.8	5.1	2	34.741	31.84	31.63058	32.73719535
5.9	5.1	-1	35.1295	32.08	31.95969	33.05639698
6	5.1	-5	35.6475	32.4	32.40143	33.48297669
6.1	5.1	-10	36.29499	32.8	32.95811	34.01770169
6.2	5.1	-17	37.20149	33.36	33.74531	34.76893472
6.3	5.1	-20	37.58999	33.6	34.0853	35.09176342
6.4	5.1	-22	37.84899	33.76	34.31278	35.30725574
6.5	5.1	-25	38.23749	34	34.65517	35.63088621
6.6	5.1	-25	38.23749	34	34.65517	35.63088621
6.7	5.1	-26	38.36698	34.08	34.76961	35.73886395
6.8	5.1	-26	38.36698	34.08	34.76961	35.73886395
6.9	5.1	-25	38.23749	34	34.65517	35.63088621
7	5.1	-23	37.97849	33.84	34.42676	35.4150812
7.1	5.1	-21	37.71949	33.68	34.19896	35.19948286
7.2	5.1	-20	37.58999	33.6	34.0853	35.09176342
7.3	5.1	-18	37.33099	33.44	33.85848	34.87648848
7.4	5.1	-10	36.29499	32.8	32.95811	34.01770169
7.5	5.1	-8	36.036	32.64	32.73486	33.80361725
7.6	5.1	-4	35.518	32.32	32.29069	33.37622935
7.7	5.1	-2	35.259	32.16	32.06982	33.16293872
7.8	5.1	2	34.741	31.84	31.63058	32.73719535
7.9	5.1	5	34.3525	31.6	31.30343	32.41864496
8	5.1	3	34.6115	31.76	31.52131	32.63093854
8.1	5.1	0	35	32	31.84978	32.94992533
8.2	5.1	8	33.964	31.36	30.97829	32.10076574
8.3	5.1	13	33.31651	30.96	30.44103	31.57251091
5	5.2		35	32	31.84978	32.94992533
5.1	5.2		35	32	31.84978	32.94992533
5.2	5.2		35	32	31.84978	32.94992533
5.3	5.2		35	32	31.84978	32.94992533
5.4	5.2	2	34.741	31.84	31.63058	32.73719535
5.5	5.2	3	34.6115	31.76	31.52131	32.63093854

5.6	5.2	5	34.3525	31.6	31.30343	32.41864496
5.7	5.2	3	34.6115	31.76	31.52131	32.63093854
5.8	5.2	2	34.741	31.84	31.63058	32.73719535
5.9	5.2	1	34.8705	31.92	31.74007	32.84352454
6	5.2	-8	36.036	32.64	32.73486	33.80361725
6.1	5.2	-16	37.07199	33.28	33.63232	34.66143794
6.2	5.2	-20	37.58999	33.6	34.0853	35.09176342
6.3	5.2	-24	38.10799	33.92	34.54089	35.52295832
6.4	5.2	-26	38.36698	34.08	34.76961	35.73886395
6.5	5.2	-28	38.62598	34.24	34.99891	35.95496536
6.6	5.2	-30	38.88498	34.4	35.22878	36.17125519
6.7	5.2	-29	38.75548	34.32	35.11378	36.06308719
6.8	5.2	-30	38.88498	34.4	35.22878	36.17125519
6.9	5.2	-28	38.62598	34.24	34.99891	35.95496536
7	5.2	-26	38.36698	34.08	34.76961	35.73886395
7.1	5.2	-24	38.10799	33.92	34.54089	35.52295832
7.2	5.2	-22	37.84899	33.76	34.31278	35.30725574
7.3	5.2	-21	37.71949	33.68	34.19896	35.19948286
7.4	5.2	-20	37.58999	33.6	34.0853	35.09176342
7.5	5.2	-16	37.07199	33.28	33.63232	34.66143794
7.6	5.2	-14	36.81299	33.12	33.40686	34.44661874
7.7	5.2	-12	36.55399	32.96	33.18212	34.23203774
7.8	5.2	-8	36.036	32.64	32.73486	33.80361725
7.9	5.2	-4	35.518	32.32	32.29069	33.37622935
8	5.2	0	35	32	31.84978	32.94992533
8.1	5.2	8	33.964	31.36	30.97829	32.10076574
8.2	5.2	12	33.44601	31.04	30.54801	31.67800424
8.3	5.2	16	32.92801	30.72	30.12153	31.25651466
5	5.3		35	32	31.84978	32.94992533
5.1	5.3		35	32	31.84978	32.94992533
5.2	5.3		35	32	31.84978	32.94992533
5.3	5.3		35	32	31.84978	32.94992533
5.4	5.3	3	34.6115	31.76	31.52131	32.63093854
5.5	5.3	2	34.741	31.84	31.63058	32.73719535
5.6	5.3	1	34.8705	31.92	31.74007	32.84352454
5.7	5.3	-1	35.1295	32.08	31.95969	33.05639698
5.8	5.3	-11	36.42449	32.88	33.07002	34.12483868
5.9	5.3	-20	37.58999	33.6	34.0853	35.09176342
6	5.3	-15	36.94249	33.2	33.51951	34.55399899

6.1	5.3	-29	38.75548	34.32	35.11378	36.06308719
6.2	5.3	-30	38.88498	34.4	35.22878	36.17125519
6.3	5.3	-32	39.14398	34.56	35.4592	36.38772598
6.4	5.3	-34	39.40298	34.72	35.69013	36.60437025
6.5	5.3	-36	39.66198	34.88	35.92156	36.8211804
6.6	5.3	-32	39.14398	34.56	35.4592	36.38772598
6.7	5.3	-30	38.88498	34.4	35.22878	36.17125519
6.8	5.3	-15	36.94249	33.2	33.51951	34.55399899
6.9	5.3	-19	37.46049	33.52	33.97181	34.98409834
7	5.3	-22	37.84899	33.76	34.31278	35.30725574
7.1	5.3	-24	38.10799	33.92	34.54089	35.52295832
7.2	5.3	-26	38.36698	34.08	34.76961	35.73886395
7.3	5.3	-22	37.84899	33.76	34.31278	35.30725574
7.4	5.3	-20	37.58999	33.6	34.0853	35.09176342
7.5	5.3	-18	37.33099	33.44	33.85848	34.87648848
7.6	5.3	-14	36.81299	33.12	33.40686	34.44661874
7.7	5.3	-11	36.42449	32.88	33.07002	34.12483868
7.8	5.3	-7	35.9065	32.56	32.62352	33.69667144
7.9	5.3	-3	35.3885	32.24	32.18015	33.26954977
8	5.3	0	35	32	31.84978	32.94992533
8.1	5.3	6	34.223	31.52	31.19483	32.31260968
8.2	5.3	12	33.44601	31.04	30.54801	31.67800424
8.3	5.3	18	32.66901	30.56	29.90977	31.0462602
5	5.4		35	32	31.84978	32.94992533
5.1	5.4		35	32	31.84978	32.94992533
5.2	5.4		35	32	31.84978	32.94992533
5.3	5.4		35	32	31.84978	32.94992533
5.4	5.4	1	34.8705	31.92	31.74007	32.84352454
5.5	5.4	0	35	32	31.84978	32.94992533
5.6	5.4	0	35	32	31.84978	32.94992533
5.7	5.4	-12	36.55399	32.96	33.18212	34.23203774
5.8	5.4	-16	37.07199	33.28	33.63232	34.66143794
5.9	5.4	-24	38.10799	33.92	34.54089	35.52295832
6	5.4	-30	38.88498	34.4	35.22878	36.17125519
6.1	5.4	-32	39.14398	34.56	35.4592	36.38772598
6.2	5.4	-34	39.40298	34.72	35.69013	36.60437025
6.3	5.4	-36	39.66198	34.88	35.92156	36.8211804
6.4	5.4	-34	39.40298	34.72	35.69013	36.60437025
6.5	5.4	-33	39.27348	34.64	35.5746	36.49602691

6.6	5.4	-28	38.62598	34.24	34.99891	35.95496536
6.7	5.4	-26	38.36698	34.08	34.76961	35.73886395
6.8	5.4	-23	37.97849	33.84	34.42676	35.4150812
6.9	5.4	-21	37.71949	33.68	34.19896	35.19948286
7	5.4	-18	37.33099	33.44	33.85848	34.87648848
7.1	5.4	-16	37.07199	33.28	33.63232	34.66143794
7.2	5.4	-14	36.81299	33.12	33.40686	34.44661874
7.3	5.4	-12	36.55399	32.96	33.18212	34.23203774
7.4	5.4	-10	36.29499	32.8	32.95811	34.01770169
7.5	5.4	-8	36.036	32.64	32.73486	33.80361725
7.6	5.4	-6	35.777	32.48	32.51238	33.58979098
7.7	5.4	-4	35.518	32.32	32.29069	33.37622935
7.8	5.4	-2	35.259	32.16	32.06982	33.16293872
7.9	5.4	-1	35.1295	32.08	31.95969	33.05639698
8	5.4	0	35	32	31.84978	32.94992533
8.1	5.4	7	34.0935	31.44	31.08644	32.2066497
8.2	5.4	13	33.31651	30.96	30.44103	31.57251091
8.3	5.4	19	32.53951	30.48	29.80426	30.94125781
5	5.5		35	32	31.84978	32.94992533
5.1	5.5		35	32	31.84978	32.94992533
5.2	5.5		35	32	31.84978	32.94992533
5.3	5.5	-3	35.3885	32.24	32.18015	33.26954977
5.4	5.5	-6	35.777	32.48	32.51238	33.58979098
5.5	5.5	-9	36.16549	32.72	32.84639	33.91062761
5.6	5.5	-12	36.55399	32.96	33.18212	34.23203774
5.7	5.5	-15	36.94249	33.2	33.51951	34.55399899
5.8	5.5	-19	37.46049	33.52	33.97181	34.98409834
5.9	5.5	-15	36.94249	33.2	33.51951	34.55399899
6	5.5	-32	39.14398	34.56	35.4592	36.38772598
6.1	5.5	-36	39.66198	34.88	35.92156	36.8211804
6.2	5.5	-38	39.92098	35.04	36.15347	37.03814878
6.3	5.5	-36	39.66198	34.88	35.92156	36.8211804
6.4	5.5	-34	39.40298	34.72	35.69013	36.60437025
6.5	5.5	-32	39.14398	34.56	35.4592	36.38772598
6.6	5.5	-30	38.88498	34.4	35.22878	36.17125519
6.7	5.5	-26	38.36698	34.08	34.76961	35.73886395
6.8	5.5	-24	38.10799	33.92	34.54089	35.52295832
6.9	5.5	-20	37.58999	33.6	34.0853	35.09176342
7	5.5	-16	37.07199	33.28	33.63232	34.66143794

7.1	5.5	-10	36.29499	32.8	32.95811	34.01770169
7.2	5.5	-6	35.777	32.48	32.51238	33.58979098
7.3	5.5	-1	35.1295	32.08	31.95969	33.05639698
7.4	5.5	0	35	32	31.84978	32.94992533
7.5	5.5	-2	35.259	32.16	32.06982	33.16293872
7.6	5.5	-6	35.777	32.48	32.51238	33.58979098
7.7	5.5	-8	36.036	32.64	32.73486	33.80361725
7.8	5.5	-4	35.518	32.32	32.29069	33.37622935
7.9	5.5	-2	35.259	32.16	32.06982	33.16293872
8	5.5	0	35	32	31.84978	32.94992533
8.1	5.5	6	34.223	31.52	31.19483	32.31260968
8.2	5.5	12	33.44601	31.04	30.54801	31.67800424
8.3	5.5	18	32.66901	30.56	29.90977	31.0462602
5	5.6		35	32	31.84978	32.94992533
5.1	5.6		35	32	31.84978	32.94992533
5.2	5.6		35	32	31.84978	32.94992533
5.3	5.6	-4	35.518	32.32	32.29069	33.37622935
5.4	5.6	-7	35.9065	32.56	32.62352	33.69667144
5.5	5.6	-11	36.42449	32.88	33.07002	34.12483868
5.6	5.6	-14	36.81299	33.12	33.40686	34.44661874
5.7	5.6	-16	37.07199	33.28	33.63232	34.66143794
5.8	5.6	-18	37.33099	33.44	33.85848	34.87648848
5.9	5.6	-20	37.58999	33.6	34.0853	35.09176342
6	5.6	-26	38.36698	34.08	34.76961	35.73886395
6.1	5.6	-30	38.88498	34.4	35.22878	36.17125519
6.2	5.6	-32	39.14398	34.56	35.4592	36.38772598
6.3	5.6	-34	39.40298	34.72	35.69013	36.60437025
6.4	5.6	-36	39.66198	34.88	35.92156	36.8211804
6.5	5.6	-38	39.92098	35.04	36.15347	37.03814878
6.6	5.6	-36	39.66198	34.88	35.92156	36.8211804
6.7	5.6	-34	39.40298	34.72	35.69013	36.60437025
6.8	5.6	-32	39.14398	34.56	35.4592	36.38772598
6.9	5.6	-28	38.62598	34.24	34.99891	35.95496536
7	5.6	-24	38.10799	33.92	34.54089	35.52295832
7.1	5.6	-21	37.71949	33.68	34.19896	35.19948286
7.2	5.6	-16	37.07199	33.28	33.63232	34.66143794
7.3	5.6	-10	36.29499	32.8	32.95811	34.01770169
7.4	5.6	-4	35.518	32.32	32.29069	33.37622935
7.5	5.6	4	34.482	31.68	31.41226	32.52475483

7.6	5.6	2	34.741	31.84	31.63058	32.73719535
7.7	5.6	0	35	32	31.84978	32.94992533
7.8	5.6	8	33.964	31.36	30.97829	32.10076574
7.9	5.6	10	33.70501	31.2	30.76268	31.88922873
8	5.6	0	35	32	31.84978	32.94992533
8.1	5.6	7	34.0935	31.44	31.08644	32.2066497
8.2	5.6	14	33.18701	30.88	30.33429	31.46709776
8.3	5.6	19	32.53951	30.48	29.80426	30.94125781
5	4.9		35	32	31.84978	32.94992533
5.1	5.7		35	32	31.84978	32.94992533
5.2	5.7	-3	35.3885	32.24	32.18015	33.26954977
5.3	5.7	-7	35.9065	32.56	32.62352	33.69667144
5.4	5.7	-10	36.29499	32.8	32.95811	34.01770169
5.5	5.7	-14	36.81299	33.12	33.40686	34.44661874
5.6	5.7	-17	37.20149	33.36	33.74531	34.76893472
5.7	5.7	-20	37.58999	33.6	34.0853	35.09176342
5.8	5.7	-25	38.23749	34	34.65517	35.63088621
5.9	5.7	-30	38.88498	34.4	35.22878	36.17125519
6	5.7	-32	39.14398	34.56	35.4592	36.38772598
6.1	5.7	-34	39.40298	34.72	35.69013	36.60437025
6.2	5.7	-36	39.66198	34.88	35.92156	36.8211804
6.3	5.7	-38	39.92098	35.04	36.15347	37.03814878
6.4	5.7	-36	39.66198	34.88	35.92156	36.8211804
6.5	5.7	-34	39.40298	34.72	35.69013	36.60437025
6.6	5.7	-31	39.01448	34.48	35.34392	36.27946843
6.7	5.7	-27	38.49648	34.16	34.88419	35.84689064
6.8	5.7	-25	38.23749	34	34.65517	35.63088621
6.9	5.7	-23	37.97849	33.84	34.42676	35.4150812
7	5.7	-19	37.46049	33.52	33.97181	34.98409834
7.1	5.7	-12	36.55399	32.96	33.18212	34.23203774
7.2	5.7	-5	35.6475	32.4	32.40143	33.48297669
7.3	5.7	7	34.0935	31.44	31.08644	32.2066497
7.4	5.7	5	34.3525	31.6	31.30343	32.41864496
7.5	5.7	3	34.6115	31.76	31.52131	32.63093854
7.6	5.7	-1	35.1295	32.08	31.95969	33.05639698
7.7	5.7	-5	35.6475	32.4	32.40143	33.48297669
7.8	5.7	-7	35.9065	32.56	32.62352	33.69667144
7.9	5.7	-3	35.3885	32.24	32.18015	33.26954977
8	5.7	0	35	32	31.84978	32.94992533

8.1	5.7	8	33.964	31.36	30.97829	32.10076574
8.2	5.7	13	33.31651	30.96	30.44103	31.57251091
8.3	5.7	18	32.66901	30.56	29.90977	31.0462602
5	5.8		35	32	31.84978	32.94992533
5.1	5.8	-4	35.518	32.32	32.29069	33.37622935
5.2	5.8	-9	36.16549	32.72	32.84639	33.91062761
5.3	5.8	-15	36.94249	33.2	33.51951	34.55399899
5.4	5.8	-19	37.46049	33.52	33.97181	34.98409834
5.5	5.8	-22	37.84899	33.76	34.31278	35.30725574
5.6	5.8	-24	38.10799	33.92	34.54089	35.52295832
5.7	5.8	-26	38.36698	34.08	34.76961	35.73886395
5.8	5.8	-29	38.75548	34.32	35.11378	36.06308719
5.9	5.8	-33	39.27348	34.64	35.5746	36.49602691
6	5.8	-36	39.66198	34.88	35.92156	36.8211804
6.1	5.8	-38	39.92098	35.04	36.15347	37.03814878
6.2	5.8	-36	39.66198	34.88	35.92156	36.8211804
6.3	5.8	-34	39.40298	34.72	35.69013	36.60437025
6.4	5.8	-30	38.88498	34.4	35.22878	36.17125519
6.5	5.8	-29	38.75548	34.32	35.11378	36.06308719
6.6	5.8	-27	38.49648	34.16	34.88419	35.84689064
6.7	5.8	-25	38.23749	34	34.65517	35.63088621
6.8	5.8	-24	38.10799	33.92	34.54089	35.52295832
6.9	5.8	-22	37.84899	33.76	34.31278	35.30725574
7	5.8	-20	37.58999	33.6	34.0853	35.09176342
7.1	5.8	-14	36.81299	33.12	33.40686	34.44661874
7.2	5.8	-12	36.55399	32.96	33.18212	34.23203774
7.3	5.8	-6	35.777	32.48	32.51238	33.58979098
7.4	5.8	2	34.741	31.84	31.63058	32.73719535
7.5	5.8	6	34.223	31.52	31.19483	32.31260968
7.6	5.8	4	34.482	31.68	31.41226	32.52475483
7.7	5.8	-1	35.1295	32.08	31.95969	33.05639698
7.8	5.8	-2	35.259	32.16	32.06982	33.16293872
7.9	5.8	-4	35.518	32.32	32.29069	33.37622935
8	5.8	0	35	32	31.84978	32.94992533
8.1	5.8	7	34.0935	31.44	31.08644	32.2066497
8.2	5.8	12	33.44601	31.04	30.54801	31.67800424
8.3	5.8	18	32.66901	30.56	29.90977	31.0462602
5	5.9	0	35	32	31.84978	32.94992533
5.1	5.9	-8	36.036	32.64	32.73486	33.80361725

5.2	5.9	-16	37.07199	33.28	33.63232	34.66143794
5.3	5.9	-20	37.58999	33.6	34.0853	35.09176342
5.4	5.9	-24	38.10799	33.92	34.54089	35.52295832
5.5	5.9	-27	38.49648	34.16	34.88419	35.84689064
5.6	5.9	-29	38.75548	34.32	35.11378	36.06308719
5.7	5.9	-31	39.01448	34.48	35.34392	36.27946843
5.8	5.9	-33	39.27348	34.64	35.5746	36.49602691
5.9	5.9	-35	39.53248	34.8	35.80579	36.71275506
6	5.9	-37	39.79148	34.96	36.03746	36.92964529
6.1	5.9	-35	39.53248	34.8	35.80579	36.71275506
6.2	5.9	-32	39.14398	34.56	35.4592	36.38772598
6.3	5.9	-30	38.88498	34.4	35.22878	36.17125519
6.4	5.9	-26	38.36698	34.08	34.76961	35.73886395
6.5	5.9	-23	37.97849	33.84	34.42676	35.4150812
6.6	5.9	-20	37.58999	33.6	34.0853	35.09176342
6.7	5.9	-20	37.58999	33.6	34.0853	35.09176342
6.8	5.9	-19	37.46049	33.52	33.97181	34.98409834
6.9	5.9	-18	37.33099	33.44	33.85848	34.87648848
7	5.9	-20	37.58999	33.6	34.0853	35.09176342
7.1	5.9	-12	36.55399	32.96	33.18212	34.23203774
7.2	5.9	-6	35.777	32.48	32.51238	33.58979098
7.3	5.9	0	35	32	31.84978	32.94992533
7.4	5.9	6	34.223	31.52	31.19483	32.31260968
7.5	5.9	12	33.44601	31.04	30.54801	31.67800424
7.6	5.9	4	34.482	31.68	31.41226	32.52475483
7.7	5.9	0	35	32	31.84978	32.94992533
7.8	5.9	-3	35.3885	32.24	32.18015	33.26954977
7.9	5.9	-1	35.1295	32.08	31.95969	33.05639698
8	5.9	2	34.741	31.84	31.63058	32.73719535
8.1	5.9	8	33.964	31.36	30.97829	32.10076574
8.2	5.9	15	33.05751	30.8	30.22779	31.36176546
8.3	5.9	19	32.53951	30.48	29.80426	30.94125781
5	6	-20	37.58999	33.6	34.0853	35.09176342
5.1	6	-21	37.71949	33.68	34.19896	35.19948286
5.2	6	-25	38.23749	34	34.65517	35.63088621
5.3	6	-27	38.49648	34.16	34.88419	35.84689064
5.4	6	-29	38.75548	34.32	35.11378	36.06308719
5.5	6	-31	39.01448	34.48	35.34392	36.27946843
5.6	6	-33	39.27348	34.64	35.5746	36.49602691

5.7	6	-35	39.53248	34.8	35.80579	36.71275506
5.8	6	-37	39.79148	34.96	36.03746	36.92964529
5.9	6	-35	39.53248	34.8	35.80579	36.71275506
6	6	-34	39.40298	34.72	35.69013	36.60437025
6.1	6	-33	39.27348	34.64	35.5746	36.49602691
6.2	6	-32	39.14398	34.56	35.4592	36.38772598
6.3	6	-30	38.88498	34.4	35.22878	36.17125519
6.4	6	-24	38.10799	33.92	34.54089	35.52295832
6.5	6	-19	37.46049	33.52	33.97181	34.98409834
6.6	6	-17	37.20149	33.36	33.74531	34.76893472
6.7	6	-15	36.94249	33.2	33.51951	34.55399899
6.8	6	-13	36.68349	33.04	33.2944	34.33929804
6.9	6	-11	36.42449	32.88	33.07002	34.12483868
7	6	-10	36.29499	32.8	32.95811	34.01770169
7.1	6	-8	36.036	32.64	32.73486	33.80361725
7.2	6	-6	35.777	32.48	32.51238	33.58979098
7.3	6	-4	35.518	32.32	32.29069	33.37622935
7.4	6	8	33.964	31.36	30.97829	32.10076574
7.5	6	18	32.66901	30.56	29.90977	31.0462602
7.6	6	20	32.41001	30.4	29.69901	30.8363395
7.7	6	16	32.92801	30.72	30.12153	31.25651466
7.8	6	8	33.964	31.36	30.97829	32.10076574
7.9	6	4	34.482	31.68	31.41226	32.52475483
8	6	10	33.70501	31.2	30.76268	31.88922873
8.1	6	14	33.18701	30.88	30.33429	31.46709776
8.2	6	17	32.79851	30.64	30.01553	31.15134603
8.3	6	19	32.53951	30.48	29.80426	30.94125781
5	6.1	-24	38.10799	33.92	34.54089	35.52295832
5.1	6.1	-26	38.36698	34.08	34.76961	35.73886395
5.2	6.1	-28	38.62598	34.24	34.99891	35.95496536
5.3	6.1	-30	38.88498	34.4	35.22878	36.17125519
5.4	6.1	-32	39.14398	34.56	35.4592	36.38772598
5.5	6.1	-34	39.40298	34.72	35.69013	36.60437025
5.6	6.1	-36	39.66198	34.88	35.92156	36.8211804
5.7	6.1	-37	39.79148	34.96	36.03746	36.92964529
5.8	6.1	-38	39.92098	35.04	36.15347	37.03814878
5.9	6.1	-36	39.66198	34.88	35.92156	36.8211804
6	6.1	-35	39.53248	34.8	35.80579	36.71275506
6.1	6.1	-34	39.40298	34.72	35.69013	36.60437025

6.2	6.1	-32	39.14398	34.56	35.4592	36.38772598
6.3	6.1	-30	38.88498	34.4	35.22878	36.17125519
6.4	6.1	-26	38.36698	34.08	34.76961	35.73886395
6.5	6.1	-18	37.33099	33.44	33.85848	34.87648848
6.6	6.1	-16	37.07199	33.28	33.63232	34.66143794
6.7	6.1	-14	36.81299	33.12	33.40686	34.44661874
6.8	6.1	-12	36.55399	32.96	33.18212	34.23203774
6.9	6.1	-10	36.29499	32.8	32.95811	34.01770169
7	6.1	-8	36.036	32.64	32.73486	33.80361725
7.1	6.1	-6	35.777	32.48	32.51238	33.58979098
7.2	6.1	-4	35.518	32.32	32.29069	33.37622935
7.3	6.1	-2	35.259	32.16	32.06982	33.16293872
7.4	6.1	2	34.741	31.84	31.63058	32.73719535
7.5	6.1	16	32.92801	30.72	30.12153	31.25651466
7.6	6.1	22	32.15101	30.24	29.48926	30.62675759
7.7	6.1	20	32.41001	30.4	29.69901	30.8363395
7.8	6.1	21	32.28051	30.32	29.59401	30.73150589
7.9	6.1	22	32.15101	30.24	29.48926	30.62675759
8	6.1	23	32.02151	30.16	29.38477	30.52209521
8.1	6.1	24	31.89201	30.08	29.28054	30.41751936
8.2	6.1	26	31.63302	29.92	29.07287	30.20862959
8.3	6.1	26	31.63302	29.92	29.07287	30.20862959
5	6.2	-23	37.97849	33.84	34.42676	35.4150812
5.1	6.2	-25	38.23749	34	34.65517	35.63088621
5.2	6.2	-27	38.49648	34.16	34.88419	35.84689064
5.3	6.2	-31	39.01448	34.48	35.34392	36.27946843
5.4	6.2	-32	39.14398	34.56	35.4592	36.38772598
5.5	6.2	-33	39.27348	34.64	35.5746	36.49602691
5.6	6.2	-34	39.40298	34.72	35.69013	36.60437025
5.7	6.2	-35	39.53248	34.8	35.80579	36.71275506
5.8	6.2	-36	39.66198	34.88	35.92156	36.8211804
5.9	6.2	-36	39.66198	34.88	35.92156	36.8211804
6	6.2	-35	39.53248	34.8	35.80579	36.71275506
6.1	6.2	-34	39.40298	34.72	35.69013	36.60437025
6.2	6.2	-32	39.14398	34.56	35.4592	36.38772598
6.3	6.2	-31	39.01448	34.48	35.34392	36.27946843
6.4	6.2	-27	38.49648	34.16	34.88419	35.84689064
6.5	6.2	-20	37.58999	33.6	34.0853	35.09176342
6.6	6.2	-16	37.07199	33.28	33.63232	34.66143794

6.7	6.2	-12	36.55399	32.96	33.18212	34.23203774
6.8	6.2	-10	36.29499	32.8	32.95811	34.01770169
6.9	6.2	-8	36.036	32.64	32.73486	33.80361725
7	6.2	-6	35.777	32.48	32.51238	33.58979098
7.1	6.2	-5	35.6475	32.4	32.40143	33.48297669
7.2	6.2	-4	35.518	32.32	32.29069	33.37622935
7.3	6.2	-2	35.259	32.16	32.06982	33.16293872
7.4	6.2	0	35	32	31.84978	32.94992533
7.5	6.2	8	33.964	31.36	30.97829	32.10076574
7.6	6.2	18	32.66901	30.56	29.90977	31.0462602
7.7	6.2	22	32.15101	30.24	29.48926	30.62675759
7.8	6.2	23	32.02151	30.16	29.38477	30.52209521
7.9	6.2	24	31.89201	30.08	29.28054	30.41751936
8	6.2	25	31.76251	30	29.17658	30.31303062
8.1	6.2	26	31.63302	29.92	29.07287	30.20862959
8.2	6.2	27	31.50352	29.84	28.96943	30.10431684
8.3	6.2	28	31.37402	29.76	28.86626	30.00009294
5	6.3	-18	37.33099	33.44	33.85848	34.87648848
5.1	6.3	-22	37.84899	33.76	34.31278	35.30725574
5.2	6.3	-26	38.36698	34.08	34.76961	35.73886395
5.3	6.3	-28	38.62598	34.24	34.99891	35.95496536
5.4	6.3	-30	38.88498	34.4	35.22878	36.17125519
5.5	6.3	-31	39.01448	34.48	35.34392	36.27946843
5.6	6.3	-32	39.14398	34.56	35.4592	36.38772598
5.7	6.3	-33	39.27348	34.64	35.5746	36.49602691
5.8	6.3	-34	39.40298	34.72	35.69013	36.60437025
5.9	6.3	-35	39.53248	34.8	35.80579	36.71275506
6	6.3	-35	39.53248	34.8	35.80579	36.71275506
6.1	6.3	-34	39.40298	34.72	35.69013	36.60437025
6.2	6.3	-33	39.27348	34.64	35.5746	36.49602691
6.3	6.3	-32	39.14398	34.56	35.4592	36.38772598
6.4	6.3	-31	39.01448	34.48	35.34392	36.27946843
6.5	6.3	-25	38.23749	34	34.65517	35.63088621
6.6	6.3	-18	37.33099	33.44	33.85848	34.87648848
6.7	6.3	-10	36.29499	32.8	32.95811	34.01770169
6.8	6.3	-5	35.6475	32.4	32.40143	33.48297669
6.9	6.3	-1	35.1295	32.08	31.95969	33.05639698
7	6.3	2	34.741	31.84	31.63058	32.73719535
7.1	6.3	4	34.482	31.68	31.41226	32.52475483

7.2	6.3	6	34.223	31.52	31.19483	32.31260968
7.3	6.3	8	33.964	31.36	30.97829	32.10076574
7.4	6.3	10	33.70501	31.2	30.76268	31.88922873
7.5	6.3	12	33.44601	31.04	30.54801	31.67800424
7.6	6.3	15	33.05751	30.8	30.22779	31.36176546
7.7	6.3	18	32.66901	30.56	29.90977	31.0462602
7.8	6.3	20	32.41001	30.4	29.69901	30.8363395
7.9	6.3	21	32.28051	30.32	29.59401	30.73150589
8	6.3	22	32.15101	30.24	29.48926	30.62675759
8.1	6.3	23	32.02151	30.16	29.38477	30.52209521
8.2	6.3	24	31.89201	30.08	29.28054	30.41751936
8.3	6.3	25	31.76251	30	29.17658	30.31303062
5	6.4	-17	37.20149	33.36	33.74531	34.76893472
5.1	6.4	-18	37.33099	33.44	33.85848	34.87648848
5.2	6.4	-20	37.58999	33.6	34.0853	35.09176342
5.3	6.4	-23	37.97849	33.84	34.42676	35.4150812
5.4	6.4	-26	38.36698	34.08	34.76961	35.73886395
5.5	6.4	-28	38.62598	34.24	34.99891	35.95496536
5.6	6.4	-30	38.88498	34.4	35.22878	36.17125519
5.7	6.4	-31	39.01448	34.48	35.34392	36.27946843
5.8	6.4	-32	39.14398	34.56	35.4592	36.38772598
5.9	6.4	-31	39.01448	34.48	35.34392	36.27946843
6	6.4	-30	38.88498	34.4	35.22878	36.17125519
6.1	6.4	-30	38.88498	34.4	35.22878	36.17125519
6.2	6.4	-31	39.01448	34.48	35.34392	36.27946843
6.3	6.4	-32	39.14398	34.56	35.4592	36.38772598
6.4	6.4	-31	39.01448	34.48	35.34392	36.27946843
6.5	6.4	-28	38.62598	34.24	34.99891	35.95496536
6.6	6.4	-22	37.84899	33.76	34.31278	35.30725574
6.7	6.4	-16	37.07199	33.28	33.63232	34.66143794
6.8	6.4	-9	36.16549	32.72	32.84639	33.91062761
6.9	6.4	-3	35.3885	32.24	32.18015	33.26954977
7	6.4	1	34.8705	31.92	31.74007	32.84352454
7.1	6.4	3	34.6115	31.76	31.52131	32.63093854
7.2	6.4	5	34.3525	31.6	31.30343	32.41864496
7.3	6.4	7	34.0935	31.44	31.08644	32.2066497
7.4	6.4	9	33.83451	31.28	30.87037	31.99495852
7.5	6.4	11	33.57551	31.12	30.65522	31.78357708
7.6	6.4	13	33.31651	30.96	30.44103	31.57251091

7.7	6.4	15	33.05751	30.8	30.22779	31.36176546
7.8	6.4	18	32.66901	30.56	29.90977	31.0462602
7.9	6.4	20	32.41001	30.4	29.69901	30.8363395
8	6.4	21	32.28051	30.32	29.59401	30.73150589
8.1	6.4	22	32.15101	30.24	29.48926	30.62675759
8.2	6.4	23	32.02151	30.16	29.38477	30.52209521
8.3	6.4	24	31.89201	30.08	29.28054	30.41751936
5	6.5	-14	36.81299	33.12	33.40686	34.44661874
5.1	6.5	-15	36.94249	33.2	33.51951	34.55399899
5.2	6.5	-17	37.20149	33.36	33.74531	34.76893472
5.3	6.5	-18	37.33099	33.44	33.85848	34.87648848
5.4	6.5	-19	37.46049	33.52	33.97181	34.98409834
5.5	6.5	-20	37.58999	33.6	34.0853	35.09176342
5.6	6.5	-21	37.71949	33.68	34.19896	35.19948286
5.7	6.5	-22	37.84899	33.76	34.31278	35.30725574
5.8	6.5	-25	38.23749	34	34.65517	35.63088621
5.9	6.5	-26	38.36698	34.08	34.76961	35.73886395
6	6.5	-27	38.49648	34.16	34.88419	35.84689064
6.1	6.5	-28	38.62598	34.24	34.99891	35.95496536
6.2	6.5	-29	38.75548	34.32	35.11378	36.06308719
6.3	6.5	-30	38.88498	34.4	35.22878	36.17125519
6.4	6.5	-30	38.88498	34.4	35.22878	36.17125519
6.5	6.5	-26	38.36698	34.08	34.76961	35.73886395
6.6	6.5	-23	37.97849	33.84	34.42676	35.4150812
6.7	6.5	-17	37.20149	33.36	33.74531	34.76893472
6.8	6.5	-12	36.55399	32.96	33.18212	34.23203774
6.9	6.5	-6	35.777	32.48	32.51238	33.58979098
7	6.5	0	35	32	31.84978	32.94992533
7.1	6.5	2	34.741	31.84	31.63058	32.73719535
7.2	6.5	4	34.482	31.68	31.41226	32.52475483
7.3	6.5	6	34.223	31.52	31.19483	32.31260968
7.4	6.5	8	33.964	31.36	30.97829	32.10076574
7.5	6.5	10	33.70501	31.2	30.76268	31.88922873
7.6	6.5	12	33.44601	31.04	30.54801	31.67800424
7.7	6.5	14	33.18701	30.88	30.33429	31.46709776
7.8	6.5	16	32.92801	30.72	30.12153	31.25651466
7.9	6.5	18	32.66901	30.56	29.90977	31.0462602
8	6.5	20	32.41001	30.4	29.69901	30.8363395
8.1	6.5	22	32.15101	30.24	29.48926	30.62675759

8.2	6.5	24	31.89201	30.08	29.28054	30.41751936
8.3	6.5	26	31.63302	29.92	29.07287	30.20862959
5	6.6	0	35	32	31.84978	32.94992533
5.1	6.6	-2	35.259	32.16	32.06982	33.16293872
5.2	6.6	-5	35.6475	32.4	32.40143	33.48297669
5.3	6.6	-8	36.036	32.64	32.73486	33.80361725
5.4	6.6	-12	36.55399	32.96	33.18212	34.23203774
5.5	6.6	-14	36.81299	33.12	33.40686	34.44661874
5.6	6.6	-16	37.07199	33.28	33.63232	34.66143794
5.7	6.6	-18	37.33099	33.44	33.85848	34.87648848
5.8	6.6	-20	37.58999	33.6	34.0853	35.09176342
5.9	6.6	-21	37.71949	33.68	34.19896	35.19948286
6	6.6	-22	37.84899	33.76	34.31278	35.30725574
6.1	6.6	-23	37.97849	33.84	34.42676	35.4150812
6.2	6.6	-24	38.10799	33.92	34.54089	35.52295832
6.3	6.6	-25	38.23749	34	34.65517	35.63088621
6.4	6.6	-25	38.23749	34	34.65517	35.63088621
6.5	6.6	-24	38.10799	33.92	34.54089	35.52295832
6.6	6.6	-22	37.84899	33.76	34.31278	35.30725574
6.7	6.6	-17	37.20149	33.36	33.74531	34.76893472
6.8	6.6	-14	36.81299	33.12	33.40686	34.44661874
6.9	6.6	-8	36.036	32.64	32.73486	33.80361725
7	6.6	-3	35.3885	32.24	32.18015	33.26954977
7.1	6.6	5	34.3525	31.6	31.30343	32.41864496
7.2	6.6	8	33.964	31.36	30.97829	32.10076574
7.3	6.6	12	33.44601	31.04	30.54801	31.67800424
7.4	6.6	14	33.18701	30.88	30.33429	31.46709776
7.5	6.6	15	33.05751	30.8	30.22779	31.36176546
7.6	6.6	9	33.83451	31.28	30.87037	31.99495852
7.7	6.6	10	33.70501	31.2	30.76268	31.88922873
7.8	6.6	11	33.57551	31.12	30.65522	31.78357708
7.9	6.6	12	33.44601	31.04	30.54801	31.67800424
8	6.6	13	33.31651	30.96	30.44103	31.57251091
8.1	6.6	14	33.18701	30.88	30.33429	31.46709776
8.2	6.6	15	33.05751	30.8	30.22779	31.36176546
8.3	6.6	16	32.92801	30.72	30.12153	31.25651466
5	6.7	3	34.6115	31.76	31.52131	32.63093854
5.1	6.7	1	34.8705	31.92	31.74007	32.84352454
5.2	6.7	-1	35.1295	32.08	31.95969	33.05639698

5.3	6.7	-3	35.3885	32.24	32.18015	33.26954977
5.4	6.7	-5	35.6475	32.4	32.40143	33.48297669
5.5	6.7	-7	35.9065	32.56	32.62352	33.69667144
5.6	6.7	-9	36.16549	32.72	32.84639	33.91062761
5.7	6.7	-11	36.42449	32.88	33.07002	34.12483868
5.8	6.7	-15	36.94249	33.2	33.51951	34.55399899
5.9	6.7	-17	37.20149	33.36	33.74531	34.76893472
6	6.7	-18	37.33099	33.44	33.85848	34.87648848
6.1	6.7	-19	37.46049	33.52	33.97181	34.98409834
6.2	6.7	-20	37.58999	33.6	34.0853	35.09176342
6.3	6.7	-23	37.97849	33.84	34.42676	35.4150812
6.4	6.7	-27	38.49648	34.16	34.88419	35.84689064
6.5	6.7	-23	37.97849	33.84	34.42676	35.4150812
6.6	6.7	-20	37.58999	33.6	34.0853	35.09176342
6.7	6.7	-18	37.33099	33.44	33.85848	34.87648848
6.8	6.7	-15	36.94249	33.2	33.51951	34.55399899
6.9	6.7	-8	36.036	32.64	32.73486	33.80361725
7	6.7	-3	35.3885	32.24	32.18015	33.26954977
7.1	6.7	0	35	32	31.84978	32.94992533
7.2	6.7	2	34.741	31.84	31.63058	32.73719535
7.3	6.7	3	34.6115	31.76	31.52131	32.63093854
7.4	6.7	4	34.482	31.68	31.41226	32.52475483
7.5	6.7	5	34.3525	31.6	31.30343	32.41864496
7.6	6.7	6	34.223	31.52	31.19483	32.31260968
7.7	6.7	7	34.0935	31.44	31.08644	32.2066497
7.8	6.7	8	33.964	31.36	30.97829	32.10076574
7.9	6.7	9	33.83451	31.28	30.87037	31.99495852
8	6.7	10	33.70501	31.2	30.76268	31.88922873
8.1	6.7	11	33.57551	31.12	30.65522	31.78357708
8.2	6.7	12	33.44601	31.04	30.54801	31.67800424
8.3	6.7	13	33.31651	30.96	30.44103	31.57251091
5	6.8	6	34.223	31.52	31.19483	32.31260968
5.1	6.8	5	34.3525	31.6	31.30343	32.41864496
5.2	6.8	3	34.6115	31.76	31.52131	32.63093854
5.3	6.8	0	35	32	31.84978	32.94992533
5.4	6.8	-2	35.259	32.16	32.06982	33.16293872
5.5	6.8	-4	35.518	32.32	32.29069	33.37622935
5.6	6.8	-6	35.777	32.48	32.51238	33.58979098
5.7	6.8	-8	36.036	32.64	32.73486	33.80361725

5.8	6.8	-10	36.29499	32.8	32.95811	34.01770169
5.9	6.8	-12	36.55399	32.96	33.18212	34.23203774
6	6.8	-14	36.81299	33.12	33.40686	34.44661874
6.1	6.8	-16	37.07199	33.28	33.63232	34.66143794
6.2	6.8	-19	37.46049	33.52	33.97181	34.98409834
6.3	6.8	-22	37.84899	33.76	34.31278	35.30725574
6.4	6.8	-24	38.10799	33.92	34.54089	35.52295832
6.5	6.8	-22	37.84899	33.76	34.31278	35.30725574
6.6	6.8	-18	37.33099	33.44	33.85848	34.87648848
6.7	6.8	-15	36.94249	33.2	33.51951	34.55399899
6.8	6.8	-12	36.55399	32.96	33.18212	34.23203774
6.9	6.8	-9	36.16549	32.72	32.84639	33.91062761
7	6.8	-5	35.6475	32.4	32.40143	33.48297669
7.1	6.8	-2	35.259	32.16	32.06982	33.16293872
7.2	6.8	1	34.8705	31.92	31.74007	32.84352454
7.3	6.8	2	34.741	31.84	31.63058	32.73719535
7.4	6.8	3	34.6115	31.76	31.52131	32.63093854
7.5	6.8	4	34.482	31.68	31.41226	32.52475483
7.6	6.8	5	34.3525	31.6	31.30343	32.41864496
7.7	6.8	6	34.223	31.52	31.19483	32.31260968
7.8	6.8	7	34.0935	31.44	31.08644	32.2066497
7.9	6.8	8	33.964	31.36	30.97829	32.10076574
8	6.8	9	33.83451	31.28	30.87037	31.99495852
8.1	6.8	10	33.70501	31.2	30.76268	31.88922873
8.2	6.8	11	33.57551	31.12	30.65522	31.78357708
8.3	6.8	12	33.44601	31.04	30.54801	31.67800424
5	6.9		35	32	31.84978	32.94992533
5.1	6.9		35	32	31.84978	32.94992533
5.2	6.9	5	34.3525	31.6	31.30343	32.41864496
5.3	6.9	3	34.6115	31.76	31.52131	32.63093854
5.4	6.9	1	34.8705	31.92	31.74007	32.84352454
5.5	6.9	-1	35.1295	32.08	31.95969	33.05639698
5.6	6.9	-3	35.3885	32.24	32.18015	33.26954977
5.7	6.9	-5	35.6475	32.4	32.40143	33.48297669
5.8	6.9	-7	35.9065	32.56	32.62352	33.69667144
5.9	6.9	-9	36.16549	32.72	32.84639	33.91062761
6	6.9	-11	36.42449	32.88	33.07002	34.12483868
6.1	6.9	-14	36.81299	33.12	33.40686	34.44661874
6.2	6.9	-17	37.20149	33.36	33.74531	34.76893472

6.3	6.9	-20	37.58999	33.6	34.0853	35.09176342
6.4	6.9	-20	37.58999	33.6	34.0853	35.09176342
6.5	6.9	-18	37.33099	33.44	33.85848	34.87648848
6.6	6.9	-16	37.07199	33.28	33.63232	34.66143794
6.7	6.9	-14	36.81299	33.12	33.40686	34.44661874
6.8	6.9	-12	36.55399	32.96	33.18212	34.23203774
6.9	6.9	-10	36.29499	32.8	32.95811	34.01770169
7	6.9	-8	36.036	32.64	32.73486	33.80361725
7.1	6.9	-6	35.777	32.48	32.51238	33.58979098
7.2	6.9	-5	35.6475	32.4	32.40143	33.48297669
7.3	6.9	-3	35.3885	32.24	32.18015	33.26954977
7.4	6.9	-3	35.3885	32.24	32.18015	33.26954977
7.5	6.9	-1	35.1295	32.08	31.95969	33.05639698
7.6	6.9	1	34.8705	31.92	31.74007	32.84352454
7.7	6.9	3	34.6115	31.76	31.52131	32.63093854
7.8	6.9	5	34.3525	31.6	31.30343	32.41864496
7.9	6.9	7	34.0935	31.44	31.08644	32.2066497
8	6.9	9	33.83451	31.28	30.87037	31.99495852
8.1	6.9	11	33.57551	31.12	30.65522	31.78357708
8.2	6.9	13	33.31651	30.96	30.44103	31.57251091
8.3	6.9	15	33.05751	30.8	30.22779	31.36176546
5	7		35	32	31.84978	32.94992533
5.1	7		35	32	31.84978	32.94992533
5.2	7		35	32	31.84978	32.94992533
5.3	7		35	32	31.84978	32.94992533
5.4	7		35	32	31.84978	32.94992533
5.5	7	2	34.741	31.84	31.63058	32.73719535
5.6	7	0	35	32	31.84978	32.94992533
5.7	7	-1	35.1295	32.08	31.95969	33.05639698
5.8	7	-3	35.3885	32.24	32.18015	33.26954977
5.9	7	-5	35.6475	32.4	32.40143	33.48297669
6	7	-7	35.9065	32.56	32.62352	33.69667144
6.1	7	-11	36.42449	32.88	33.07002	34.12483868
6.2	7	-14	36.81299	33.12	33.40686	34.44661874
6.3	7	-16	37.07199	33.28	33.63232	34.66143794
6.4	7	-16	37.07199	33.28	33.63232	34.66143794
6.5	7	-14	36.81299	33.12	33.40686	34.44661874
6.6	7	-12	36.55399	32.96	33.18212	34.23203774
6.7	7	-10	36.29499	32.8	32.95811	34.01770169

6.8	7	-7	35.9065	32.56	32.62352	33.69667144
6.9	7	-4	35.518	32.32	32.29069	33.37622935
7	7	-3	35.3885	32.24	32.18015	33.26954977
7.1	7	-2	35.259	32.16	32.06982	33.16293872
7.2	7	-1	35.1295	32.08	31.95969	33.05639698
7.3	7	-1	35.1295	32.08	31.95969	33.05639698
7.4	7	-3	35.3885	32.24	32.18015	33.26954977
7.5	7	-5	35.6475	32.4	32.40143	33.48297669
7.6	7	-2	35.259	32.16	32.06982	33.16293872
7.7	7	0	35	32	31.84978	32.94992533
7.8	7	2	34.741	31.84	31.63058	32.73719535
7.9	7	4	34.482	31.68	31.41226	32.52475483
8	7	6	34.223	31.52	31.19483	32.31260968
8.1	7	8	33.964	31.36	30.97829	32.10076574
8.2	7	10	33.70501	31.2	30.76268	31.88922873
8.3	7	12	33.44601	31.04	30.54801	31.67800424
5	7.1		35	32	31.84978	32.94992533
5.1	7.1		35	32	31.84978	32.94992533
5.2	7.1		35	32	31.84978	32.94992533
5.3	7.1		35	32	31.84978	32.94992533
5.4	7.1		35	32	31.84978	32.94992533
5.5	7.1		35	32	31.84978	32.94992533
5.6	7.1		35	32	31.84978	32.94992533
5.7	7.1		35	32	31.84978	32.94992533
5.8	7.1	0	35	32	31.84978	32.94992533
5.9	7.1	-2	35.259	32.16	32.06982	33.16293872
6	7.1	-4	35.518	32.32	32.29069	33.37622935
6.1	7.1	-6	35.777	32.48	32.51238	33.58979098
6.2	7.1	-8	36.036	32.64	32.73486	33.80361725
6.3	7.1	-10	36.29499	32.8	32.95811	34.01770169
6.4	7.1	-8	36.036	32.64	32.73486	33.80361725
6.5	7.1	-6	35.777	32.48	32.51238	33.58979098
6.6	7.1	-4	35.518	32.32	32.29069	33.37622935
6.7	7.1	-2	35.259	32.16	32.06982	33.16293872
6.8	7.1	-1	35.1295	32.08	31.95969	33.05639698
6.9	7.1	0	35	32	31.84978	32.94992533
7	7.1	2	34.741	31.84	31.63058	32.73719535
7.1	7.1	4	34.482	31.68	31.41226	32.52475483
7.2	7.1	6	34.223	31.52	31.19483	32.31260968

7.3	7.1	4	34.482	31.68	31.41226	32.52475483
7.4	7.1	2	34.741	31.84	31.63058	32.73719535
7.5	7.1	0	35	32	31.84978	32.94992533
7.6	7.1	-2	35.259	32.16	32.06982	33.16293872
7.7	7.1	-2	35.259	32.16	32.06982	33.16293872
7.8	7.1	0	35	32	31.84978	32.94992533
7.9	7.1	2	34.741	31.84	31.63058	32.73719535
8	7.1	4	34.482	31.68	31.41226	32.52475483
8.1	7.1	6	34.223	31.52	31.19483	32.31260968
8.2	7.1	8	33.964	31.36	30.97829	32.10076574
8.3	7.1	10	33.70501	31.2	30.76268	31.88922873
5	7.2		35	32	31.84978	32.94992533
5.1	7.2		35	32	31.84978	32.94992533
5.2	7.2		35	32	31.84978	32.94992533
5.3	7.2		35	32	31.84978	32.94992533
5.4	7.2		35	32	31.84978	32.94992533
5.5	7.2		35	32	31.84978	32.94992533
5.6	7.2		35	32	31.84978	32.94992533
5.7	7.2		35	32	31.84978	32.94992533
5.8	7.2		35	32	31.84978	32.94992533
5.9	7.2		35	32	31.84978	32.94992533
6	7.2	-1	35.1295	32.08	31.95969	33.05639698
6.1	7.2	-3	35.3885	32.24	32.18015	33.26954977
6.2	7.2	-5	35.6475	32.4	32.40143	33.48297669
6.3	7.2	-7	35.9065	32.56	32.62352	33.69667144
6.4	7.2	-5	35.6475	32.4	32.40143	33.48297669
6.5	7.2	-3	35.3885	32.24	32.18015	33.26954977
6.6	7.2	-1	35.1295	32.08	31.95969	33.05639698
6.7	7.2	2	34.741	31.84	31.63058	32.73719535
6.8	7.2	3	34.6115	31.76	31.52131	32.63093854
6.9	7.2	5	34.3525	31.6	31.30343	32.41864496
7	7.2	7	34.0935	31.44	31.08644	32.2066497
7.1	7.2	9	33.83451	31.28	30.87037	31.99495852
7.2	7.2	11	33.57551	31.12	30.65522	31.78357708
7.3	7.2	9	33.83451	31.28	30.87037	31.99495852
7.4	7.2	6	34.223	31.52	31.19483	32.31260968
7.5	7.2	3	34.6115	31.76	31.52131	32.63093854
7.6	7.2	0	35	32	31.84978	32.94992533
7.7	7.2	-1	35.1295	32.08	31.95969	33.05639698

7.8	7.2	-1	35.1295	32.08	31.95969	33.05639698
7.9	7.2	1	34.8705	31.92	31.74007	32.84352454
8	7.2	3	34.6115	31.76	31.52131	32.63093854
8.1	7.2	5	34.3525	31.6	31.30343	32.41864496
8.2	7.2	7	34.0935	31.44	31.08644	32.2066497
8.3	7.2	9	33.83451	31.28	30.87037	31.99495852

APPENDIX B

Graph of Basement Depth, Conrad depth and crustal thickness obtained from Spectral results

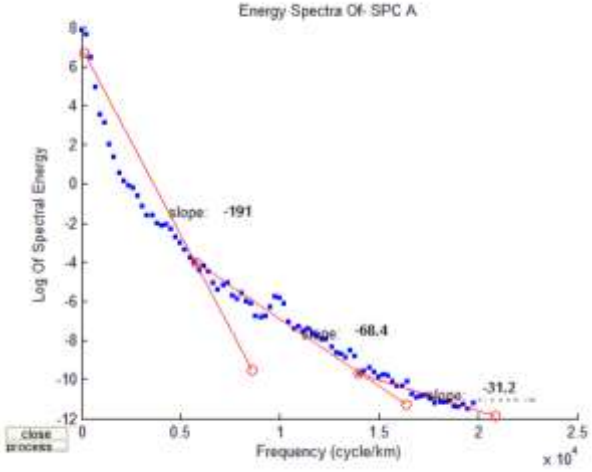

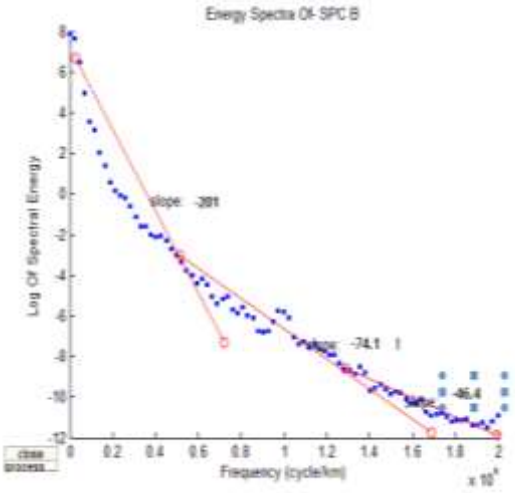

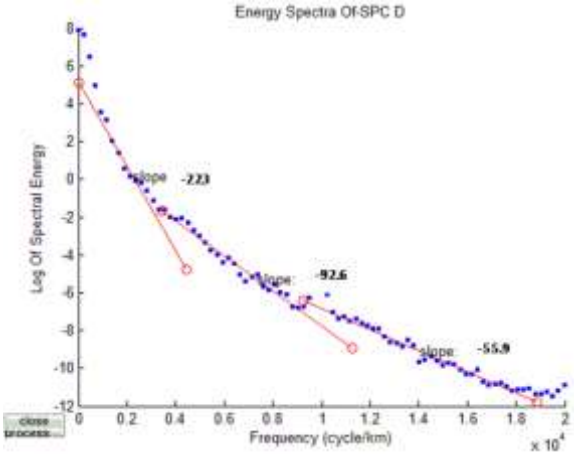

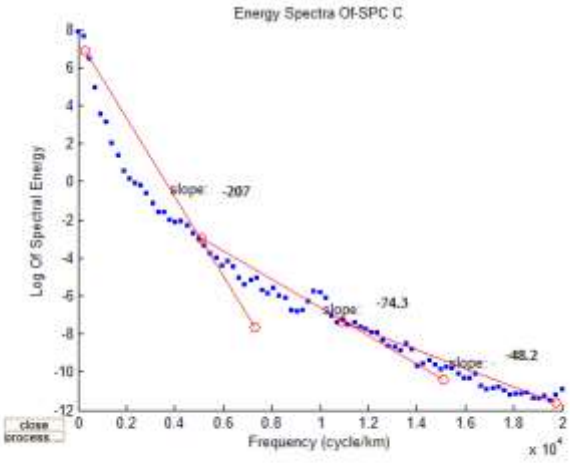

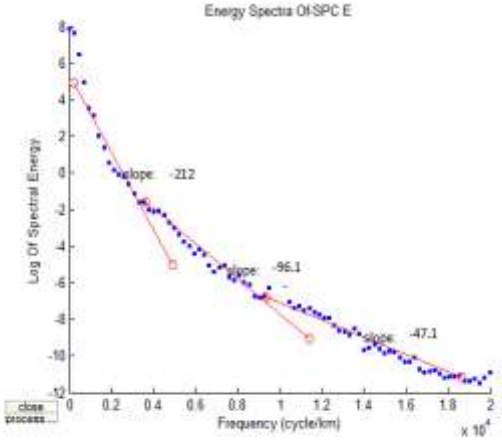

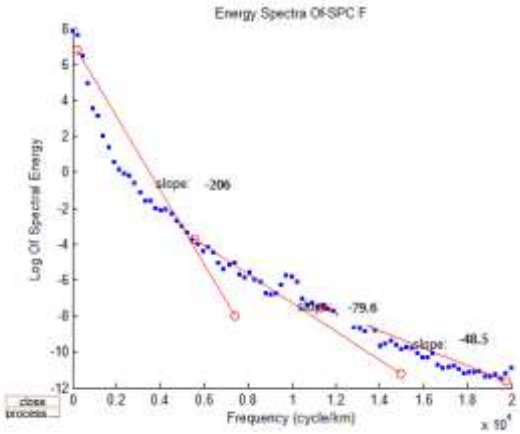

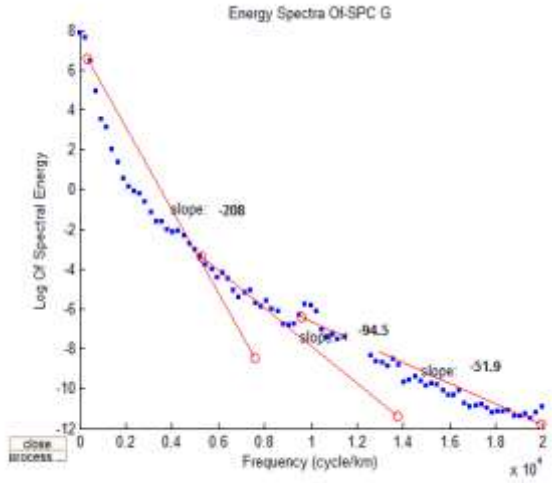
Energy Spectra Of-SPC G
Log Of Spectral Energy
Frequency (cycle/km)
x 10^4
slope: -208
slope: -94.5
slope: -51.9
close process

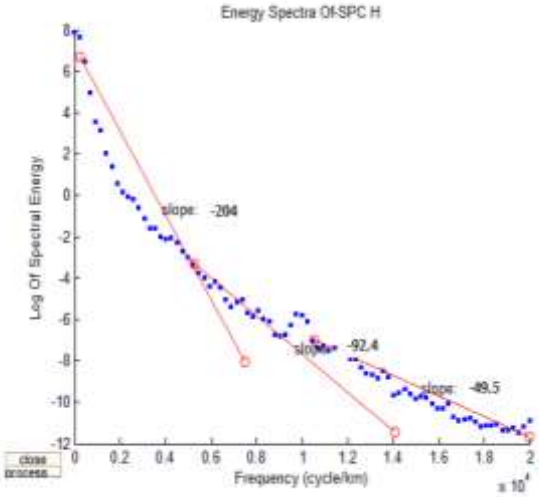
Energy Spectra Of-SPC H
Log Of Spectral Energy
Frequency (cycle/km)
x 10^4
slope: -204
slope: -92.4
slope: -89.5
close process

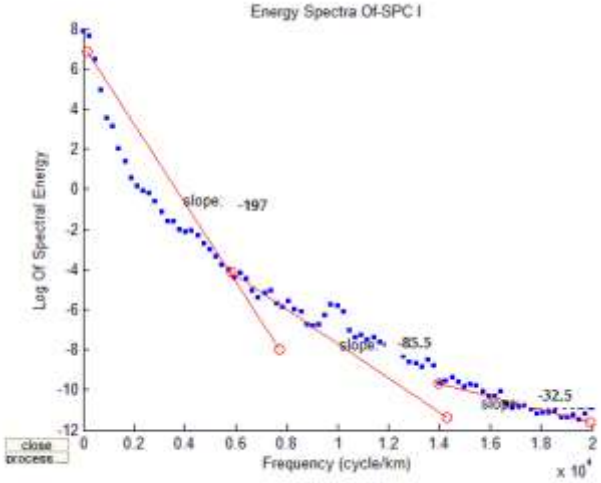
Energy Spectra Of-SPC I
Log Of Spectral Energy
Frequency (cycle/km)
x 10^4
slope: -197
slope: -85.5
slope: -32.5
close process

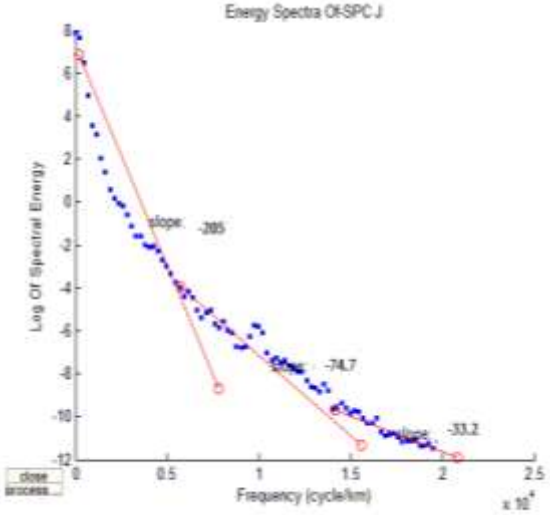
Energy Spectra Of-SPC J
Log Of Spectral Energy
Frequency (cycle/km)
x 10^4
slope: -205
-74.7
-33.2
close process

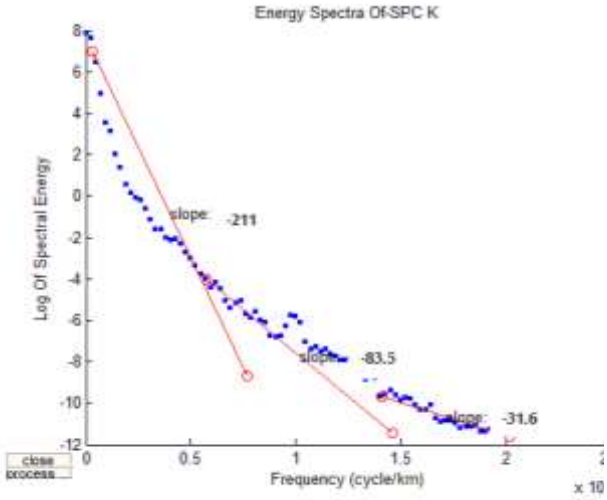
Energy Spectra Of-SPC K
Log Of Spectral Energy
Frequency (cycle/km)
slope: -211
slope: -83.5
slope: -31.6
close process

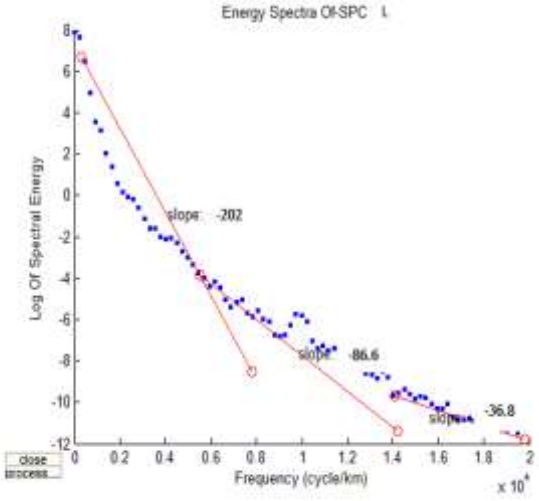
Energy Spectra Of-SPC L
Log Of Spectral Energy
Frequency (cycle/km)
x 10^4
slope: -202
slope: -86.6
slope: -36.8
close process

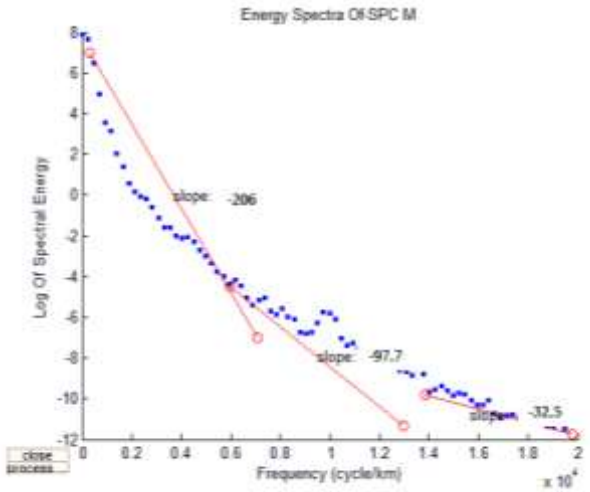
Energy Spectra Of-SPC M
Log Of Spectral Energy
Frequency (cycle/km)
x 10^4
slope: -206
slope: -97.7
slope: -32.5
close process

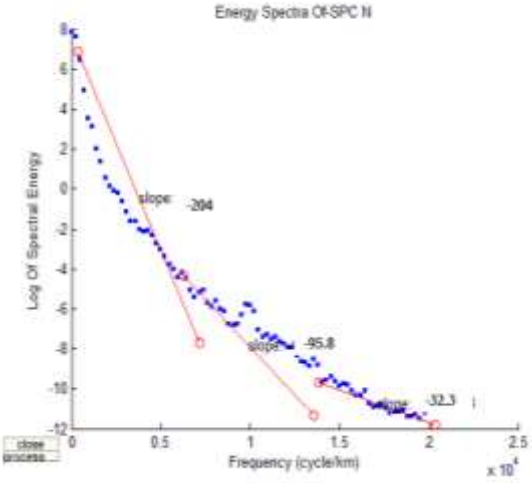
Energy Spectra Of-SPC N
Log Of Spectral Energy
Frequency (cycle/km)
x 10^4
slope: -204
slope: -95.8
slope: -32.3
close process

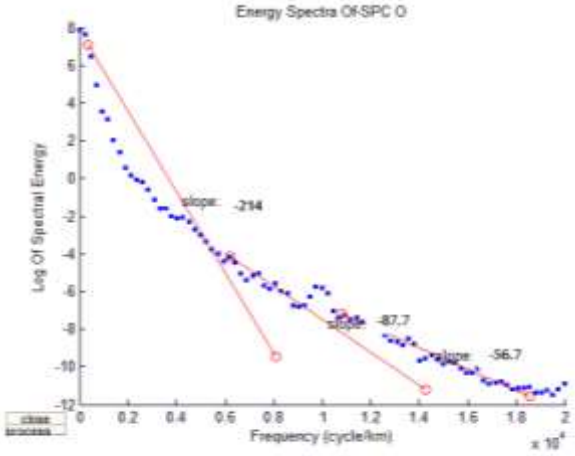
Energy Spectra Of-SPC O
Log Of Spectral Energy
Frequency (cycle/km)
x 10^4
slope: -214
slope: -87.7
slope: -56.7
close process

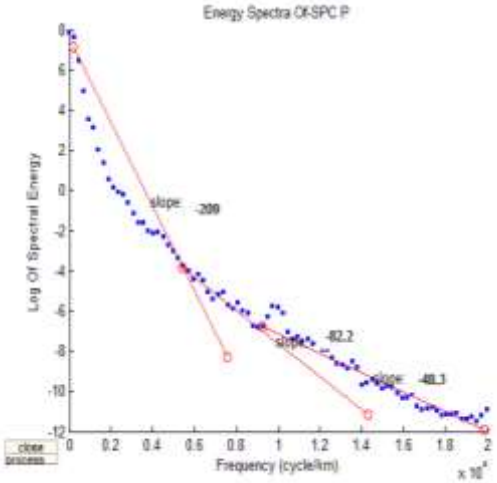
Energy Spectra Of-SPC P
Log Of Spectral Energy
Frequency (cycle/km)
x 10^4
slope: -209
slope: -82.2
slope: -48.3
close process

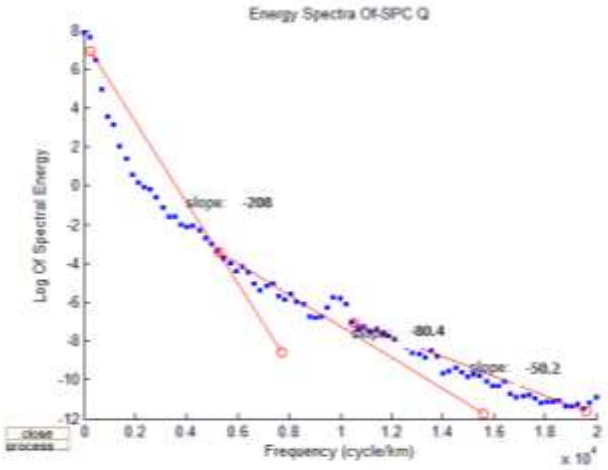
Energy Spectra Of-SPC Q
Log Of Spectral Energy
Frequency (cycle/km)
x 10^4
slope: -208
slope: -80.4
slope: -58.2
close process

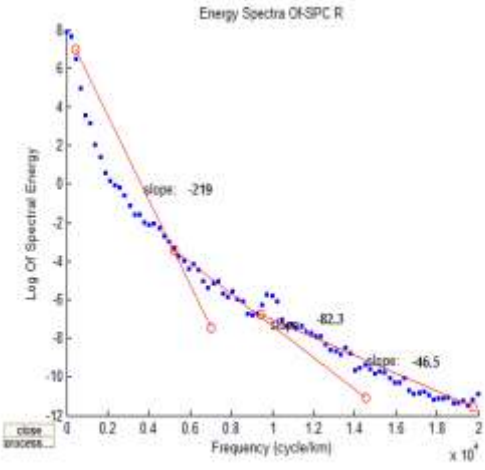
Energy Spectra Of-SPC R
Log Of Spectral Energy
Frequency (cycle/km)
x 10^4
slope: -219
slope: -82.3
slope: -46.5
close process

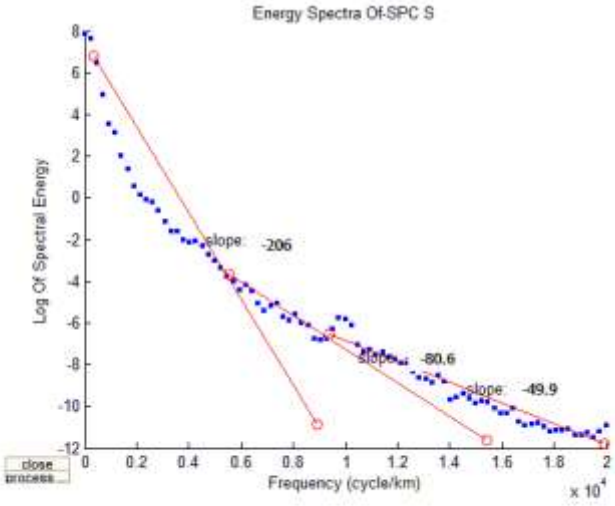
Energy Spectra Of-SPC S
Log Of Spectral Energy
Frequency (cycle/km)
x 10^4
slope: -206
slope: -80.6
slope: -49.9
close process

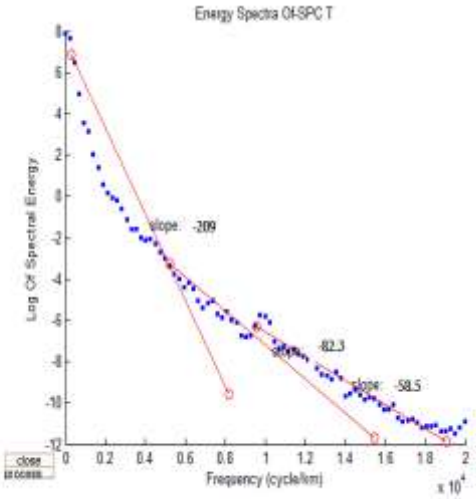
Energy Spectra Of-SPC T
Log Of Spectral Energy
Frequency (cycle/km)
x 10^4
slope: -209
slope: -82.3
slope: -58.5
close process

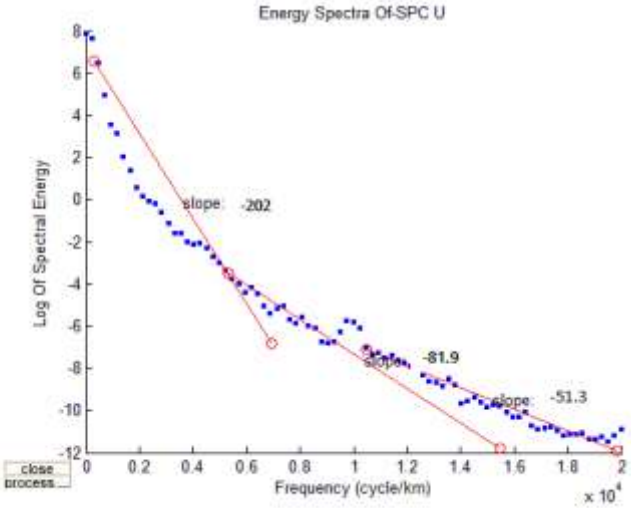
Energy Spectra Of-SPC U
Log Of Spectral Energy
Frequency (cycle/km)
x 10^4
slope: -202
slope: -81.9
slope: -51.3
close process

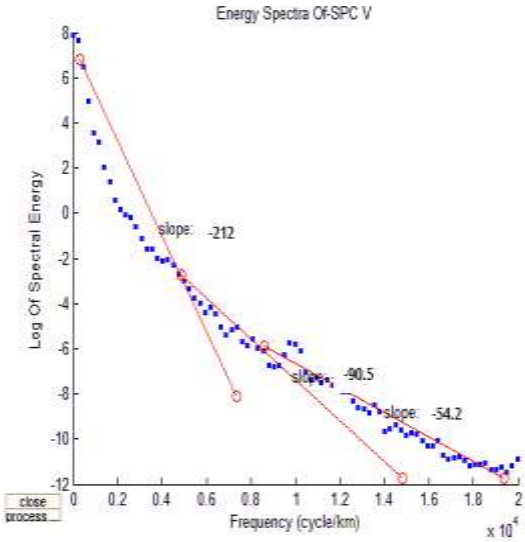
Energy Spectra Of-SPC V
Log Of Spectral Energy
Frequency (cycle/km)
x 10^4
slope: -212
slope: -90.5
slope: -54.2
close process

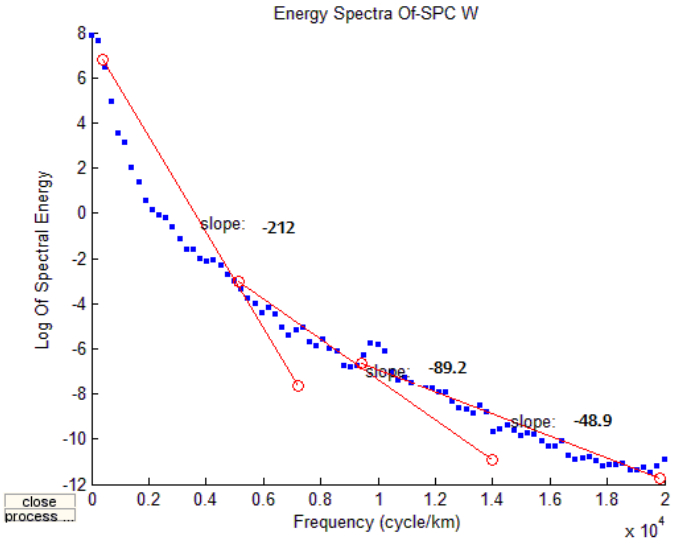
Energy Spectra Of-SPC W
Log Of Spectral Energy
Frequency (cycle/km)
x 10^4
slope: -212
slope: -89.2
slope: -48.9
close process

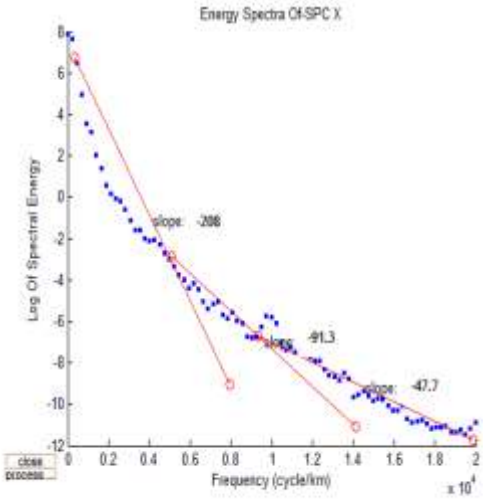
Energy Spectra Of-SPC X
Log Of Spectral Energy
Frequency (cycle/km)
x 10^4
slope: -208
slope: -91.3
slope: -47.7
close process

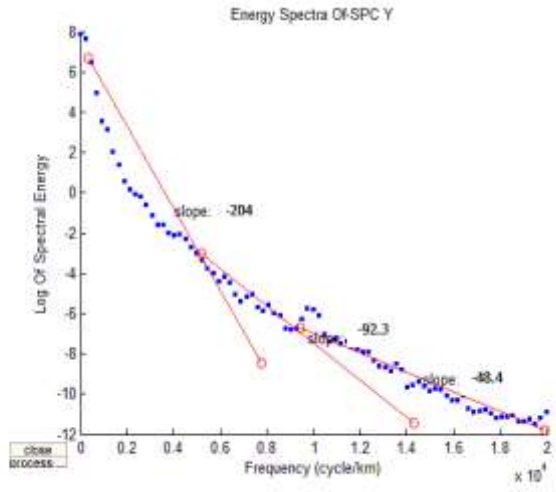
Energy Spectra Of-SPC Y
Log Of Spectral Energy
Frequency (cycle/km)
x 10^4
slope: -204
-92.3
-48.4
close
process...

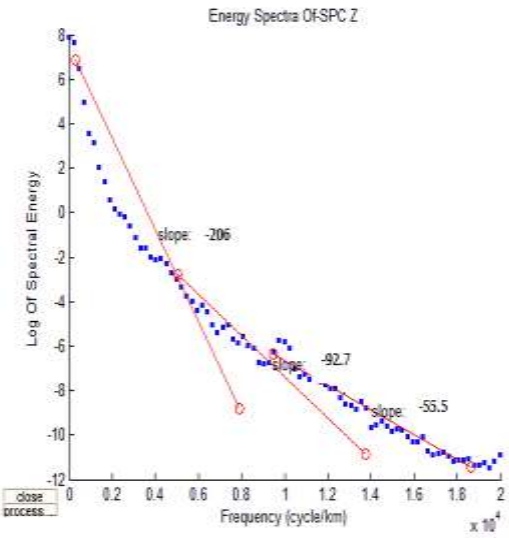
Energy Spectra Of-SPC Z
Log Of Spectral Energy
Frequency (cycle/km)
x 10^4
slope: -206
-92.7
-55.5
close
process...

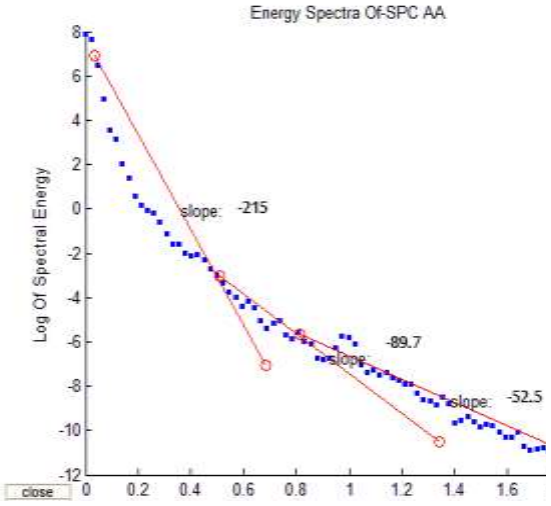
Energy Spectra Of-SPC AA
Log Of Spectral Energy
slope: -215
-89.7
-52.5
close

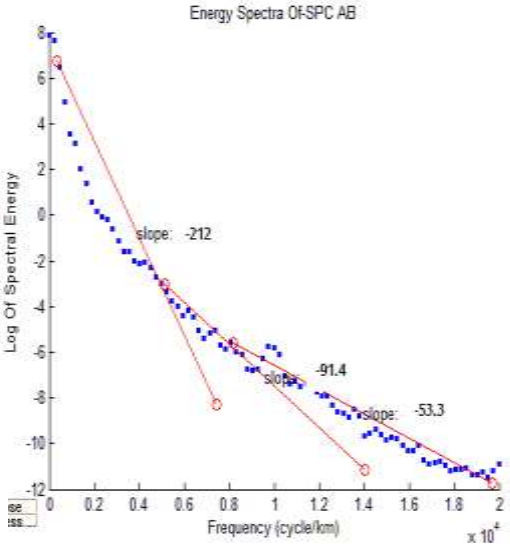
Energy Spectra Of-SPC AB
Log Of Spectral Energy
Frequency (cycle/km)
x 10^4
slope: -212
-91.4
-53.3

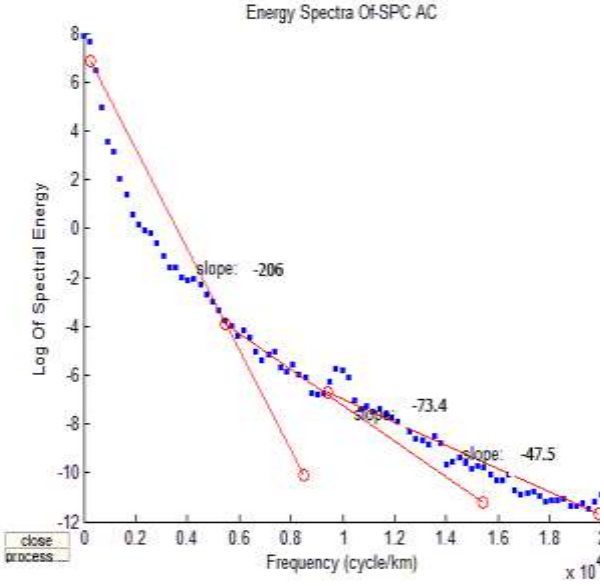
Energy Spectra Of-SPC AC
Log Of Spectral Energy
Frequency (cycle/km)
x 10^4
slope: -206
-73.4
-47.5
close
process...

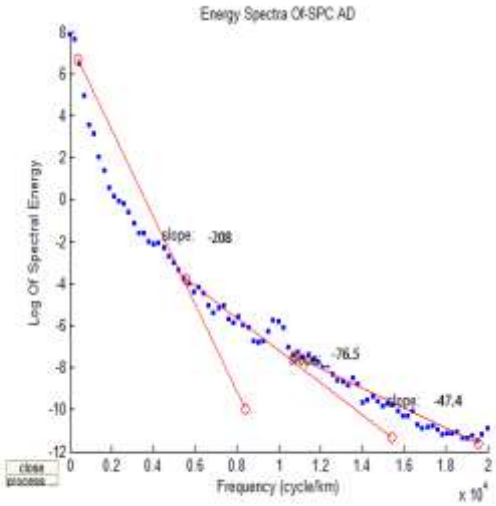
Energy Spectra Of-SPC AD
Log Of Spectral Energy
Frequency (cycle/km)
x 10^4
slope: -208
-76.5
-47.4
close
process...

APPENDIX C

Table 4.5: Complete Results of Average crustal thickness obtained from 2-D modelling of 2D plot and 3D surface plot.

LONGITUDE (Degree)	LATITUDE (Degree)	CRUSTAL THICKNESS (km)
6.22	7.08	-34
6.26	6.95	-35
6.63	6.62	-28
6.31	6.65	-29
6.37	6.95	-32
6.33	5.95	-34
6.32	5.94	-35
6.31	6.13	-35
6.23	5.88	-36
6.27	5.89	-35
6.33	5.97	-34
6.37	6.95	-33
6.22	5.89	-35
6.16	5.87	-36
6.22	5.89	-32
6.37	6.95	-34
6.63	6.62	-36
6.54	6.06	-38
5.12	6.26	-38
5.32	6.31	-37
5.42	6.31	-39
5.52	6.26	-38
5.55	6.28	-39
5.32	6.31	-37
5.19	6.28	-38
5.11	6.25	-39
5.27	5.84	-38
5.29	5.71	-39
5.29	5.61	-37
5.29	5.42	-36
5.22	5.73	-35
5.31	5.86	-36
5.35	5.85	-35
5.39	5.86	-38
5.11	6.25	-37
5.19	6.28	-39
5.66	7.14	-38

5.68	7.03	-37
5.68	6.91	-38
5.69	6.79	-37
5.75	6.61	-36
5.77	6.58	-38
5.88	6.46	-38
5.91	6.42	-39
5.99	6.74	-38
6.04	6.82	-39
5.94	6.41	-38
5.98	6.46	-39
6.02	6.56	-38
6.07	6.78	-38
6.09	6.88	-38
5.76	6.92	-37
5.53	6.95	-36
5.72	6.98	-39